ABSTRACT

KIRBY N. SMITH: Computer Modeling of Contaminant Jet Flow into Local Exhaust Hoods. (Under the direction of Assistant Professor, Michael R. Flynn, Sc.D.).

A computer model was developed and coded in BASIC to predict the streamline that a jet of gaseous sulfur hexafluoride will follow in the flow field of a flanged circular exhaust hood (FCH). This approximate solution is based on the vector addition of a modified potential flow solution for the FCH, and a jet flow solution. The assumptions underlying the equations describing jet flow are those of the Prandtl mixing length hypothesis. The computer program generates streamlines for the combined flow by means of iterative vector addition. The interactive program prompts the user for the hood and jet diameters and flows, and the distance from the hood at which the jet is placed. A graphic plot of the predicted streamline followed by the gas jet is displayed.

The program is used to predict the critical distance $[Z/D]_{50}$, the distance along the hood centerline (Z), as a fraction of the hood diameter (D), where the jet can be placed such that 50% of the jet contaminant flow is captured. A series of such $[Z/D]_{50}$ values was generated for twenty-one hood and jet flow combinations.

The program was validated in the laboratory. A probe was placed in the duct of a flanged circular exhaust hood and was connected to an electron-capture gas chromatograph, to determine the concentration of SF_6 in the hood. Capture efficiencies (ratios of "captured" gas concentrations at various jet-hood distances to concentrations in the duct when the jet flow is fully captured) were determined for jet positions at intervals along the hood centerline. Five replicate measurements were collected per position, for all combinations of jet and hood flow.

Results indicate that the model is quite accurate when crossdrafts are accounted for, except for predicted $[Z/D]_{50}$ values of less than 0.7, which occur quite close to the hood face. The approximate model errs in this region because it neglects the effects on the jet of the static pressure gradient created by the flow of the exhaust hood, and the shear turbulence of the interacting streamlines of jet and hood flow.

The model may be expanded in the future to include definitive crossdraft variations, other jet locations or directions, hoods of other shapes, or heat and gas buoyancy effects.

Key Words: Critical distance, flanged circular exhaust hood, capture efficiency, ventilation.

TABLE OF CONTENTS

LIST OF FIGURES

LIST OF TABLES

LIST OF APPENDICES

ACKNOWLEDGMENTS

My sincere thanks are due to Dr. Michael R. Flynn for his direction and enthusiasm for this research project. His occasional suggestions were helpful, as was the freedom he allowed me in pursing my intellectual curiosity regarding adjunct issues. Appreciation is also extended gratefully to my committee members Drs. Cass T. Miller and David Leith. Dr. Leith provided the cyclone and Venturi meter, without which this project would not have been possible.

I. INTRODUCTION

Industrial hygienists typically use a variety of control measures to abate the danger to workers of inhaling toxic materials. These may include engineering or administrative controls, and possibly the use of personal protective equipment. Because inhaled toxic materials may give rise to a variety of deleterious health effects, it is important to minimize such exposures.

Engineering controls are easily the more desirable of protective measures because they ensure that the worker is actually exposed to the toxin or otherwise hazardous material as little as possible. Engineering controls in general do not require active participation on the part of the worker to be effective (controls are "designed in"), and are therefore recommended over measures requiring considerable training and, especially, supervision, such as personal protective equipment or even administrative rotation [1].

Ventilation is a desirable and useful engineering control. Dilution ventilation reduces the air concentration of toxin in the entire work area by bringing in uncontaminated air with which it is diluted. Dilution ventilation is useful when the contaminant concentration or toxicity is fairly low, if the contaminant is released reasonably uniformly in the workroom, and if the worker(s) are somewhat removed in location from the process.

Otherwise, dilution ventilation is insufficient. Local exhaust ventilation is particularly necessary for close work with concentrated toxic materials.

Local exhaust ventilation (LEV) is most usefully designed so the contaminant does not have a chance to escape in quantity into the room air. When LEV is properly designed, other forms of protection, such as masks and/or respirators may not be necessary. The basic elements of LEV consist of a hood or hoods, ductwork, fan(s) and an air cleaning system [2].

Hoods preferably are designed to be enclosures encompassing the exhaust from the entire process. When this is not possible, the hood may be placed to receive or capture the bulk of the air flow from a process, and should be placed as close to the process as possible. Receiving hoods are placed so that the contaminant material will flow into them. Grinding wheel hoods and canopies over hot processes are receiving hoods. "Capture" hoods on the other hand must be designed so the ventilation system creates a strong enough flow field to entrain and capture the contaminant. LEV hood design will be reviewed in the next section.

The contaminant in air is removed through the ductwork to the air cleaning device by the fan. By creating in the ductwork a static pressure differential negative to the atmosphere, the specifically-chosen fan moves a quantity of air with a certain velocity. Ductwork and air cleaner design depend on the process employed, its temperature, the particle size and density of the material expelled, the toxicity thereof, and the cleaning efficiency required [Figure 1].

The air cleaning device removes the contaminant from the airstream brought to it by the ventilation system described above. Air is usually exhausted to the outside atmosphere through an exhaust stack once the particulates and toxins have been largely removed. Under certain circumstances, e.g., where atmospheric air would have to be excessively heated or otherwise conditioned, some proportion of exhaust air may be recirculated.

Designs of the LEV systems have remained fairly stagnant since World War II, partially because the older methods were seen as "adequate." Until the 1980s a relative lack of theoretical work was available which would affect system design concepts. The goal of such theoretical work is not only to understand better the fundamentals, but is also to provide workers with better protection for the engineering dollar spent.

FIGURE 1.

EXHAUST AIR SYSTEM

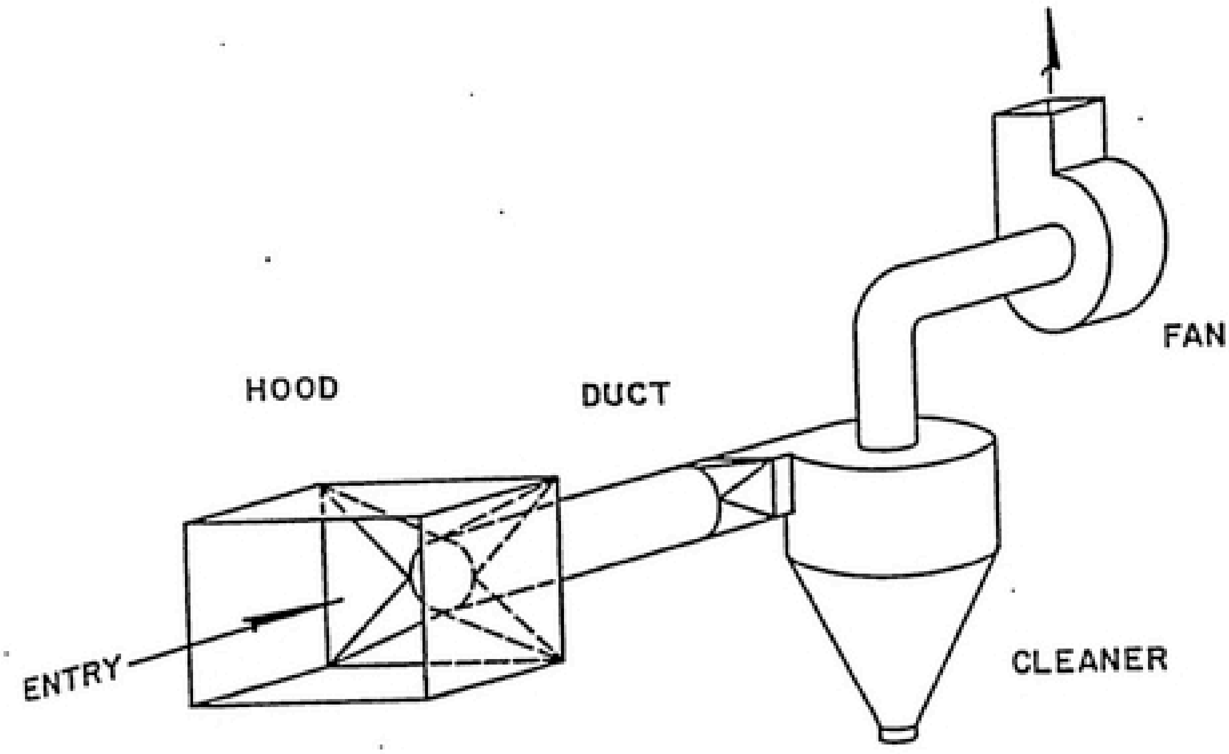

SOURCE: REFERENCE 3

II. LOCAL EXHAUST VENTILATION DESIGN

A. CAPTURE VELOCITY CONCEPTS

Many different configurations of hood designs are possible for control of the exhaust of every conceivable industrial process. Nonetheless there are a few standard designs that are used routinely, and which have been tested widely. Slots, rectangular and round openings are the most common; cabinets and booths are used to enclose whole processes, and canopies are placed over evaporative processes [Figure 2]. Traditionally, local exhaust ventilation designs relied on a single unifying concept, that of "capture velocity." The design equations developed by Dalla Valle and Silverman in the 1930s all rely on this design parameter, and it is the primary focus of designs still promulgated by the ACGIH, in their Industrial Ventilation Manual [3].

Velocity must be sufficient to entrain the contaminant in the airflow toward the hood so it does not disperse or settle out before being "captured" by the exhaust system. Particular processes generate contaminants of different characteristics (gaseous vs. particulate; light vs. heavy or dense particles; contaminants released with low or very high initial velocity). Each characteristic should contribute to the evaluation of the capture velocity necessary [Table 1]. Then the volumetric flow (Q) necessary may be calculated

FIGURE 2.

HOOD DESIGN TYPES

HOOD TYPE	DESCRIPTION	ASPECT RATIO $\frac{W}{L}$
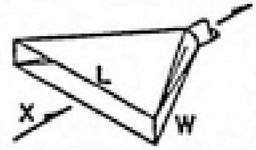	SLOT	0.2 OR LESS
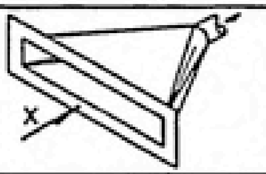	FLANGED SLOT	0.2 OR LESS
 A=WL (sq.ft.)	PLAIN OPENING	0.2 OR GREATER AND ROUND
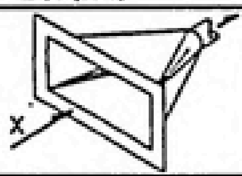	FLANGED OPENING	0.2 OR GREATER AND ROUND
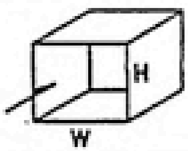	BOOTH	TO SUIT WORK
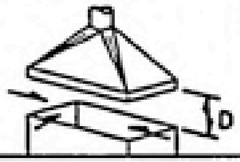	CANOPY	TO SUIT WORK

SOURCE: REFERENCE 3

TABLE 1.

CAPTURE VELOCITIES

Condition of Dispersion of Contaminant	Examples	Capture Velocity, fpm
Released with practically no velocity into quiet air.	Evaporation from tanks; degreasing, etc.	50-100
Released at low velocity into moderately still air.	Spray booths; intermittent container filling; low speed conveyor transfers; welding; plating; pickling	100-200
Active generation into zone of rapid air motion	Spray painting in shallow booths; barrel filling; conveyor loading; crushers	200-500
Released at high initial velocity into zone of very rapid air motion.	Grinding; abrasive blasting, tumbling	500-2000

In each category above, a range of capture velocity is shown. The proper choice of values depends on several factors:

Lower End of Range	Upper End of Range
1. Room air currents minimal or favorable to capture.	1. Disturbing room air currents.
2. Contaminants of low toxicity or of nuisance value only.	2. Contaminants of high toxicity.
3. Intermittent, low production.	3. High production, heavy use.
4. Large hood—large air mass in motion.	4. Small hood—local control only.

SOURCE: REFERENCE 3

easily, in conjunction with the use of a "VS Print" (a plan of a ventilation system typical for the process) taken from or adapted from the ACGIH Manual.

For standard hood configurations such as round or rectangular, flanged or unflanged hoods, Dalla Valle [4] developed the original "rule-of-thumb" equations. He mathematically related several variables he found to be characteristic of hood velocity values he measured at various locations in front of LEV hoods. In general Dalla Valle established the concept of the centerline velocity gradient as a function of distance from the hood (X), volume airflow (Q), and hood shape and flanging. He showed that the surfaces of equal velocity into an exhaust hood were of the same shape and relative position for all similarly shaped hoods. While he mistakenly equated equal velocity contours with equipotential surfaces, in alluding to potential theory as a possible basis for description of streamlines of airflow, he not only formed the basis for the capture velocity concept, but also paved the way for the theory which superceded it.

The use of a modified Pitot tube allowed Dalla Valle to map the equal velocity contours of various exhaust hoods [Figure 3]. A general equation was the result of his studies:

$$f(Y) = m/(X^n), \quad (1)$$

where: n = a constant: -1.91;

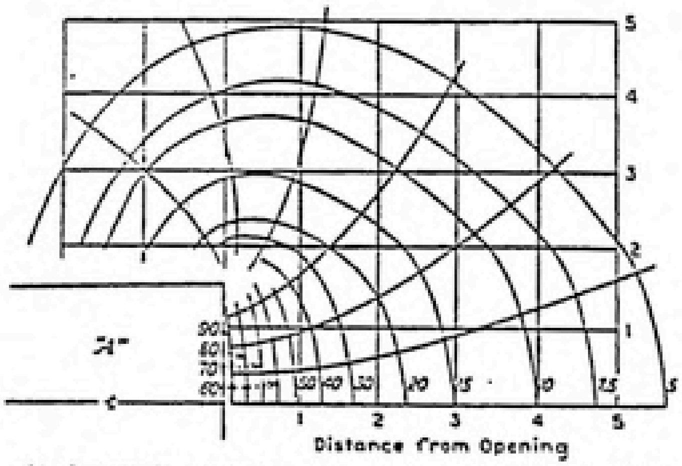

(A, Contours in center-plane, perpendicular to long side of opening.)

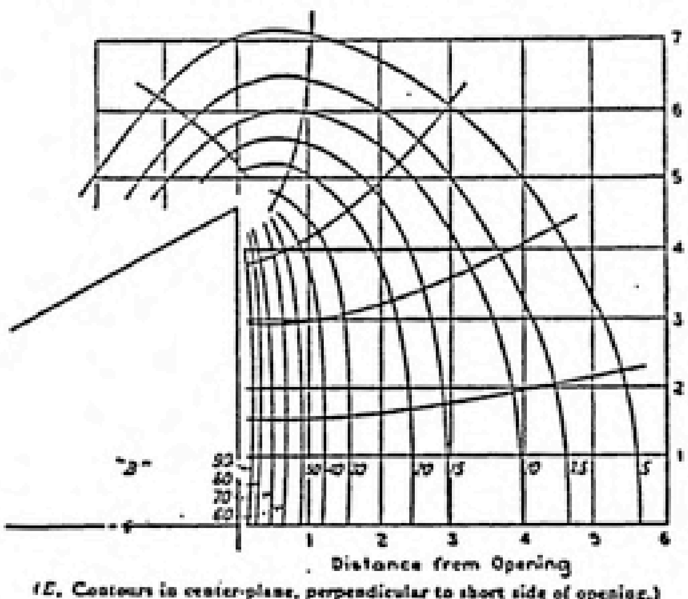

(B, Contours in center-plane, perpendicular to short side of opening.)

FIG. 3 VELOCITY CONTOURS FOR 3-INCH BY 9-INCH OPENING

SOURCE: REFERENCE 4

X = the horizontal distance from the hood along its centerline;

$m = bA^k$,

where: b depends on the aspect ratio of a rectangular hood, or = 0.0825 for round hoods;

A = the hood face area;

k = a constant: 1.04; and

f(Y) = the point velocity at X, as fraction of Y = the average face velocity.

Dalla Valle later simplified this model for round hoods, or rectangular hoods with aspect ratio (AR = width/length) greater than 0.2. This simplification has been rearranged in the Ventilation Manual as:

$$V = Q/(10X^2 + A), \qquad (2)$$

where: $X \leq 3/2\ D$;

D = the hood diameter or side length;

V = the air velocity in feet per minute (fpm);

Q = volume flow in cubic feet per minute (cfm).

Dalle Valle believed that flanges reduce the volume flow required by about 33% for the same required capture velocity, so the simplified (ACGIH) equation for flanged hoods became:

$$V = Q/[.75(10X^2 + A)], \qquad (3)$$

which Garrison [10] says is good for the region beyond about .4D away from the hood face.

Several years after Dalla Valle's work Silverman continued his investigations [5]. While he was unable to improve upon Dalla Valle's simple equations for round hoods and rectangular hoods of aspect ratios of >0.2, Silverman was able to provide handy equations for slots (defined as having AR ≤ 0.2). His empirical solutions were:

for unflanged: $$V = 23.8\ Q[(W+1)/W]/XL; \text{ and} \tag{4}$$

for flanged: $$V = 55.4\ Q/XL, \tag{5}$$

where: L = the length of the slot hood;

W = the width of the slot hood; and

X is defined as in the Dalla Valle equations.

These equations have been reduced and corrected in the ACGIH Ventilation Manual to the following:

for unflanged: $$V = Q/(3.7LX); \text{ and} \tag{6}$$

for flanged: $$V = Q/(2.6LX). \tag{7}$$

A much more extensive investigation of the effect of aspect ratio on the centerline velocity gradient was conducted by Fletcher [6]. For fixed volume flows and hood areas, the velocity at any given point X on the hood centerline increased as the AR decreased (became more slot-like). Fletcher developed an equation for unflanged slot hoods of AR's from 1:1 to 1:16 relating these variables, and then constructed a convenient nomogram [Figure 4]. Fletcher's equation is:

$$V/V_o = 1/(0.93 + 8.58a^2), \tag{8}$$

where: $a = [X/A^{.5}]\ [W/L]^{-B}$; and

$B = 0.2[X/A^{.5}]^{-1/3}$; and

V_o= hood face velocity; and

other variables are defined as before.

The effects of flanging on the centerline velocity were studied subsequently by Fletcher [7]. Because flanges cut down significantly on the volume flow necessary to produce a given centerline velocity, they increase the efficiency and decrease the cost of ventilation systems which use them [8]. He was able to demonstrate that the optimum flange width equalled the square root of the hood opening area, and the effect of the flange increases as the aspect ratio decreases (becomes more slot-like). An adjacent surface [9] likewise increases the centerline velocity of an exhaust hood by cutting down the air volume from which flow is drawn into the hood. Equal centerline velocities may be obtained in either case with the use of lower total volume flows.

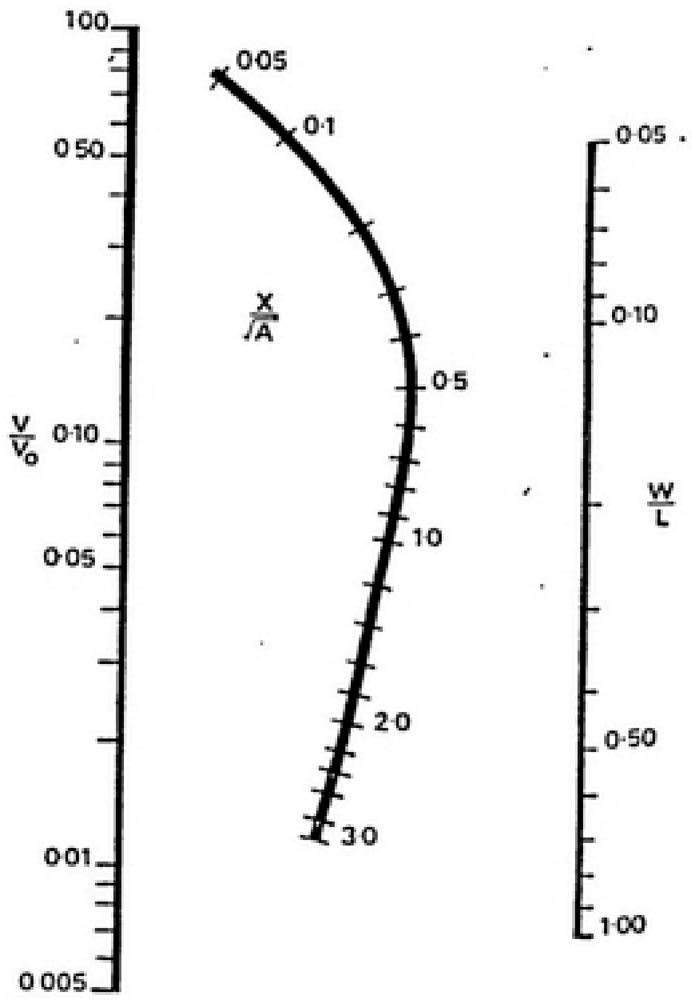

FIGURE 4.

HOOD FLOW NOMOGRAM

(FLETCHER)

SOURCE: REFERENCE 6

More recently, Garrison [10] has studied high velocity-low volume (HVLV) systems and compared the results to the work of Dalla Valle and followers. Generally, he found that the ACGIH Ventilation Manual equations were suitable, but disagreed that flanging added 33% to centerline velocity gradient values. He suggested that the actual increase is probably between 10 to 30%. Silverman's equations cannot be used very near the hood face, because as X approaches zero, V at X becomes indeterminate; Garrison suggests that a limit of accuracy of Silverman's equations (or their simplifications in the ACGIH Manual) is reached when centerline distance X to hood diameter or width ratios X/D or X/W = 0.4.

Garrison subsequently [11] conducted analyses of the relationship of non-dimensional velocity ratios to non-dimensional distance ratios for circular, rectangular and slot hoods, for flanged and unflanged cases, and for various aspect ratios. V, the centerline velocity at any given X distance, may be related in a ratio to the hood face velocity V_o: $Y = V/V_o$. Likewise, the centerline distance X may be related in a ratio to hood diameter D, rectangular hood width W, or slot hood length L: $X_{DW} = X/D$ or X/W or X/L. Then non-dimensional ratios Y and X_{DW} may be related to one another through empirically derived equations:

$$Y_{(\text{"near"})} = a(b)^{X_{DW}}; \text{ and} \tag{9}$$

$$Y_{(\text{"far"})} = a(X_{DW})^{b}, \tag{10}$$

where: a and b are empirical constants, which vary depending on hood characteristics.

Later, Garrison expanded his explorations to include other practice design concepts using various graphical techniques for a number of "real-world" situations [12]. Obstacles and surfaces frequently block ideal airflow streamlines, and methods such as sketching, conformal mapping, and velocity vector addition may assist in the evaluation of two-dimensional velocity gradients on the hood centerline [Table 2].

A great deal of work has been done, summarized briefly above, using capture velocity as the core theoretical concept upon which practical design of exhaust hoods, and analysis of exhaust hood flow, has been built. However, there are significant deficiencies therein.

Recently, a number of investigators have criticized the capture velocity concept. Heinson and Choi [13] have provided a good summary of the problems associated with this design method. It is as follows:

1) Contaminant concentration in the vicinity of the source cannot be predicted;

2) The effect of changes in design (such as system dimensions or volumetric flow) on the performance of a system cannot be estimated;

TABLE 2.

Empirical Design Data for Nondimensional Centerline Velocity Gradients

Nozzle End Shape	Nozzle Profile Shape	$Y = a(b)^{X_{ow}}$				$Y = a(X_{ow})^b$					Specific Y Values at X_{ow} =	
		$0 \leq X_{ow} < 0.5$		$0.5 \leq X_{ow} < 1.0$				$1.0 \leq X_{ow} \leq X_{ow_{max}}$				
		a	b	a	b	a	b	a	b	$X_{ow_{max}}$	0.5	1.0
Circular	Plain	110	0.06	--	--	8	-1.7	8	-1.7	1.5	26	8
	Flanged	110	0.07	--	--	10	-1.6	10	-1.6	1.5	30	10
	Flared	90	0.20	90	0.20	--	--	18	-1.7	2.0	40	18
	Rounded	98	0.50	145	0.23	--	--	33	-2.2	2.5	69	33
Square (WLR=1.0)	Plain	107	0.09	--	--	10	-1.7	10	-1.7	1.5	32	10
	Flanged	107	0.11	--	--	12	-1.6	12	-1.6	1.5	36	12
Rectangular (WLR=0.50)	Plain	107	0.14	--	--	18	-1.2	18	-1.7	2.0	41	18
	Flanged	107	0.17	--	--	21	-1.1	21	-1.6	2.0	45	21
Rectangular (WLR=0.25)	Plain	107	0.18	--	--	23	-1.0	23	-1.5	2.5	46	23
	Flanged	107	0.22	--	--	27	-0.9	27	-1.4	3.0	50	27
Narrow slot (WLR=0.10)	Plain	107	0.19	--	--	24	-1.0	24	-1.2	3.5	48	24
	Flanged	107	0.22	--	--	29	-0.8	29	-1.1	4.0	50	29

SOURCE: REFERENCE 12

3) Even though the performance of a particular system is known, the effect of geometrically scaling it up or down is unpredictable;

4) An engineer designing a system for a new process (one for which an LEV design does not appear in published literature) is left to design basically from scratch with little knowledge of the effectiveness of the resulting system;

5) The idea of providing a certain velocity to capture contaminants is inconsistent with the laws of fluid mechanics.

For example, Fletcher and Johnson [14] show that traditional design methods are adequate for gases and micron-sized particles released on the centerline of an LEV hood at low velocities. But, especially if the direction of release is away from the hood, if the release velocity is higher than a certain low amount (0.21 m/sec in a certain set of cases), higher "capture velocities" are required. Moreover, as Ellenbecker et al. [16] point out, crossdrafts and other air disturbances cannot be accounted for, energy expenditure optimization is difficult, and there are significant uncertainties in shaping the hood to distribute velocity contours for efficient capture in three dimensions. Only qualitative predictions of hood performance can be obtained using capture velocity concepts as the theoretical foundation.

B. CAPTURE EFFICIENCY CONCEPTS

Capture efficiency is a notion which may be used to evaluate hood performance comprehensively. It is useful because hood and system designs of all types may be compared effectively to one another, and the effects of changes in any design parameter may be evaluated along a single scale.

Dalla Valle was quite aware of the inadequacies of the theoretical approach in use at the time he was doing his original work. He states [4]: "Without attempting to minimize the importance of experience in engineering design, it seems proper to point out that most of the past experience in the design of local exhaust hoods has not been associated with quantitative studies of the actual efficiency of dust removal."

The first study using capture efficiency as the central concept for the evaluation of hoods was conducted by Burgess and Murrow [15]. Field conditions of contaminant generation from machining operations were modeled in the laboratory, and hood shape was demonstrated by the authors to be a primary factor in the efficiency of contaminant control.

Once the central concept underlying hood design changed, a new era in ventilation research began. However, a careful definition of the new parameter was required.

Capture efficiency, η, is defined by Ellenbecker, et al. [16] as "the fraction of the airborne contaminants generated by a source that is captured by the LEV system controlling it," or mathematically as:

$$\eta = G'/G \tag{11}$$

where: G' = the exhaust contaminant capture rate in grams per second (g/s), and

G = the contaminant generation rate, g/s.

The capture efficiency is a function of at least five variables:

- Q, the volume flow of the hood;
- A, the hood face area;
- X, the centerline distance of the hood to the source;
- V_c, the crossdraft velocity; and
- T, the temperature of the source.

When the temperature variable can be ignored, the others may be analysed more easily. It is found by application of the Buckingham π Theorem (see the relevant discussion later in this section) that the capture efficiency is related to a function of two (dimensionless) ratios: the crossdraft velocity to hood face velocity; and the centerline distance of source to hood divided by the square root of the hood area:

$$\eta = K(V_c/V_o)^a \, (X/\sqrt{A})^b \tag{12}$$

The specific functional variable (K) and exponents (a, b) defining the relationship are determined by experiment.

The limiting conditions which apply are:

$$\eta = 0 \text{ when } X \rightarrow \infty; \tag{13}$$

$$\eta = 0 \text{ when } V_o = 0; \tag{14}$$

$$\eta = 0 \text{ when } V_c \rightarrow \infty; \tag{15}$$

$$\eta = 1 \text{ when } X = 0; \tag{16}$$

$$\eta = 1 \text{ when } V_c = 0. \tag{17}$$

Actual measurement of capture efficiency in the laboratory entails direct measurement of contaminant concentrations in the duct of the exhaust hood. One must assure good mixing within the hood's duct. Direct measurement is made in the duct of the exhaust hood for the contaminant concentration. The source is placed just within the hood itself, to obtain the "100%" value. Then, the source is placed at various distances X away from the hood. The latter contaminant concentration values are compared at every time interval measured with the 100% value, and the ratio of the two is capture efficiency.

A subsequent paper by Flynn and Ellenbecker [17] offered an analytically detailed approach to capture efficiency, specifically to flanged circular exhaust hoods (FCH). Their approach was based on the intuitive idea that capture efficiency depends upon the interaction of three flow fields: 1) that generated by the hood; 2) the flow field generated by the contaminant source; and 3) the flow field due to perturbing crossdrafts [Figure 5]. It is the interactions of these flow fields that ultimately determine whether a contaminant enters the exhaust hood. Velocity vector average values were determined for each field by mathematical functions; in addition they accounted for some degree of variability about these averages due to turbulence.

In their model, Flynn and Ellenbecker calculated by vector addition the path of streamlines of a contaminant issuing in all directions from a point source, as they were affected by the flow fields of the hood, and by a crossdraft. They based their model on the modified potential flow solution for airflow into flanged circular hoods [18].

The cylindrical coordinate system is assumed in this model such that the FCH centerline is the Z-axis. The crossdraft is assumed to blow at velocity V_c perpendicular to the Z-axis, from the $\theta = 180°$ to the $\theta = 0°$ half-planes. The model assumes irrotational incompressible air flow, Q. A series of point sources of isothermal nonbouyant gas release at flow volume Q_s, at some point (at distance Z) from the FCH. Flynn and Ellenbecker developed a computer model for the IBM XT personal computer [17] which maps the streamlines for the contaminant flow. It displays a visual plot of a semicircle of point-source streamlines, as they

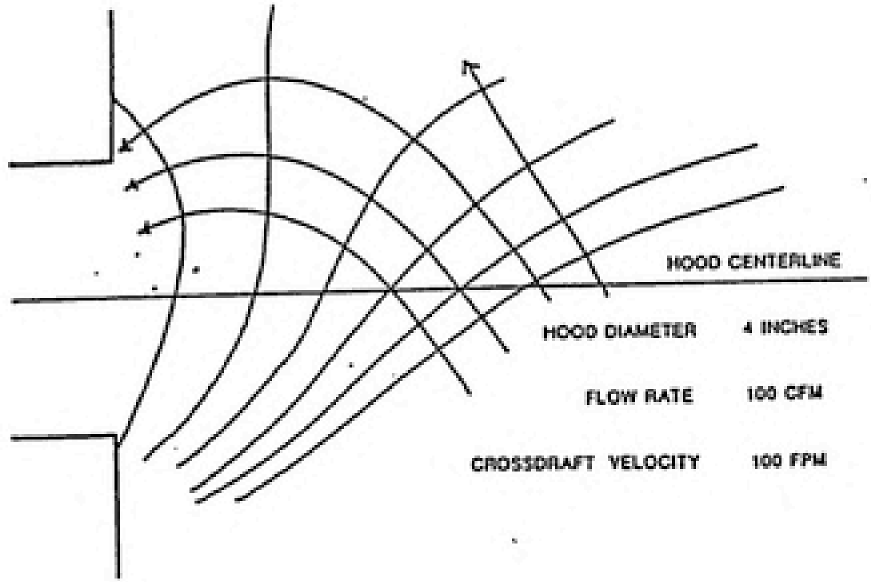

Figure 5 — Theoretical potential lines and streamlines for a flanged circular hood operating in the presence of a crossdraft perpendicular to the hood centerline.

SOURCE: REFERENCE 18

exist in the plane of the Z axis, and shows whether or not, when under the combined influence of the hood flow and crossdraft flow, they enter the FCH [Figure 6].

Previously developed similar models include Fialkovskaya's simplified point-sink model in which he described equations for the streamline which would just enter a hood in the presence of a cross-draft [19], and Strauss' modified n-sinks model allowing iterative processing [20]. Empirical studies have validated Flynn and Ellenbecker's "Final Model" [21]; their work recently has been extended to mathematical analysis and quantitative evaluation of potential flow modeling for hoods of other configurations [22].

To calculate capture efficiencies in such systems, one must apply the Buckingham π theorem. The π stands for the Product of variables. Each π is a dimensionless group of variables formed by application of the theorem. The theorem assures that for a process depending on n dimensional variables, then a reduction to k dimensionless variables is possible, where $n-k = j$, where j is the maximum number of variables which do not form a π among themselves. The reduction number j is always less than or equal to the number of dimensions (time, length, mass, temperature), m, in the n descriptive variables. The choice of the n dimensional variables is critical; if one is inadvertently omitted, then the analysis will be incorrect.

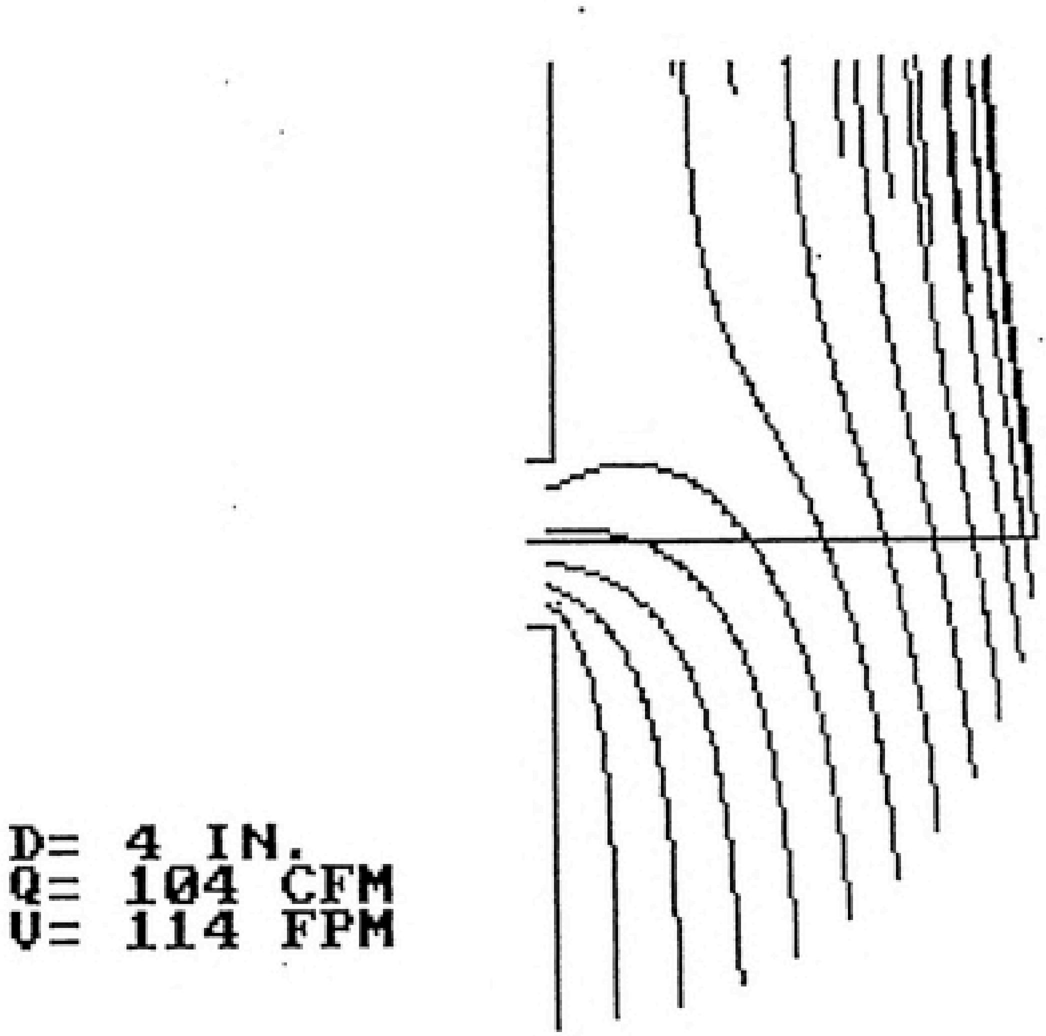

FIGURE 6.

IDEALIZED CONTAMINANT STREAMLINES

SOURCE: REFERENCE 21

In the capture efficiency analysis, each of the following variables:

D = diameter of the hood;

Z = distance to the point of origin;

Q = the volume flow of the hood in cfm; and

V_c= the velocity of the crossdraft,

must be considered. Application of the Buckingham π theorem suggests that one dimensionless group will be [Z/D], and the second will be $[V_f/V_c]$, where the hood face velocity is extracted from the hood flow variable. A third dimensionless group, $[Q_s/Q]$ will appear when the contaminant source flow $[Q_s]$ is considered with the other variables.

However, the functional relationship between the π's cannot be specified explicitly without experiment. The [Z/D] is the ratio of the hood-source distance to the diameter of the hood. It will have a profound effect on capture efficiency. Near the hood, most of the source of flow will be captured by the hood's flow field; if the source is far away the hood's field is weak. The second group $[V_f/V_c]$ is the ratio of face velocity to that of the crossdraft. The weaker the crossdraft, the less distorted are the effects of the hood and its flow field. Similarly with $[Q_s/Q]$, the hood flow field will have predominance over a contaminant source with a low flow rate.

The use of plotted streamlines from the source to the hood is important; each streamline either does or does not enter the hood. Thus whatever proportion of multiple streamlines enter the hood defines the capture efficiency for that particular set of conditions [Figure 6].

Alternatively, when a single streamline is calculated from a point source, it may be seen statistically as the first moment of distribution of the flow from that source; turbulence and dispersion are assumed to be equally distributed around such a streamline. When such a streamline hits the edge of the hood, half the flow is assumed captured and half is not. The distance Z from the hood to the contaminant source then forms a dimensionless ratio with the hood diameter D; and at the point of probable 50% capture, is designated $[Z/D]_{50}$, the "critical distance." It is assumed that turbulence is primarily accounted for by the $[V_f/V_c]$ ratio; it is used as a predictor for the effects of turbulent diffusion on contaminant dispersion around the streamline. The computer model can be used iteratively to obtain the $[Z/D]_{50}$ for any given combination of other variables. Then one determines the regression between the π groups.

III. BACKGROUND TO THE COMPUTER MODEL

A. ELEMENTS OF POTENTIAL THEORY

Since Flynn and Ellenbecker's model [17, 21] is based on the potential flow solution [18], they are assuming that the airflow into the exhaust hood is incompressible and irrotational. Moreover, in potential flow, frictional forces are negligible, so that inviscid flow is assumed. Laplace's equation:

$$\nabla^2 \phi = 0 \tag{18}$$

is used to describe such a flow field.

Laplace's equation is derived from the continuity equation:

$$[\partial\rho/\partial t] + \nabla \cdot (\rho \vec{v}) = 0 \tag{19}$$

where: ρ = the fluid density;

t = the elapsed time;

∇ = del, the gradient operator; and

$\vec{v}$ = the velocity vector.

The continuity equation is the summary of conservation of mass requirements in fluid mechanics. Continuity is said to exist wherever the volume flow, Q, equals the area of any hypothetical velocity contour surface times the velocity magnitude through that surface.

Incompressibility of a fluid means that density changes are negligible, so the first term drops out, and the continuity equation becomes:

$$\nabla \cdot \vec{v} = 0, \qquad (20)$$

and it is said that the "divergence" of the velocity field is zero. "Divergence" is a measure comparing flow into and out of a defined differentially small control volume in space. When it is zero, all fluid flowing into such a volume leaves at the same rate. The velocity field then is neither converging (volume shrinking with increasing density) nor diverging (getting larger with decreasing density). About 330 ft/sec is the upper velocity limit for incompressible flow of standard air.

The gradient operator, ∇, can be written out as:

$$\nabla(\ ) = [\partial(\ )/\partial x]\vec{i} + [\partial(\ )/\partial y]\vec{j} + [\partial(\ )/\partial z]\vec{k} \qquad (21)$$

in a three dimensional (x, y, z) coordinate system. The gradient operator converts a scalar to a vector function, and when solved gives the direction and maximum rate of increase of the function.

An irrotational fluid flow has no vorticity or "curl." In the mathematical description of an irrotational fluid, the cross-product of the gradient operator and the velocity vector function must always equal zero:

$$\nabla \times \vec{v} = 0 \qquad (22)$$

because the angular momentum of an irrotational flow is zero.

From this it follows directly (partly by definition) that the velocity vector function is the gradient of a "potential" function:

$$\vec{v} = \nabla \Phi \tag{23}$$

where Φ is the (scalar) potential function. Substituting equation (23) into equation (20) yields Laplace's equation (18).

The "potential" function, Φ, is defined for every point in space (x, y, z) as "the sum of the potential of the extraneous impulsive forces by which the actual motion at any instant could be produced instantaneously from rest" [27]. The potential function may be analysed as the product of time and force, divided by area and density: $tF/A\rho$; simplified, the units are usually cm^2/sec.

Viscous forces are negligible in potential flow. Inviscid flow occurs where no solid surfaces exist over which boundary layers would form. It is assumed in the strict potential flow model for FCH's that all hood flow is potential flow. This simplifying assumption yields results which are inaccurate only at points close to the hood face.

Using the assumptions of potential flow, and within certain boundary conditions, one can use Laplace's equation to define the velocity flow field. Boundary conditions are discussed in the next section.

B. POTENTIAL FLOW SOLUTIONS FOR FLANGED CIRCULAR HOODS

The potential flow solution is described in detail in Flynn and Ellenbecker's original papers [18, 21]. The potential flow model for the FCH was developed because it is amenable to practical application, in contrast to the more accurate, but difficult, constant velocity analytic solutions of Lamb [27] and Drkal [28].

In contrast to centerline velocity gradient studies, potential flow solutions describe the velocity field of airflow into the hood in three dimensions. This is particularly useful and important where sources are not on the centerline, where there is significant dispersion, where the direction of contaminant generation is not directly toward the hood face, or where there is a crossdraft.

Boundary conditions and simplifying assumptions for the potential flow model for the FCH are:

1) an infinite flange;

2) no flow through the flange: $\partial\Phi/\partial z = 0$, for the conditions $z = 0$, $r > a$, where a = the hood radius;

3) constant potential, Φ, at the hood face; and

4) $\Phi \rightarrow 0$, as $X \rightarrow \infty$.

The strict potential flow solution however, is not entirely adequate. The assumptions of inviscid, irrotational flow begin to break down in the region near the flange and the hood face, because of the increasing importance of shear stress due to turbulence of the boundary layer, and vena contracta formation. Real centerline velocities at the hood face are about twice the predicted value. Additionally, the strict potential flow solution predicts infinite velocity along the edge of the hood. However, turbulence there considerably reduces actual air velocity.

To address these anomalies in the theory, Flynn and Ellenbecker noted that Dalla Valle's equal velocity contours are elliptical. They make the assumption that the velocity vector field is uniform everywhere along each confocal ellipsoid equipotential surface provided by the theory. (In reality, the velocity field is the gradient of the potential.) For their modified potential flow solutions, a set of conditions, similar to the boundary conditions for the strict solution, apply, with the exception that in addition the hood face velocity is constant. The derived expression for velocity at every point in the field is then reasonably consistent with experiment. Additionally, because Laplace's equation is linear, other potential flows may be added vectorially at any given point. Thus, crossdraft effects and source vectors can be added to affect the velocity vector field of the hood.

In the validation of their solution [21], Flynn and Ellenbecker considered three versions of their model. The first was the strict potential flow solution. The second was the modification just discussed. They distinguish between an "inconsistent" model and one which contains a singularity. While "an inconsistent model is one that is not exact mathematically, a singularity refers to a region where unrealistic fluid behavior occurs." Thus while Model 1 is a consistent model, it is also a singular one. Model 2, however, is inconsistent due to the "inexact" approximation made to obtain it. The modified velocity field equation cannot be integrated to give the true Q; for example, the theoretical (Model 2) average face velocity is 87% of the true value.

Flynn and Ellenbecker's Final Model employed a radial correction factor C_r, a strong function of the eccentricity, where: $C_r = 2.6\ \epsilon^{18} + 0.853$. The eccentricity, ϵ, is the ratio of the hood diameter to the sum of the distances from the edges of the hood opening to the point in question:

$$\epsilon = \frac{2\ a}{(\Gamma_1 + \Gamma_2)}\ . \tag{24}$$

Here, $\Gamma_1 = \sqrt{[z^2+(a^2+r^2)]}$, and $\Gamma_2 = \sqrt{[z^2+(a^2-r^2)]}$. The radial correction was necessary because the radial velocity as measured increased more rapidly than predicted as the eccentricity approached 1 (i.e. near the hood face).

Additionally, the theoretical axial velocity calculations were also adjusted, by a factor of 0.9, based on the graphical results of the validation experiments. These empirical corrections were an attempt to overcome the mathematical inconsistency previously discussed.

The modified potential flow solution calculates the velocity at any point in the hood coordinate system (R, Θ', Z) as:

$$V_{T2} = \frac{\sqrt{3}\ Q\ \epsilon^2}{2\ \pi\ a^2\ \sqrt{(3-2\epsilon^2)}}\ . \qquad (25)$$

The Final Model component velocity vectors are:

$$V_R = -C_r\ V_{T2}\ (\sin\beta);\ \text{and} \qquad (26)$$

$$V_Z = -0.9\ V_{T2}\ (\cos\beta); \qquad (27)$$

where: $$\beta = \tan^{-1}(V_{R1}/V_{Z1}),\ \text{and} \qquad (28)$$

where V_{R1} and V_{Z1} are calculated as defined in both papers [18, 21].

The Final Model was incorporated into an interactive BASIC program, which required the input of three variables:

D = the hood diameter in inches;

Q = the hood flow in cubic feet per minute, cfm;

V_c= the crossdraft velocity, feet per minute, fpm.

The output for one of the possible combinations of these variables is seen in [Figure 6]. Through this program it is possible to "define the regions under control of the hood, and those that are dominated by the crossdraft." Some level of control will be exerted over contaminant processes located in those regions from which the streamlines are drawn into the hood. The program just described forms the basis of both the experiments and program modifications for this thesis; the contaminant source will be a jet.

C. CIRCULAR JET FLOW AND THE SCHLICHTING EQUATIONS

An ideal circular jet of fluid, flowing into a still medium, maintains constant static pressure throughout itself. However, the flow, Q, the area, A, and the jet width, b, are not at all constant; they are continually increasing with the entrainment of the surrounding air [Figure 7]. Its energy losses are likewise proportional to jet length, almost entirely in kinetic energy (i.e. in velocity) [Figure 8]. The momenta of external forces on a jet entering still air sum to zero, so the momentum of the mass flow of air (kinematic momentum) throughout such a jet remains constant [19].

The kinematic momentum, K, can be calculated for a jet of known flow. Since, in cylindrical coordinates

$$K = 2\pi \int_{o}^{\infty} V_z^2 \, r \, dr, \tag{29}$$

where: V_z = velocity in the axial direction of the jet, and

r = the radius of the jet flow at z; and

since at $z = 0$, V_z is not a function of r, then simple integration will yield:

$$K = \pi r^2 \, V_z^2 = QV_z, \tag{30}$$

Fig. 7. Pattern of streamlines in a circular, turbulent free jet

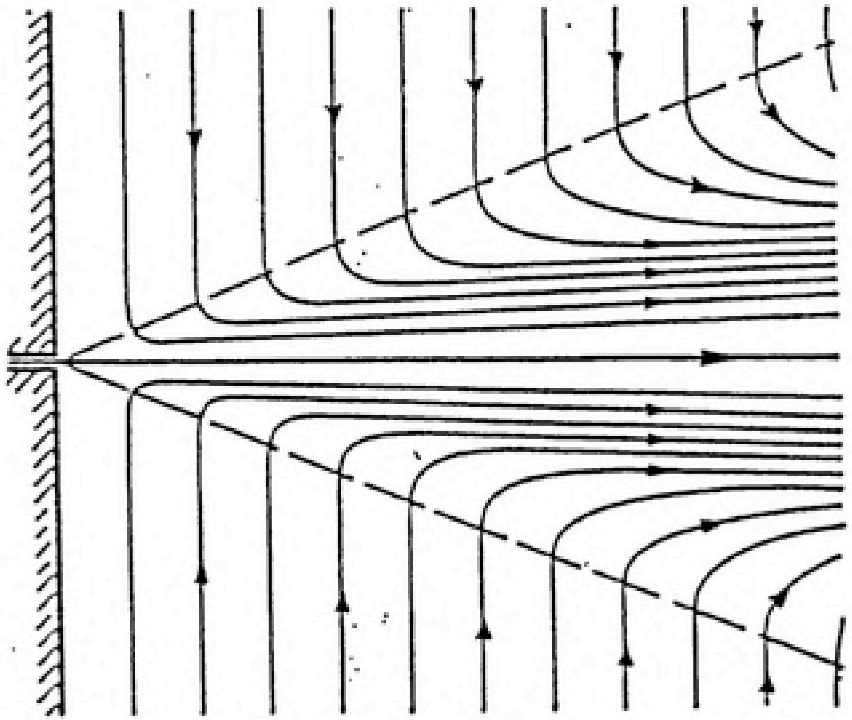

SOURCE: REFERENCE 23

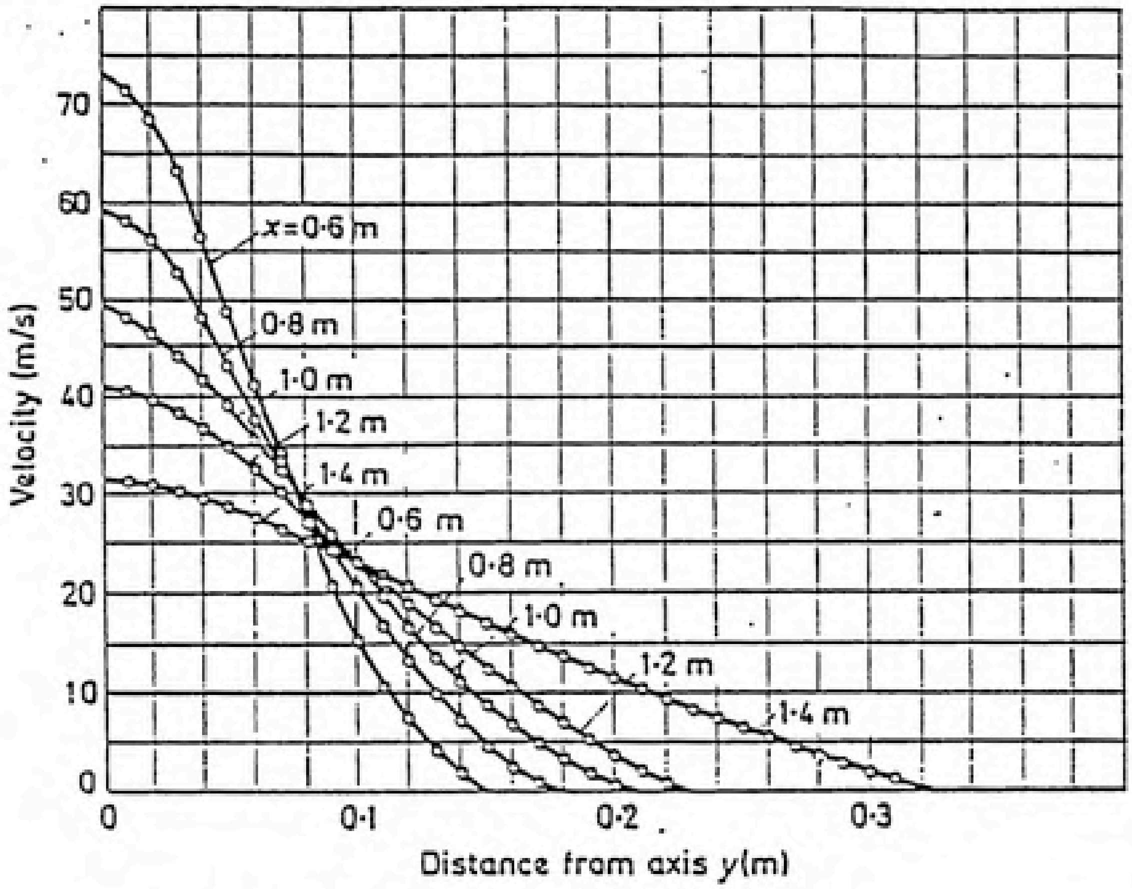

FIG. 8. Velocity profiles for axisymmetric jet.

SOURCE: REFERENCE 23

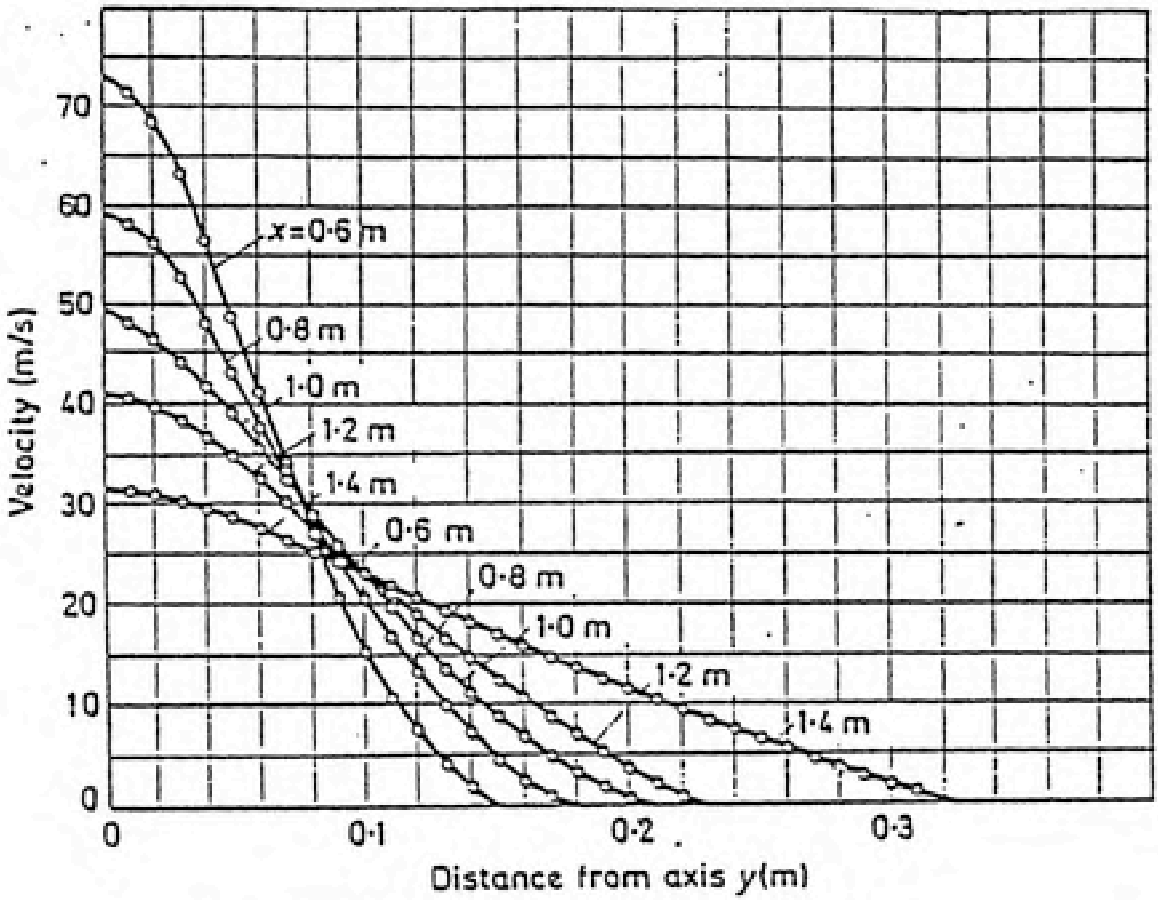

FIG. 8. Velocity profiles for axisymmetric jet.

SOURCE: REFERENCE 23

since flow equals the product of area and velocity. For any given jet flow, Q, and starting velocity, V, we can thus calculate K.

The spread of a circular jet can be described [23] as beginning at a single point ("pole" or "virtual point") [Figure 9]. Experimentally, it has been discovered that for a cylindrical jet the virtual point is located 1.86 times the jet opening diameter, inside its opening [19]. It is there that the flow calculations must begin. See the program, located in the Appendix.

Lines drawn from the virtual point through the orifice edges then extend outward such that they form the boundary of the mixing zone. With increasing distance from the origin, the material in the jet core becomes diffused by mixture with the surrounding air. In the core (in the "initial section"), the velocity profile remains square, and the temperature and concentration remain constant. The core tapers. In the "main section," the velocity profile widens and flattens. Throughout, the velocity profiles are symmetric, and similar.

Turbulent jet flow is characterized by a cross-transfer of vortices, and as these move beyond the limits of the jet, impart their momentum to surrounding layers of air. Successive cone-shaped layers of air are entrained in the jet motion. This incorporation retards the boundary layer. The thickness of the turbulent boundary zone increases with the increasing distance from the jet source, until from the

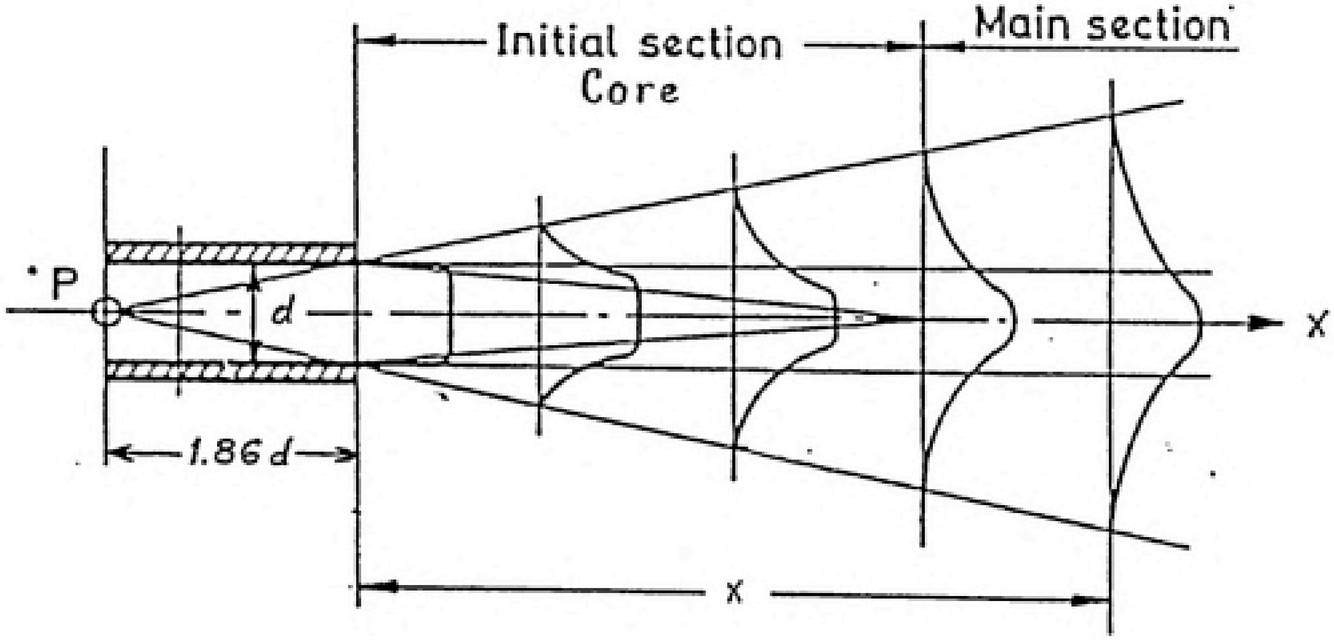

FIG. 9. Axisymmetric jet.

SOURCE: REFERENCE 19

entire periphery it "meets itself" on the axis of the jet [Figure 9]. In the main section of the jet, the entire flow is turbulent.

In a circular jet, the amount of turbulent shear stress associated with the boundary layer can be analyzed by Prandtl's modified mixing length theory. To visualize a physical interpretation of "mixing length" one must use a simple model of turbulent flow of a jet along a wall [Figure 10]. This is the simplest case of parallel flow, in which velocity is assumed to vary only from streamline to streamline. As the flow progresses and turbulent mixing zones move longitudinally, they also may move transversely, while retaining their momentum.

Prandtl's mixing length, l, is defined as "that (transverse) distance which must be covered by an agglomeration of fluid particles, travelling with its original velocity, in order to make the difference between its velocity and the velocity in the new lamina equal to the mean transverse fluctuation in turbulent flow" [23].

The overall variations in the velocity contours of the jet are controlled by this transverse movement of turbulence eddies. The thickness and rate of motion of the mixing layers is a critical determinant in the calculation of the magnitude and direction of the velocity vectors at any given point in the jet.

The difference in forward velocity, between the laminae defining lateral movement, is related quantitatively to the

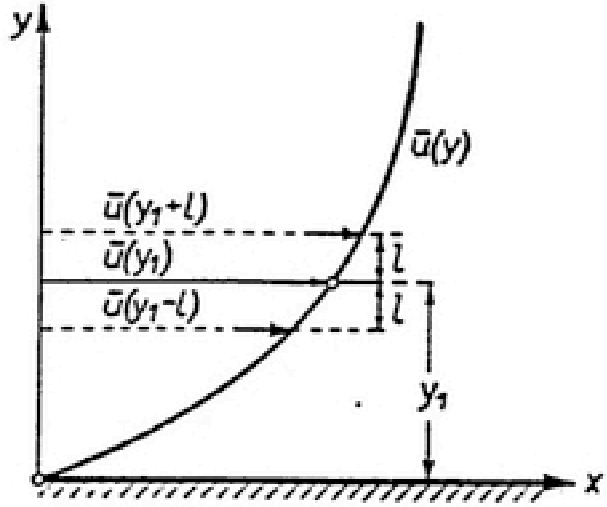

Fig. 10. Explanation of the mixing-length concept

SOURCE: REFERENCE 23

extent of lateral movement. Prandtl's mixing length hypothesis combines the equation describing this relation, with the equation for the shearing stress of the turbulent flow, and obtains an equation hypothetically describing the turbulent shear stress, τ_t, in terms of:

ρ = the density of the flowing medium;

l = the thickness of the laminae defining lateral movement; and

$d\bar{u}/dy$ = the rate of change of mean velocity between laminae:

$$\tau_t = \rho\ l^2\ |d\bar{u}/dy|\ d\bar{u}/dy, \tag{31}$$

where the absolute value operator is to ensure the proper sign of the result. Equation 31 is the formal definition of Prandtl's mixing length hypothesis.

Turbulent flow contains both time-average (mean) motions, and fluctuating (eddying) motions, in all three directions. Over a sufficient length of time, the time-average of all the eddying motions sum to zero. However, these fluctuations influence the mean motion such that the mean motion exhibits an apparent increase in resistance to deformation: the apparent (or virtual) viscosity, or "eddy viscosity." A mixing coefficient has been introduced in the fluid dynamics literature, A_τ, for this Reynolds stress of turbulent flow. It is analogous to the Stokes coefficient of viscosity for laminar flow, μ_1, and it likewise relates the (turbulent) shear stress to the velocity gradient:

$\tau_t = A_\tau\, d\bar{u}/dy$. It is not, however, a fluid property like the coefficient of viscosity, and its value depends on the mean fluid velocity. The apparent *kinematic* viscosity, ϵ_τ, is likewise analogous to the derivation of kinematic viscosity of laminar flow, v_1, and is defined as the mixing coefficient divided by the fluid density.

In order to cure a theoretical defect in the calculation of the apparent kinematic viscosity, ϵ_τ, based on Equation 31 and its assumptions, Prandtl modified its derivation. The modification is valid only in free turbulent flow, and is derived from extensive experimental data. The original hypothesis had assumed that the volumes of fluid moving transversely during turbulent mixing had diameters very small compared to the transverse dimensions of the movement. The modified hypothesis [23] assumes the diameters of the transversely-moving volumes of fluid are of the same order of magnitude as that of the mixing zone. "The virtual kinematic (eddy) viscosity, ϵ_τ, is now formed by multiplying the maximum difference in the time-mean flow velocity with a length which is assumed to be proportional to the width, b, of the mixing zone":

$$\epsilon_\tau = x_1\, b\, (\bar{u}_{max} - \bar{u}_{min}), \tag{32}$$

where x_1 is a dimensionless experimentally-derived constant; with this treatment, ϵ_τ remains constant throughout the width of every cross-section of flow. Due to the direct proportionality of length and width of the jet, and the simple inverse proportionality thereof to velocity, the virtual kinematic viscosity of turbulent flow, ϵ_T, becomes a constant, ϵ_o, over the entire length of the jet.

As a result, the velocity distribution differential equations become formally similar to those of laminar jets; only the term therein for kinematic viscosity of laminar flow (v_1) needs to be replaced by that for the virtual kinematic viscosity (ϵ_o) of turbulent flow.

To calculate the vector equations, one must know how to calculate ϵ_o. According to measurements by Reichardt [referenced in 23], the half-width, $b_{½}$, of a circular turbulent jet at the point where V_z = one-half the maximum centerline velocity, is given by:

$$b_{\frac{1}{2}} = 0.0848\ z, \tag{33}$$

where: z = the distance from the nozzle.

Reichardt's measurements also yielded an equation:

$$b_{\frac{1}{2}} = (5.27\ z\ \epsilon_o) / \sqrt{K} \tag{34}$$

that can be used in conjunction with the previous one, such that for any given value of z, and with K determined as previously discussed, ϵ_o, the virtual or apparent kinematic ("eddy") viscosity can be directly calculated.

In summary, given a few fairly reasonable simplifying assumptions, it is possible to calculate two critical characteristics of the flow of a circular turbulent jet. The kinematic momentum, K, and the eddy viscosity, ϵ_o, are calculated by knowing: 1) the flow, Q, and initial velocity, V; and 2) the axial distance, z, of any particular point in the jet.

As alluded to earlier, there is formal similarity of the equations for the velocity vectors of turbulent flow with those of laminar flow. For a turbulent jet, V_z is the magnitude of the velocity vector in the direction of the jet axis (z):

$$V_z = \frac{3K}{8\ \pi\ \epsilon_o\ z\ [1+.25\eta^2]^2}\ \text{, and} \tag{35}$$

V_r is the magnitude of the velocity vector in the radial direction (r):

$$V_r = \frac{\sqrt{3K}\ \ [\eta-.25\eta^3]}{4\ \sqrt{\pi}\ z\ [1+.25\eta^2]^2}\ , \tag{36}$$

where in either case:

$$\eta = \frac{r\ \sqrt{3K}}{4\ \sqrt{\pi}\ \epsilon_o\ z}. \tag{37}$$

Reichardt evaluated this model by comparing the predicted velocity distribution of a circular turbulent jet with the distribution of experimentally-determined velocity values, for three different axial distances [Figure 11]. The axes of Figure 11 are in dimensionless ratios. There is impressive correspondence between the experimental findings and the model predictions.

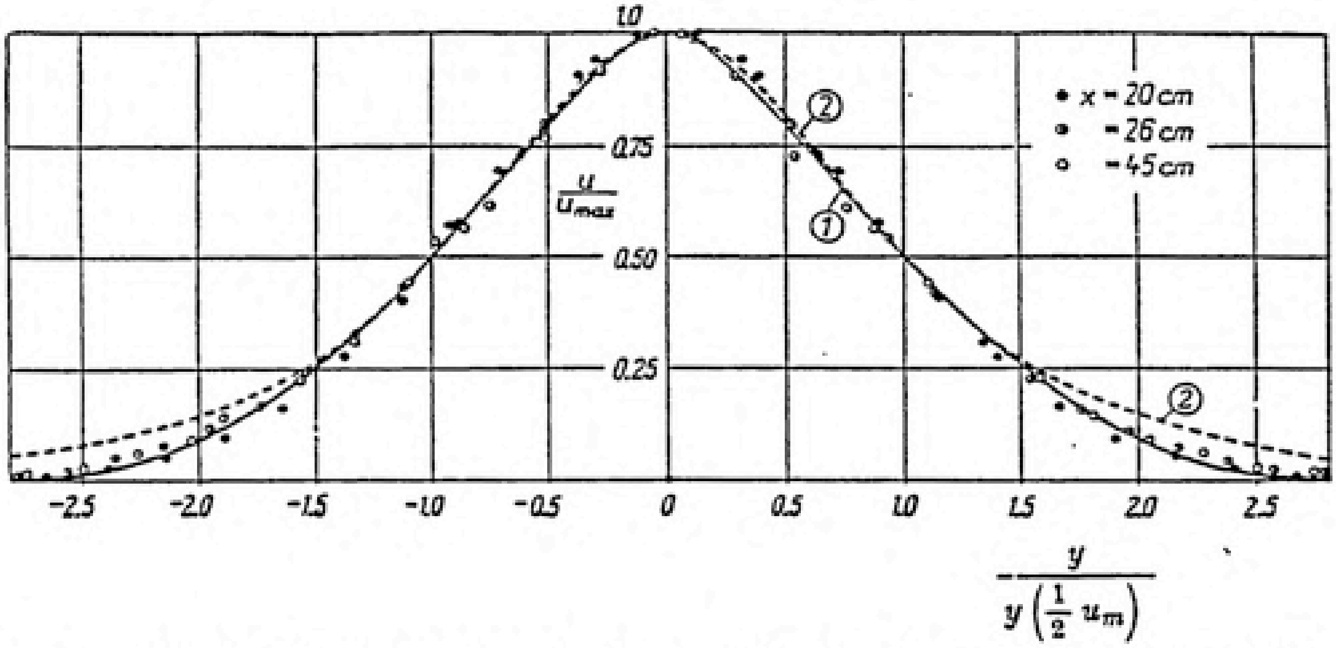

Fig. 11. Velocity distribution in a circular, turbulent jet. Measurements due to Reichardt

SOURCE: REFERENCE 23

IV. PURPOSE AND OBJECTIVES

The purpose of this work is to validate a computer model that predicts the streamline that a jet of gaseous contaminant will follow in the flow field of a flanged circular hood. These studies will assist in developing reliable estimates of breathing zone concentrations of gaseous or other jets of workplace contaminants.

The objectives of this research are:

1. To write a new interactive computer program to describe the flow of a circular turbulent contaminant jet within the flow field of a flanged circular exhaust hood. This is accomplished by combining a modified BASIC computer program from Flynn and Ellenbecker [21], for the validated potential flow solution for airflow into a flanged circular hood, with the appropriate expressions for the velocity vectors of the flow of a circular jet;

2. To run the program for a matrix of hood and jet flows, and distance values of the jet from the hood face, to create predictions of the specific hood centerline locations of the jet, $[Z/D]_{50}$, at which half of the jet flow would be captured by the exhaust hood; and

3. To perform replicate laboratory experiments for each combination of hood and jet flows and distances, to determine actual $[Z/D]_{50}$ values for each, and to compare the results statistically with the predictions.

A basic premise of potential theory is that of a free field, in which there is unbounded, unobstructed flow. Inviscid flow may be assumed, and this assumption allows the neglect of friction. The use of strict potential theory in the description of hood flow yields an analysis in which the gradient of potential (the magnitude of velocity vectors) varies strongly along the confocal ellipsoids of equal potential. For the modified potential flow solution, a simplifying assumption is made [18], equivalent to Dalle Valle's original error. It is that the equal velocity contours found in experimental work are equivalent to the equipotential confocal ellipsoidal surfaces described in potential flow field theory. This simplification, with appropriate correction factors [21], yields a quite accurate descriptive model of an unobstructed FCH flow field.

When plumes of jet contaminant are introduced, an appropriate jet-flow theory must be used. The Prandtl mixing-length hypothesis for turbulent jet flow, which assumes a constant virtual kinematic viscosity, and yields a constant kinematic momentum, seems to be applicable; viscosity is an important consideration in its derivation. The Schlichting equations calculate the velocity vectors of any given point in the flow field of the jet. It is assumed that each of these vector components can be added to those velocity vector quantities calculated for each corresponding point along streamlines of the flow field of the hood. Vector additions are made iteratively at desired increments, to obtain the entire combined streamline.

This model of combined flow is validated experimentally. Computer predictions are made of the specific locations along the hood centerline of the jet, such that a 50% capture efficiency is achieved by the hood. This is necessary to determine if the velocity vectors of the two parts of this model, one (for the hood flow) which ignores viscosity, and the other (for the jet) which assumes its significance, can be added together to predict jetstream trajectory while in the flow field of the hood. If so, then the entire field of points of actual jet location can be mapped such that the capture efficiency of the hood is at least 50%.

V. METHODS

A. COMPUTER MODEL

The computer model is composed of the union of two parts, with accompanying reminders, explanatory notes, and instructions for graphic display and printouts. The two parts of the computer model are: 1) those that describe and calculate the flow field of the flanged circular exhaust hood; and 2) those that describe and calculate the flow of a free turbulent gas jet. Each of these parts of the overall program calculates the vector magnitude and direction of velocity in its own cylindrical coordinate system. These are denoted as (r, Θ, z) for the jet, and (R, Θ', Z) for the hood.

The jet is arranged in relation to the hood such that its tip is in front of the hood on the hood centerline, and the jet centerline (z) axis is perpendicular to the centerline (Z) axis of the hood. The "base plane," in which all calculations are done, is the plane of the two (hood and jet) centerlines.

Vector transformations are contingent upon the original orientation of the jet to the hood. The hood's R directional axis for calculation purposes was in the half-plane of the base plane in the direction of original jet flow. Additionally, only the r-vector of the jet in the base plane was considered for calculation purposes. Due to the specific arrangement of jet to hood axes chosen, there was no θ component (rotation out of the base plane) to be considered for either jet or hood. In the base plane, r- and z-direction vector magnitudes of the jet were transformed into the coordinate system of the hood, prior to the calculation of their combined magnitude. They were also calculated to account for the distance of the virtual point, within the tip of the jet tube, from the tip of the jet nozzle.

In order to account for the effects of the flange of the hood on the flow of the jet, use is made in the computer program of an image jet located "behind" the flange, the vector calculations for which are assumed to be equal and opposite to its real counterpart. It is necessary for the proper calculation of the velocity vectors of jet flow. Any given velocity vector for the real jet equals the scalar sum of the corresponding velocity vectors of both the real and imaginary jets. Thus, when combined, jet velocity vectors will be calculated to yield streamlines which follow a path which "sees" the barrier the flange presents.

The velocity vectors of the hood and jet flows are iteratively calculated and added (once transformed to the same coordinate system) for the entire length of the centerline flow of the jet within the flow field of the hood. The program directs the display of the jet's calculated centerline in relation to a cross section of the hood, and the hood centerline. Each time the program is run, it may be used to calculate the jet trajectory for any given hood flow (Q_h), jet flow (Q_j), jet-to-hood distance (z), and crossdraft velocity (V_c) parallel to the axis of the jet.

The program can be run, using the given assumptions, with the jet pointing along any quadrant line. The jet could be placed pointing away from the hood ---0° to the hood Z axis--- or toward the hood (180°) along its axis. In contrast, the arrangement tested for the experiments reported in this thesis is placement of the jet axis perpendicular to the hood axis. Note that, without a crossdraft, a 270° placement is equivalent to 90°.

The program displays, for each run, the following variables:

a) Q_h/Q_j = Ratio of hood to jet flows;

b) V_h/V_j = Ratio of hood to jet velocities;

c) D_h/D_j = Ratio of hood to jet diameter;

d) Z/D = Ratio of the distance of the jet from the hood face, to the hood diameter;

e) Q_h = Hood flow, cfm;

f) V_h = Hood face velocity, fpm;

g) R_h = Hood radius, ft.;

h) Q_j = Jet flow, cfm;

i) V_j = Jet face velocity, fpm;

j) "Jet X" (Hood Z) = Distance along hood centerline of jet tip, in.;

k) "Jet Y" (Hood R) = Hood radial distance of the jet tip from the centerline, in.;

l) Ang = Angle of jet from hood centerline;

m) Jet Orig = Distance inside jet tip from which spread of jet begins, in.

n) Jet D = Jet diameter, in.;

o) Xdrft = Crossdraft velocity (in the base plane of the jet and hood centerlines), fpm;

p) Xdf Ang = Angle of the crossdraft from the hood axis.

The hood-to-jet distance, such that the jet trajectory loops over to just reach the edge of the hood opening, is called the "critical distance." See the computer program printouts in the Appendix.

It is assumed that the spread of the jet is symmetrical around its centerline. Therefore, when the jet begins at the critical distance, it is predicted that 50% of the jet flow is captured, while 50% of the jet flow escapes capture. The escaping contaminant potentially endangers nearby workers by entering their breathing zones.

Computer-predicted critical distances, $[Z/D]_{50}$'s, for any given (operator-entered) set of hood and jet flows can be determined by use of the program. This was done for a set of 21 combinations of hood and jet flow. The matrix of experimental design conditions, all [Z/D] distance ratios tested for each of the 21 [Q_h/Q_j] values comprising the experiment, is shown [Figure 12].

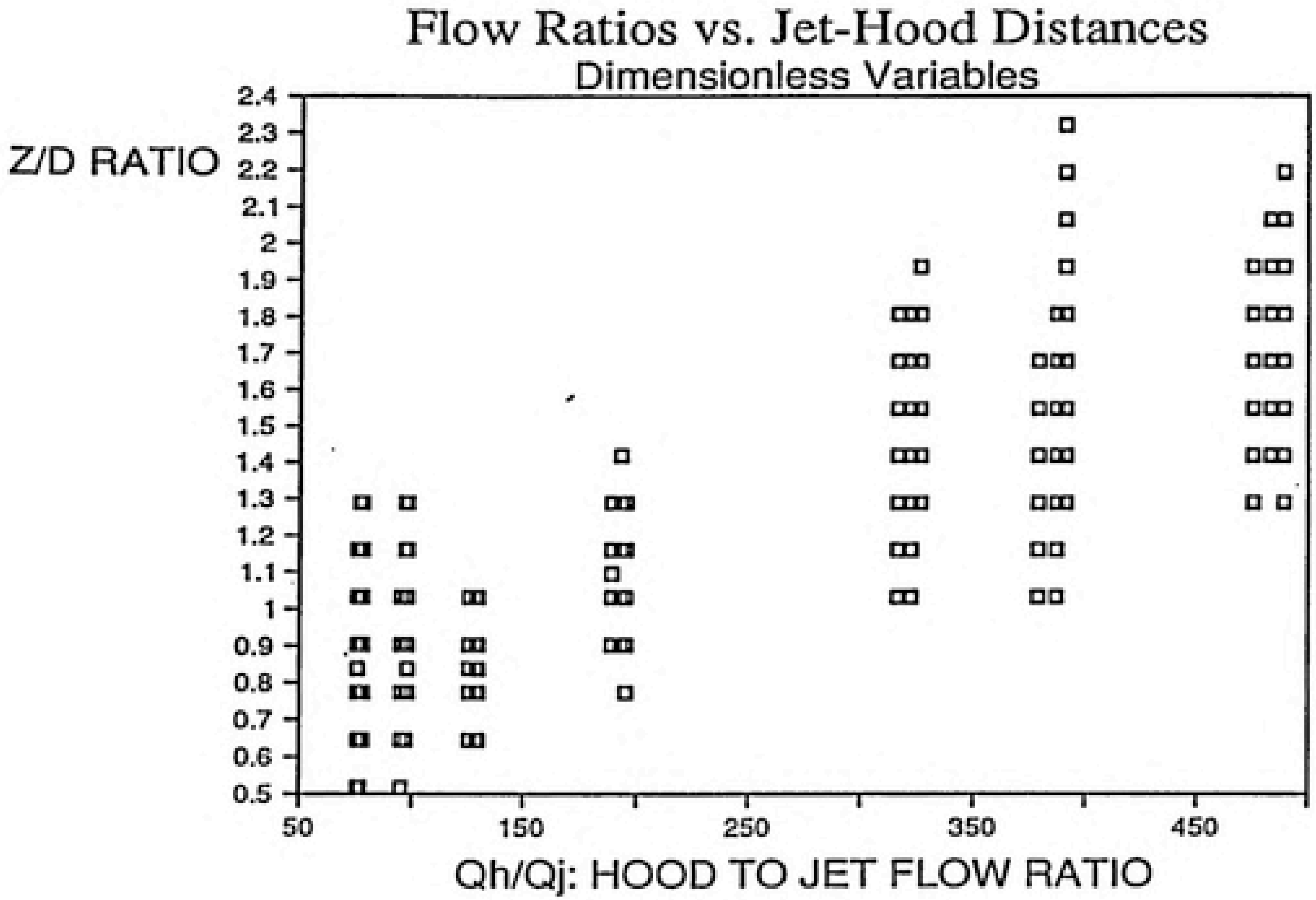

FIGURE 12. EXPERIMENTAL DESIGN

B. LABORATORY VALIDATION

The experimental set-up consisted of the jet and gas source, the FCH and fan, devices to control flow through each, and the calibration apparatus.

The jet was made of a machined steel cylinder 0.25 inches diameter, and eight inches long, connected to tubing, rotameters, and a laboratory air pump. Sulfur hexafluoride (SF_6) tracer gas at 900 ppm was drawn into the jet by the flow-induced vacuum created by the force of a laboratory air source. The individual flows were monitored carefully. Sulfur hexafluoride (SF_6) was used as the tracer primarily because of its low toxicity and low flammability and its relative ease of detection.

The jet axis was placed perpendicular to the hood centerline, and so that its tip was on the hood centerline. This created a geometrical plane, the "base plane," in which all flow calculations were made.

A machined flanged circular exhaust hood, 3.875 inches in inside diameter, with a 4 inch wide flange, was used as the primary opening. It was connected to a flexible duct, through which air was drawn at various flow rates by an industrial fan. Flows were measured by means of a manometer which measured the pressure drop across a Venturi constriction in the intake pipe of the fan.

The detector probe consisted of a steel cylinder six inches long, 0.125" in diameter, with a handle through which the passage continued, connected to a flexible tube. The probe was placed well behind the hood face opening, through and into the hood's flexible duct, so that its tip reached the duct centerline. The probe was placed about 15 hood diameters back of the hood face, two 90° bends away, so there was complete mixing of the captured contaminant jet gases with the hood flow. The probe drew samples of duct air to an ITI gas chromatograph (GC), to be analyzed for the concentration of indicator gas, SF_6, being drawn into the exhaust hood. Peak heights were displayed on a chart recorder.

The GC generated a current proportional to the concentration of tracer gas being used. Quantitation was possible by calibrating concentration vs. peak height, which, over suitable ranges, is linear. The calibration equipment consisted of the exponential dilution flask, a gas-tight syringe, the SF_6 gas source, a chart recorder, and a stopwatch or its equivalent. The exponential dilution flask had a volume of 3.7 liters, and was stirred with paddle blades to achieve to achieve gas concentrations of

$$C_t = C_o \exp[-Qt/V] \tag{38}$$

where: t = the elapsed time;

C_o =the initial concentration;

Q = the flow through the flask; and

V = the flask volume.

The initial flask concentration can be determined from the concentration of the SF_6 source gas (900 ppm), the flask volume, and the amount injected.

Capture efficiency is a relative measurement and therefore actual concentrations are not as important as the relative changes in peak height. The calibrations were least squares regressions of peak height with concentration. Calibrations were performed before every run of measurements.

Capture efficiency measurements were made with the GC. It was calculated as the relative concentration of SF_6 in the hood duct when the jet source was located at some hood centerline position Z, to the concentration in the hood duct when the jet source was located at the hood face.

$$\eta = C_Z/C_f \tag{39}$$

The experimental design consisted of twenty-one combinations (ratios) of hood to jet flows. Three hood flows were used (220, 145 and 75 cfm), by setting the fan volume flows with a damper, and reading the calibrated manometer settings.

The actual laboratory source air jet flow was carefully regulated. First, the known hood flow was divided by the desired experimental ratio, and the desired total jet flow was obtained. From this was subtracted the value in cfm of the SF_6 flow necessary to obtain a preliminary 100% reading in the calibration procedure. The SF_6 and laboratory air source flows both were set by carefully calibrated rotameters, so that the total jet flow just equaled the desired value.

A large laboratory exhaust hood was located above the experimental set-up, and was used primarily to draw off any excess SF_6 escaping into the room. The essentially vertical crossdraft periodically was measured, but was so apparently low (average 25 fpm) that it was not expected originally to have an effect on the results.

For each of the the twenty-one hood to jet flow ratios tested, the jet was moved incrementally out along the hood centerline away from the hood. At each position, five or more measurements of SF_6 concentration in the hood duct were taken. The capture efficiencies for each were calculated; then for every jet location, for each hood-to-jet flow combination [Q_h/Q_j], the capture efficiency (η) averages and standard deviations were calculated.

C. STATISTICAL EVALUATION

At each incremental position of the jet along the hood centerline, for 21 experimental hood-to-jet flow $[Q_h/Q_j]$ ratios, the average of five or more capture efficiencies was calculated. It has been found previously [17] that logit transformation is a useful treatment of capture efficiency data. Each of the calculated average capture efficiency values, η, was treated with the logistic transform:

$$y = \ln\,[\eta/\ 1-\eta], \tag{40}$$

and

$$x = Z/D \tag{41}$$

where y is the natural logarithm of the odds of being captured, and x is the dimensionless centerline distance.

These values may be related to one another by simple linear (least squares) regression procedures, the form of which is:

$$y = \alpha x + \beta. \tag{42}$$

A consistent strong relationship would suggest that capture efficiency is described by a cumulative logistic function with the form:

$$\eta = 1/(1 + \exp[(x-\mu)/\omega]), \tag{43}$$

where: $w = -1/\alpha$; and

$\mu = w\beta$.

The values of α and β are taken from the slope and intercept, respectively, of the regression of y on x.

For the logistic model, the parameter w is analogous to a standard deviation in a normal distribution. However, the distribution of the logistic model is much narrower (leptokurtic, or more peaked) than a normal distribution; 92.4% of the logistic distribution lies between $-w$ to $+w$. The probability distribution function is, of course, readily obtainable from the cumulative distribution.

The experimentally estimated "true" $[Z/D]_{50} = \mu$. In the logistic function, $\mu = w\beta$. Restated,

$$\mu = -\beta/\alpha. \tag{44}$$

VI. RESULTS AND DISCUSSION

A. LOGIT CAPTURE EFFICIENCY, y, REGRESSION ON JET DISTANCE TO HOOD DIAMETER RATIO, x

1. Summary of Equations:

a) $y = \ln[\eta/(1-\eta)]$, (40)

where: η = capture efficiency.

b) $x = Z/D$, (41)

where: D = hood diameter; and

Z = jet to hood distance.

c) Regression: $y = \alpha x + \beta$, (42)

where: α is the regression slope; and

β is the y-intercept value.

d) Predicted $[Z/D]_{50}$: $\mu = -\beta/\alpha$. (44)

2. Results and Analysis

The raw data tables and graphs, including regressions, are in the Appendix.

The summary results of the regressions are tabulated [Table 3] for each of the $[Q_h/Q_j]$ ratios employed experimentally. Logistic function estimates, μ, of each $[Z/D]_{50}$ may or may not fall within the range between the two neighboring hood axial distances actually experimentally determined. Therefore, μ can be modified to do so, and is

-----TABLE 3-----

-----SUMMARY INITIAL RESULTS-----

Qh/Qj ratio	Logit C. E. vs. (Z/D) Regression y=ax+b R^2	p-value CorrCoeff	Experimental (Z/D)50 modlogit	Vc=0 fpm: Predicted (Z/D)50	Vc=25fpm: Predicted (Z/D)50
76	0.932	0.000	0.87	0.548	0.484
77	0.925	0.001	1.11	0.548	0.484
78	0.892	0.005	1.03	0.548	0.484
95	0.859	0.023	0.75	0.677	0.548
97	0.918	0.003	0.94	0.677	0.613
98	0.860	0.023	0.92	0.677	0.677
126	1.000	0.000	0.86	0.937	0.742
129	0.953	0.024	0.82	0.939	0.806
130	0.905	0.013	0.84	0.948	0.871
189	0.948	0.005	1.14	1.388	0.935
193	0.928	0.037	1.15	1.413	1.129
195	0.919	0.010	1.03	1.452	1.194
316	0.830	0.004	1.41	2.199	1.258
322	0.765	0.023	1.41	2.243	1.516
326	0.960	0.001	1.69	2.252	1.710
379	0.973	0.000	1.43	2.529	1.323
387	0.945	0.000	1.59	2.568	1.645
391	0.882	0.000	2.07	2.613	1.903
475	0.775	0.021	1.52	2.987	1.387
483	0.972	0.000	1.76	3.000	1.839
489	0.939	0.000	1.98	3.065	2.097

denoted μ_{mod}. The predicted $[Z/D]_{50}$, determined by this modified logit transformation of the capture efficiency data, may be referred to as "modified logit" or even "modlogit." Computer program predictions of the $[Z/D]_{50}$'s are also displayed, for comparison, at two crossdraft velocity values.

Regressions of the true logit of capture efficiency, y, on the jet distance to hood diameter ratios, x, yield R^2 values of which two-thirds are greater than 0.9, and none is less than 0.75. In addition, p-values for the significance of the correlation coefficient in the regression equations are uniformly less than 0.05, and two-thirds are equal to or less than 0.01.

These results suggest that the logit transformation is a useful treatment, and that estimates of critical distances, $[Z/D]_{50}$'s, can be made with validity from capture efficiency data with this statistical procedure.

B. PREDICTED VS. EXPERIMENTAL $[Z/D]_{50}$ CRITICAL DISTANCES

Actual conditions may differ from those specified or assumed in the model. They do so appreciably near the hood face. There, the hood flow creates a strong static pressure gradient; there is shear turbulence between the flows of jet and hood; and frictional forces in the hood boundary layer become important. Predictions made for a jet entering a uniform flow field may not be borne out in this region.

The experimental findings near the hood face are consistent with this evaluation. See the graph of experimental vs. predicted $[Z/D]_{50}$ [Figure 13], and the tabulated values [Table 3]. The strong static pressure gradient, shear turbulence, and the turbulence (frictional) effects of viscous flow near the hood face create conditions of increased capture efficiency (longer $[Z/D]_{50}$'s) there compared to predicted values. This is true where the predicted critical distance of the jet from the hood is less than about seven-tenths of a hood diameter, i.e. where the predicted hood-to-jet flow ratios, $[Q_h/Q_j]$, necessary to capture 50% or more of the jet flow are less than 100.

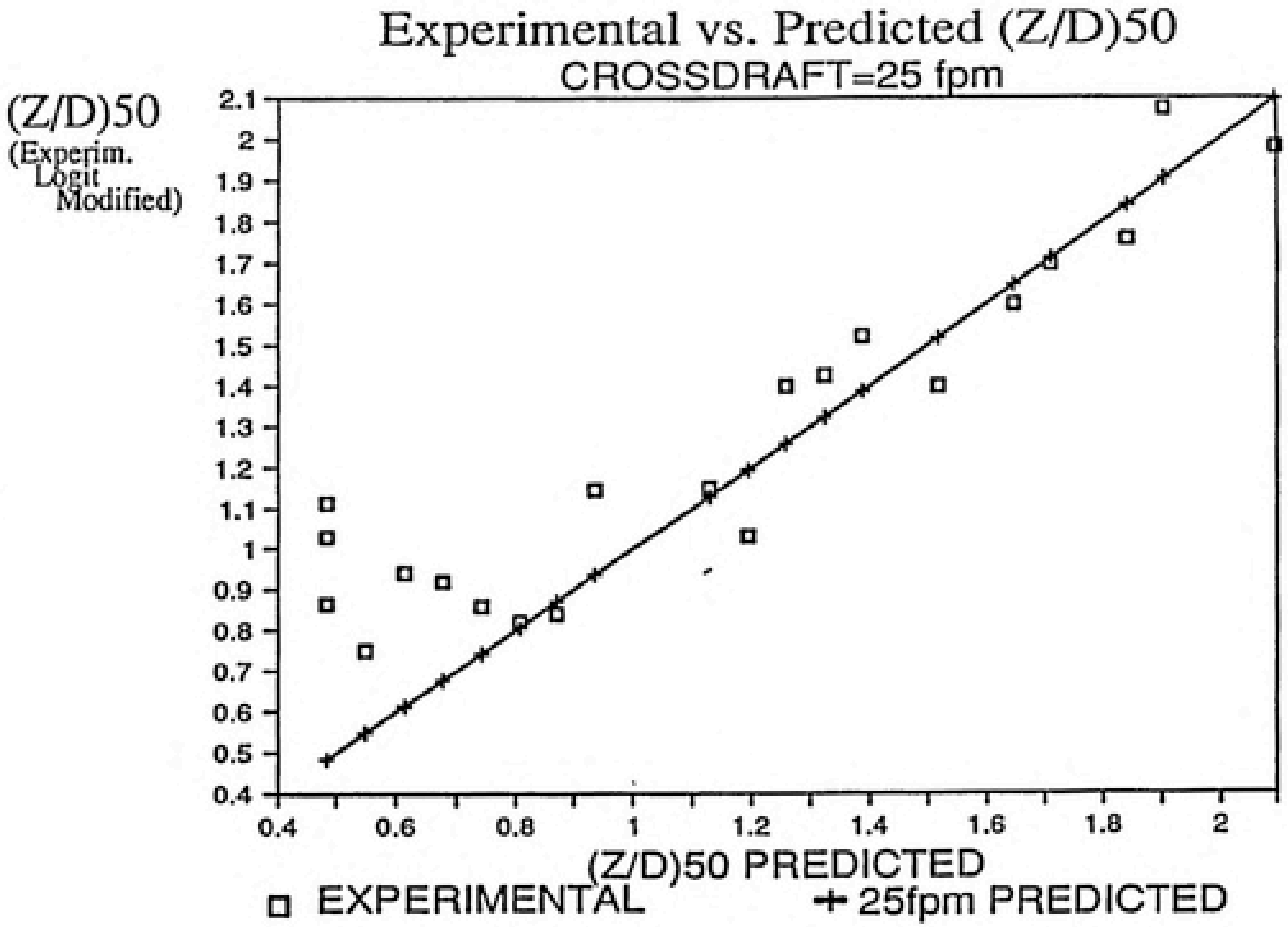
Experimental vs. Predicted (Z/D)50
CROSSDRAFT=25 fpm
(Z/D)50
(Experim. Logit Modified)
2.1
2
1.9
1.8
1.7
1.6
1.5
1.4
1.3
1.2
1.1
1
0.9
0.8
0.7
0.6
0.5
0.4
0.6
0.8
1
1.2
1.4
1.6
1.8
2
(Z/D)50 PREDICTED
EXPERIMENTAL
25fpm PREDICTED

FIGURE 13.

Turbulence may be classified in a number of ways. A useful set of distinctions is between shear turbulence (turbulence generated in free space between interacting streams of fluid); and wall turbulence (generated by fluid interactions with solid surfaces and characterized by boundary layers).

Both types of turbulence are occurring in this case; shear turbulence between a) the jet streams with each other; b) jet and hood streams; c) hood flow streams with each other; and d) each of the above with any crossdraft streams. Wall turbulence is occurring near the hood face along the entire reach of the flanges, and at the corners of the flanges with the duct.

Flynn and Ellenbecker [17] could assume that the characteristics of turbulence were primarily determined by the interaction of hood flow with crossdraft flow. They had no velocity component from their point contaminant source(s), let alone a jet, with which to contend. See [Figure 6], a depiction of the trajectories of single idealized contaminant streamlines (ICS) in a flow field of interacting hood and crossdraft effects.

Therefore, in their analysis, the $[V_f/V_c]$ ratio (hood face velocity to crossdraft velocity) serves them as a suitably predictive dimensionless variable for the effects of turbulent diffusion around each ICS. Thus Flynn and Ellenbecker rationalize the use of ω, the spread parameter in the logistic function, to describe in probabilistic terms the likely distribution of the turbulent diffusion of single streamlines. They therefore can relate mathematically predictions of the spread parameter, ω, to the dimensionless velocity ratio $[V_f/V_c]$. From this they can simplify their model so that capture efficiency, η, may be predicted directly as a function of the actual, x, and experimentally estimated, μ, ratios of centerline distances of the source from the hood face to the hood diameter.

However, a spreading turbulent jet creates a flow field very different indeed from that of Flynn and Ellenbecker's idealized contaminant streamlines (ICS), primarily by imparting significant turbulence to the hood flow field, and thus creating strong velocity gradients within it [Figure 10]. They acknowledged [17] that the velocity field into the hood (without a jet) already shows considerable gradients both in the direction of mean flow, as well as perpendicular to the streamlines, and that this indicates a non-homogenous turbulent field.

There is evidence [24] that the turbulence intensity in shear flows is quite large, and that the bulk of the transport by turbulent diffusion occurs both quickly and near the source. This suggests [17] that "the effects of turbulent diffusion may be largely determined by conditions at the source."

One might therefore suspect that the turbulence intensity near a jet source may be sufficient to cause contaminant gas dispersion into the hood flow field near the jet source. Thus, when the jet is within a short distance of the hood face, these effects are combined with those of a strong static pressure gradient across the jet created by the hood flow, so that more than predicted amounts of contaminant are captured, even at hood jet flow ratios of less than 100.

Where the predicted critical distance for the jet is farther than 0.7 hood diameters from the hood face (where the required hood-to-jet flow ratios are higher than 100), the predicted $[Z/D]_{50}$ and the experimentally estimated (modified logit procedure) $\mu_{mod} = [Z/D]_{50}$ are very close. If the crossdraft is nominally assumed to be 25 fpm (about the average of laboratory measurements), regression of all μ_{mod} on all predicted $[Z/D]_{50}$ values yields:

$$\mu_{mod} = 0.713\ [Z/D]_{50} + 0.451 \qquad (45)$$

with an $R^2 = 0.852$.

For those values of the predicted $[Z/D]_{50} > 0.7$ (i.e. where $[Q_h/Q_j] > 100$), under the same conditions, this regression yields:

$$\mu_{mod} = 0.915\ [Z/D]_{50} + 0.139, \qquad (46)$$

with an $R^2 = 0.924$.

This is excellent agreement in the outer region between predicted and experimental critical distances. There is, however, no discernible relationship between ω with the hood face to assumed average crossdraft velocity ratio, $[V_f/V_c]$, probably because, while the statistical concept of ω, the spread parameter, was useful for a single ICS from a point source, it is irrelevant in turbulent spreading jet flow.

C. HOOD TO JET FLOW RATIOS VS. $[Z/D]_{50}$'s: PREDICTIONS AND CROSSDRAFT EFFECTS

The effects of the crossdraft were apparent in the relationships of the dimensionless predictor variables [Z/D] and $[Q_h/Q_j]$. Regressions of μ_{mod} (modified logit estimated experimental $[Z/D]_{50}$) on the computer program prediction of $[Z/D]_{50}$ are more significant at V_c = 25 fpm than they are, for example, at 0 fpm (no) crossdraft.

Moreover, in the graphical representation [Figure 14] of μ_{mod} vs. $[Q_h/Q_j]$, and predicted $[Z/D]_{50}$ also vs. $[Q_h/Q_j]$, there is complete overlap (except for a single data point) of the modified logit-transformed experimental $[Z/D]_{50}$ with the computer program-predicted values, for all predicted $[Z/D]_{50}$'s > 0.7, when the crossdraft is set at 25 fpm. (When the program crossdraft value was fixed at 0 fpm, or at 5 fpm, however, there is no meaningful overlap [Figures 15 and 16].) There is a significant spreading of the predictions of $[Z/D]_{50}$ in proportion to the [Qh/Qj] ratio in the presence of a crossdraft. As the programmed crossdraft gets larger, that predicted spread becomes wider until, at 25 fpm, the experimental findings are nearly completely encompassed.

The three lines in Figures 14 and 16 represent the predictions of the $[Z/D]_{50}$ for each $[Q_h/Q_j]$, for each of three $[V_f/V_c]$ ratios tested. There are three $[V_f/V_c]$ ratios

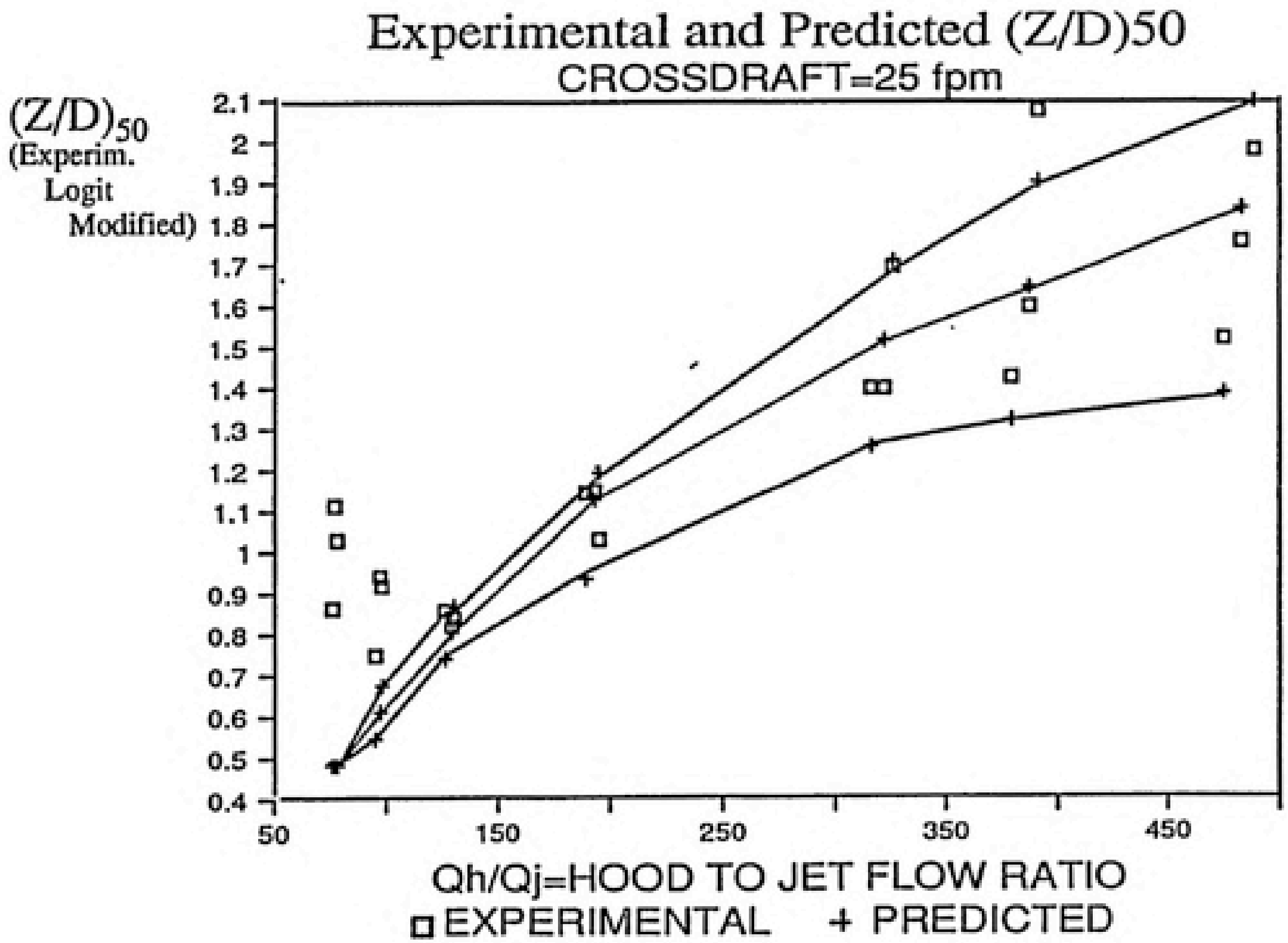

Experimental and Predicted (Z/D)50
CROSSDRAFT=25 fpm
(Z/D)50 (Experim. Logit Modified)
2.1
2
1.9
1.8
1.7
1.6
1.5
1.4
1.3
1.2
1.1
1
0.9
0.8
0.7
0.6
0.5
0.4
50
150
250
350
450
Qh/Qj=HOOD TO JET FLOW RATIO
EXPERIMENTAL
+ PREDICTED

FIGURE 14

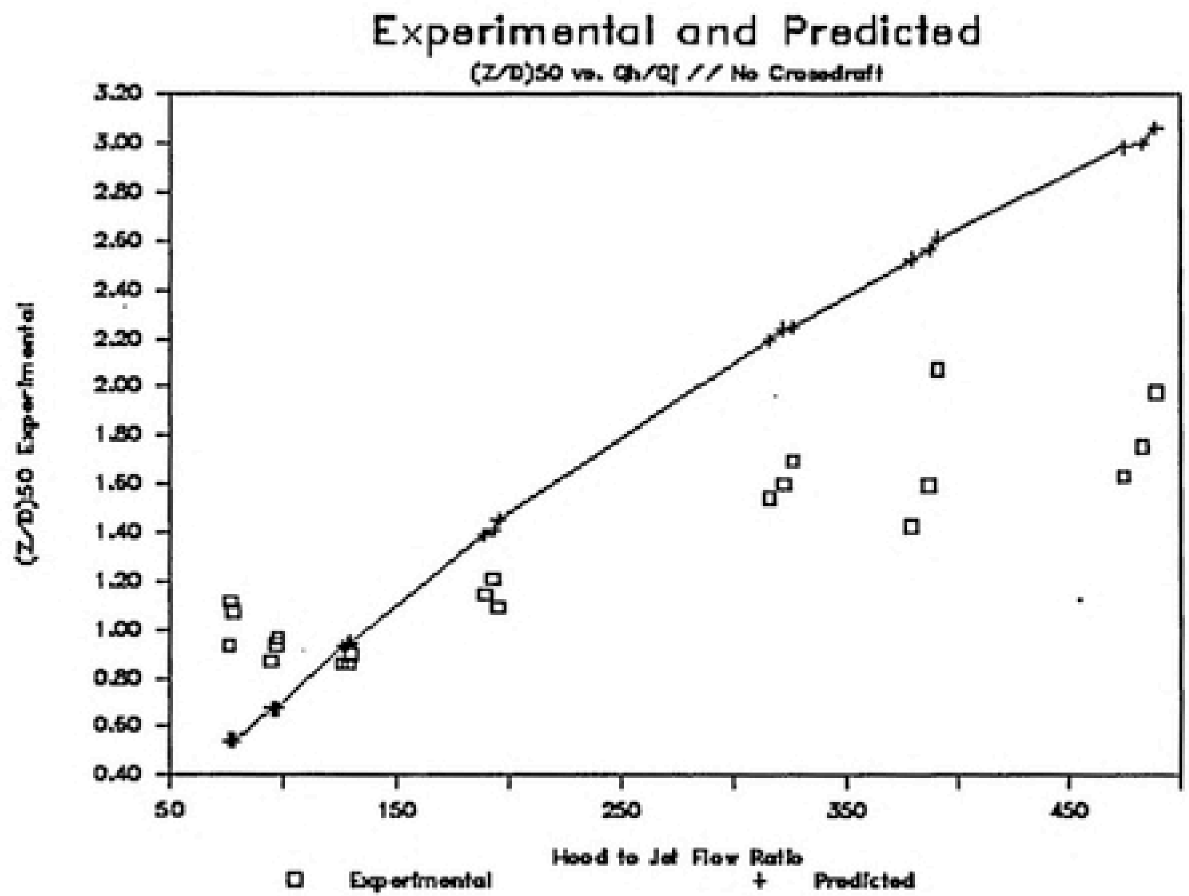

Experimental and Predicted
(Z/D)50 vs. Qh/Qj // No Crossdraft
(Z/D)50 Experimental
3.20
3.00
2.80
2.60
2.40
2.20
2.00
1.80
1.60
1.40
1.20
1.00
0.80
0.60
0.40
50
150
250
350
450
Hood to Jet Flow Ratio
Experimental
Predicted

FIGURE 15

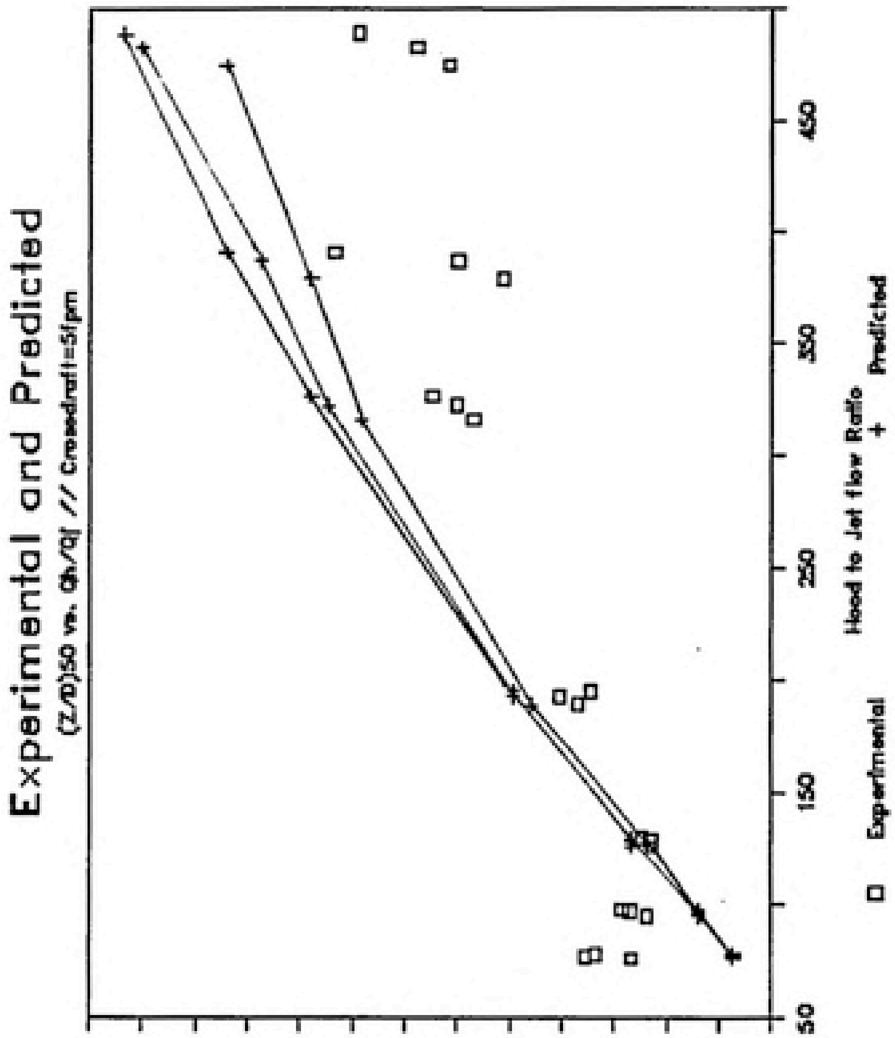

Experimental and Predicted
(Z/D)50 vs. Qh/Qj // Crossdraft=5fpm
(Z/D)50 Experimental
3
2.8
2.6
2.4
2.2
2
1.8
1.6
1.4
1.2
1
0.8
0.6
0.4
50
150
250
350
450
Hood to Jet flow Ratio
Experimental
Predicted

FIGURE 16

because there were three hood face velocities in the experiments (three Q_h's tested). It is assumed that a non-zero crossdraft is constant. In Figure 15, for no (0 fpm) crossdraft, these three prediction lines simply overlap.

With the crossdraft fixed at 25 fpm, power regression analysis was conducted for values of μ_{mod}, modified experimental estimates of $[Z/D]_{50}$, upon values of the corresponding $[Q_h/Q_j]$ ratios, for each of the $[V_f/V_c]$ ratios. The results are:

For $[V_f/V_c] = 36.64$:

$$\mu_{mod} = .144\ [Q_h/Q_j]^{0.387}, \tag{47}$$

with $R^2 = 0.922$.

For $[V_f/V_c] = 70.82$:

$$\mu_{mod} = .211\ [Q_h/Q_j]^{0.331}, \tag{48}$$

with $R^2 = 0.729$.

For $[V_f/V_c] = 107.44$:

$$\mu_{mod} = .107\ [Q_h/Q_j]^{0.471}, \tag{49}$$

with $R^2 = 0.804$.

To confirm the validity of the program when incorporating the average measured value of the crossdraft velocity (25 fpm), the computer program was re-run. This time, the variables were set such that for every $[Q_h/Q_j]$ ratio tested, the program [Z/D] (jet location) ratio was set at the best statistically evaluated laboratory value for each experiment. Then the program crossdraft velocity, V_c, was sequentially altered until the predicted jet trajectory within the hood flow curved until it just hit the edge of the computer-displayed hood opening, i.e. until that particular [Z/D] became the critical distance, the $[Z/D]_{50}$. For all $[Q_h/Q_j]$ ratios over 100, the average value of the crossdrafts necessary in the computer program to cause the predicted $[Z/D]_{50}$ to match the real one was 24.33 fpm [Table 4].

-----TABLE 4-----

VALUES REQUIRED TO MATCH COMPUTER
---------MODEL PREDICTIONS OF [Z/D]50 WITH---------
EXPERIMENTAL (mod. logit) [Z/D]50

---EXPERIMENTAL CRITERIA---			Eddy Viscosity, epsilon-sub-O, Required:		
Qh/Qj	modlogit [Z]50,in.	modlogit [Z/D]50	at Vc=0 fpm	at Vc=25fpm	Crossdraft fpm Required:
76	3.35	0.87	4.3E+00	6.9E+00	N/A
77	4.32	1.11	1.2E+01	2.1E+01	N/A
78	3.99	1.03	1.7E+01	1.9E+01	N/A
95	2.91	0.75	2.1E+00	2.7E+00	N/A
97	3.65	0.94	3.9E+00	6.5E+00	N/A
98	3.57	0.92	5.9E+00	7.8E+00	N/A
126	3.33	0.86	5.0E-01	1.6E+00	5
129	3.18	0.82	7.0E-01	2.0E+00	24
130	3.26	0.84	1.0E+00	1.3E+00	32
189	4.43	1.14	2.0E-01	1.4E+00	10
193	4.46	1.15	2.0E-01	1.3E+00	21
195	3.99	1.03	5.0E-05	1.0E-02	59
316	5.43	1.40	1.0E-06	1.0E+00	16
322	5.43	1.40	2.0E-06	4.0E-03	33
326	6.58	1.70	2.0E-05	5.0E-01	25
379	5.52	1.43	5.0E-07	6.9E-01	19
387	6.19	1.60	3.0E-06	1.3E-01	28
391	8.04	2.07	1.0E-05	1.5E+00	17
475	5.89	1.52	4.0E-07	5.5E-01	20
483	6.81	1.76	2.0E-06	1.1E-01	27
489	7.67	1.98	3.0E-06	2.0E-02	29
					Avg.= 24.333fpm

D. THE ROLE OF ϵ_o, THE VIRTUAL OR APPARENT KINEMATIC ("EDDY") VISCOSITY

To clarify a little the events occurring when the jet location is set within one hood diameter's distance of the hood face, and additional effects of the crossdraft on the system, a new program was written, EPSILON. This program is a modification of the original, constructed to change iteratively the value of ϵ_o, the eddy (apparent kinematic) viscosity of the jet flow.

Viscosity is a natural property of fluids and is a measure of resistance to shear forces. Kinematic viscosity is calculated as the viscosity divided by the fluid density. The apparent kinematic viscosity of a fluid is an analytic concept useful in helping account for the retarding effects on flow due to the excess frictional forces of turbulence.

The program was written to assist in the determination of the approximate value of ϵ_o such that when inserted into the original program, the computer program would actually predict the best statistically evaluated $[Z/D]_{50}$ values determined experimentally for all sets of trial conditions. The incorporation of a nominal crossdraft was critical in this determination, and had its most significant effect on the value of the necessary ϵ_o at the higher hood to jet flow $[Q_h/Q_j]$ ratios, where the $[Z/D]_{50}$ distances are large, i.e. where real crossdrafts would have the most relative effect [Table 4].

Moreover, where the $[Q_h/Q_j]$ ratios are less than 100, the crossdraft seems to have no relative effect on the ϵ_o values required at all; this is expected because the jet is located within one hood diameter of the hood opening. In this region, the value of the required eddy viscosity value, ϵ_o, of the jet flow is generally much greater than it is with the jet further away from the hood face. Since viscous forces in turbulent flow are approximately proportional to the square of the mean velocity, the fact that the eddy viscosity rises when the jet is near the hood face is expected.

VII. CONCLUSIONS AND RECOMMENDATIONS

The object of local exhaust ventilation is to reduce of workers' breathing zone concentrations of toxic materials. Industrial hygiene has developed rapidly in recent years in the analysis of the mechanisms of operation of local exhaust outlets, after a fallow period in the 1950's and 1960's. From the core concept of centerline velocity gradients as the basis of evaluation (and installation - it is still used by the ACGIH), the profession has recently moved to analytic and numerical solutions based in fluid mechanics theory, and to the concept of capture efficiency. These analyses have yielded promising results, and may be even more productive than the past "practical" approach.
This thesis is a piece of a larger body of ongoing research work in the field. Analytic evaluations of capture efficiency concepts, hood flows in various configurations, and experimental validations of applied potential flow theory have formed some of the background to this paper. Although frictional forces are ignored in the potential flow solution, in its modified form it has been found to be highly predictive in evaluating flows into both flanged round and rectangular hoods, both with and without crossdrafts.

Jets of contaminant gases are commonly found in industrial settings. They may include gas jets of various kinds, intentionally occurring and accidental; spray paint jets; jets of welding fume, and many other examples. It is important to remove these dangerous materials as efficiently as possible from the industrial workers' environment; where they contaminate the breathing zone of a stationary worker, local exhaust ventilation is a critical need.

This thesis describes a computer program written to address this problem and act as a first step in its solution. Schlichting's derivation of velocity vectors for a circular free jet was used as the basis of the jet flow in the program. The assumptions used were those inherent in the mixing length hypothesis of Prandtl. Viscous forces are of importance in the theoretical derivations. (In contrast, viscous forces are neglected in the potential theory model of hood flow.) The program adds iteratively the vectors of hood and jet flow at every point along the jet's hypothetical centerline. The computer program calculates the velocity vector values for any diameter flanged circular hood of any specified flow, if the jet tip is perpendicular to and on the centerline of the hood. A crossdraft parallel to the jet (either direction) can be programmed in.

The program, by predicting the critical distance of the jet from the hood, where 50% of the contaminant will be captured by the hood, forms a basis for future work. Outside of the zone within about seven-tenths of one hood diameter of the hood face, the program quite accurately predicts the critical distance. Within that short region, the critical distance is found experimentally to be longer than expected (the error is in a hypothetical worker's favor). The discrepancy near the hood face is due to: 1) the steep static pressure gradient created by the hood flow upon a jet placed within it; 2) turbulent eddies propagating from the shear between interacting streamlines of hood and jet flow; and 3) turbulence effects near the flange not accounted for in the potential flow solution. Values of the apparent or virtual kinematic (eddy) viscosity of the jetstream are high when the jet is located near the hood face.

The jet is circular, and is flowing freely in a conical dispersion pattern. This, and the real turbulence effects described above, are the reason that ω, the spread parameter of a single idealized streamline, when analyzed in a logistic function, does not describe either statistically or analytically the distribution of jet flow in the hood velocity field.

Even very weak crossdrafts have strong effects outside about one hood diameter away from the hood face. It is recommended that systematic experimental variations be made of the crossdraft velocity in a wind tunnel to confirm the strong probable effect demonstrated here of the average crossdraft velocity on the $[Z/D]_{50}$ and, thus on the capture efficiency of flanged circular exhaust hoods for a jet of contaminant.

The described computer model adds the vectors for the potential flow field into a local exhaust hood with those of a free turbulent jet model in which viscous forces are important. The program does not attempt to solve Navier-Stokes or any of the energy equations of accurate fluid mechanics models. Numerical simulations of such problems are very expensive in time, computer power and code development. Recently, investigators have evaluated the interactions of crossdraft and jets using such methods [25, 26]. The program is, however, useful as an approximate model, for building upon in the design of effective local exhaust ventilation systems, and for further research work into the interactions of hood, jet and crossdraft flow fields.

REFERENCES

1. National Institute for Occupational Safety and Health (1973). The Industrial Environment - Its Evaluation and Control. U. S. Government Printing Office, Washington, D. C.

2. McDermott, H.J. (1976). Handbook of Ventilation for Contaminant Control. Ann Arbor Science, Ann Arbor, MI.

3. American Conference of Governmental Industrial Hygienists (1986). Industrial Ventilation - A Manual of Recommended Practice, 19th Edition. ACGIH, Cincinnati, OH.

4. Dalla Valle, J.M. and Hatch, T. "Studies in the Design of Local Exhaust Hoods," presented at the 6th Annual Wood-Industries Meeting of the American Society of Mechanical Engineers, Winston-Salem, North Carolina. Oct. 15-16, 1931.

5. Silverman, L. (1942). "Centerline Velocity Characteristics of Narrow Exhaust Slots," Journal of Industrial Hygiene and Toxicology, Vol. 24, No. 9, pp. 267-276.

6. Fletcher, B. (1977). "Centerline Velocity Characteristics of Rectangular Unflanged Hoods and Slots Under Suction," Annals of Occupational Hygiene, Vol. 20, pp. 141-146.

7. Fletcher, B. (1978). "Effects of Flanges on the Velocity in Front of Exhaust Ventilation Hoods," Annals of Occupational Hygiene, Vol. 21, pp. 265-269.

8. National Safety Council (1979). Fundamentals of Industrial Hygiene, 2nd Edition, New York, N.Y.

9. Fletcher, B. and Johnson, A.E. (1982). "Velocity Profiles Around Hoods and Slots and the Effects of an Adjacent Plane," Annals of Occupational Hygiene, Vol. 25, pp. 365-372.

10. Garrison, R. (1981). "Centerline Velocity Gradients for Plain and Flanged Local Exhaust Inlets," American Industrial Hygiene Association Journal, Vol. 42, No. 10, pp. 739-746.

11. Garrison, R. (1983). "Velocity Calculation for Local Exhaust Inlets - Empirical Design Equations," American Industrial Hygiene Association Journal, Vol. 44, No. 12, pp. 937-940.

12. Garrison, R. (1983). "Velocity Calculation for Local Exhaust Inlets - Graphical Design Concepts," American Industrial Hygiene Association Journal, Vol. 44, No. 12, pp. 941-947.

13. Heinson, R.J. and Choi, M.S. "Advanced Design Methods in Industrial Ventilation", Ventilation '85 - Proceedings of the 1st International Symposium on Ventilation for Contaminant Control, Toronto, Canada, Oct. 1-3, 1985.

14. Fletcher, B. and Johnson, A. E. "The Capture Efficiency of Local Exhaust Ventilation Hoods and the Role of Capture Velocity", Ventilation '85 - Proceedings of the 1st International Symposium on Ventilation for Contaminant Control, Toronto, Canada, Oct. 1-3, 1985.

15. Burgess, W.A. and Murrow, J. (1976). "Evaluation of Hoods for Low Volume - High Velocity Exhaust Systems", American Industrial Hygiene Association Journal, Vol. 37, No. 9, pp. 546-549.

16. Ellenbecker, M. J., Gempel, R. F., and Burgess W.A. (1983). "Capture Efficiency of Local Exhaust Ventilation Systems", American Industrial Hygiene Association Journal, Vol. 44, No. 10, pp. 752-755.

17. Flynn, M.R. and Ellenbecker, M.J. (1986). "Capture Efficiency of Flanged Circular Local Exhaust Hoods," Annals of Occupational Hygiene, Vol. 30, No. 4, pp. 497-513.

18. Flynn, M.R. and Ellenbecker, M.J. (1985). "The Potential Flow Solution for Air Flow into a Flanged Circular Hood," American Industrial Hygiene Association Journal, Vol. 46, No. 6, pp. 318-322.

19. Baturin, V. V. (1972). Fundamentals of Industrial Ventilation. Pergamon Press, Elmsford, N.Y.

20. Strauss, H.J. (1973). "On an Approximation to the Determination of Flow Fields for Exhaust Hoods", Staub Reinhaltung der Luft in English, Vol. 33, No. 3, pp. 142-146.

21. Flynn, M.R. and Ellenbecker, M.J. (1987). "Empirical Validation of Theoretical Velocity Fields into Flanged Circular Hoods", American Industrial Hygiene Association Journal, Vol. 48, No. 4, pp. 380-389.

22. Conroy, L.M., Ellenbecker, M.J., and Flynn, M.R. (1988). "Prediction and Measurement of Velocity into Flanged Slot Hoods", American Industrial Hygiene Association Journal, Vol. 49, No. 5, pp. 226-234.

23. Schlichting, H. (1979). Boundary-Layer Theory, translated by J. Kestin, 4th English edition. McGraw-Hill Book Co., New York, N.Y.

24. Hinze. J. O. (1959). Turbulence. An Introduction to its Mechanism and Theory. McGraw-Hill Book Co., New York, N.Y.

25. Patankar, S. V., Basu, D. K., and Alpay, S. A. (1977). "Prediction of the Three-Dimensional Velocity Field of a Deflected Turbulent Jet." Journal of Fluids Engineering. Transactions of the American Society of Mechanical Engineers, pp. 758-762.

26. Sykes, R. I., Lewellen, W. S., and Parker, S. F. (1986). "On the Vorticity Dynamics of a Turbulent Jet in a Crossflow," Journal of Fluid Mechanics, Vol. 168, pp. 393-413.

27. Lamb, Sir H. (1945). Hydrodynamics, 6th edition. Dover, New York, N.Y.

28. Drkal, F. (1970). Theoretical Solution--Flow Conditions for Round Suction Openings with a Flange. HLH--Heizung, Luftung, Klimatechnik, Haustechnik, Vol. 21, No. 8, p.271.

APPENDIX A

RESEARCH COMPUTER PROGRAM

```
10 CLS
20 DIM P(1600,2)
30 PI=3.1415927#
40 PRINT "WELCOME"
50 'Author: This program was prepared by Kirby N. Smith.
60 'Date:   This program was finalized in October,1987.
70 'Purpose:To describe the contaminant jet flow near a flanged circular
80 '        hood, from a jet pointing in any axial or radial direction
            (0,90,180,270,360 degrees) in the base plane of the hood.
90 'Method: The flow field into the hood is described with the equations
100 '       of potential theory, which assumes inviscid, irrotational and in-
            compressible flow.  The equations of the Prandtl mixing length hypo-
            thesis, which takes viscosity into account, describe the jet flow.
110 '       These two types of equations are added vectorially at every point
            in the base (R-Z) plane of the hood. The jet flow is portrayed
            graphically in the printout.
120 '       The line of 50% Capture Efficiency can be determined with a function
            of the dimensionless variables (Qh/Qj) and (Z/D)50. and e-o.
130 'Initial Variables: Variables containing "J" are for the jet. Jet direction
             is in hood coordinates.  Initial inquiries are self-explanatory.
140 '       Constants in the program and/or input variables, or even whether a
            certain value should be a constant or an input variable, may be
            altered at the user's careful discretion.
150 SCREEN 0
160 PRINT "THE HOOD DIAMETER IS 3 7/8 IN."
170 DH=3.875
180 RH=DH/2
190 A=RH/12                '''''Note:A is the hood radius in feet.
200 INPUT "WHAT IS THE HOOD FLOW IN CFM";Q
210 VH=Q/(PI*A^2)
220 PRINT "THE JET DIAMETER JD=.25 INCHES."
230 JD=.25
240 DJ=JD/12
250 RJ=DJ/2
260 AJ=PI*(RJ)^2
270 INPUT "WHAT IS THE JET FLOW IN CFM";QJ
280 VJ=QJ/AJ
290 INPUT "WHERE IS THE JET FACE IN HOOD AXIAL COORD.(0to12in.)";XJFIN
300 PRINT "THE RADIAL COORD.(-12to+12 IN) OF JET FACE, YJFIN=0."
310 YJFIN=0
320 XJF=XJFIN/12
330 YJF=YJFIN/12
340 'Note:  (+Z) is to the right. Negative Z is into the hood.  Positive R
             is up on the screen.  The R-Z plane is the base plane.
350 PRINT "JET DIRECTION DIR=90 DEG. FROM THE HOOD(+Z) AXIS"
360 DIR=90
370 RADIANS=PI*DIR/180
380 PRINT "THE CROSSDRAFT ANGLE XDFA=90 DEG."
390 XDFA=90
400 VC=25
410      '''''INPUT"WHAT IS THE CROSSDRAFT VELOCITY";VC
420 PRINT"THE CROSSDRAFT VELOCITY IS";VC"FPM."
430 RDXDF=PI*XDFA/180
440 PRINT "THE INCREMENT TO RECALCULATION IS .03 FT."
450 INC=.03
460 ' Note: The virtual point in the Prandtl mixing length hypothesis of jet
             flow is taken as the actual origin of the jet.
470 PRINT "THE JET ORIGIN IS"1.86*JD"IN.INSIDE THE JET TIP."
480 PRINT "THE JET VELOCITY IS";VJ;"FPM."
490 PRINT "THE HOOD VELOCITY IS";VH"FPM."
500 INPUT "ENTRIES OK(Y/N)";A$
```

```
510 IF A$="N" OR A$="n" THEN GOTO 150 ELSE 520
520 CLS
530 COLOR 5
540 PRINT "PLEASE STAND BY."
550 'Note:  The following three equations set the angle of the image jet.
560 IF RADIANS=0 THEN RADIM=PI
570 IF 0<RADIANS<=PI THEN RADIM=PI-RADIANS
580 IF PI<RADIANS<2*PI THEN RADIM=(3*PI)-RADIANS
590 '  Note:The following equations set the angle of the image crossdraft.
600 IF RDXDF=0 THEN XDFIM=PI
610 IF 0<RDXDF<=PI THEN XDFIM=PI-RDXDF
620 IF PI<RDXDF<2*PI THEN XDFIM=(3*PI)-RDXDF
630 'Note:  The following equations calculate the vectors for each increment
            of hood flow.
640 'Note:  Hood coordinates Z and R are named in hood flow calculations
            as X and Y, respectively.
650 X=XJF
660 Y=YJF
670 FOR I=1 TO 1600
680 GAMMA1=SQR(X^2+(A+Y)^2)
690 GAMMA2=SQR(X^2+(A-Y)^2)
700 ECC=(2*A)/(GAMMA1+GAMMA2)
710 ECC2=ECC^2
720 T1=A+Y
730 T2=Y-A
740 T3=GAMMA1+GAMMA2
750 T4=GAMMA1*GAMMA2
760 T5=4*A^2
770 T6=SQR(T3^2-T5)
780 T7=-Q/PI
790 T8=(T1*GAMMA2)+(T2*GAMMA1)
800 T9=T3*T4*T6
810 VR1=(T8/T9)*T7
820 VZ1=(T7*X)/(T4*T6)
830 V=SQR(VR1^2+VZ1^2)
840 VTF=(Q*ECC2*SQR(3))/(2*PI*A^2*SQR(3-2*ECC2))
850 VR2=(VR1/V)*VTF
860 VZ2=(VZ1/V)*VTF
870 VRC=(2.6*ECC^18+.853)*VR2
880 VZC=.9*VZ2
890 'Note:  The following equations transform the coordinates of the jet and
            its image to the coordinates of the hood.
900 IF DIR=0 OR DIR=360 THEN GOTO 910 ELSE 960
910 Z=X-XJF+(1.86*DJ)
920 R=YJF-Y
930 ZI=2*(1.86*DJ)-(2*XJF)-Z
940 RI=-R
950 GOTO 1140
960 IF DIR=90 THEN GOTO 970 ELSE GOTO 1020
970 Z=Y-YJF+(1.86*DJ)
980 R=X-XJF
990 ZI=Z
1000 RI=(2*XJF)+R
1010 GOTO 1140
1020 IF DIR=180 THEN GOTO 1030 ELSE GOTO 1080
1030 Z=XJF-X+(1.86*DJ)
1040 R=Y-YJF
1050 ZI=2*((1.86*DJ)+XJF)-Z
1060 RI=-R
1070 GOTO 1140
1080 IF DIR=270 THEN GOTO 1090 ELSE GOTO 350
1090 Z=YJF-Y+(1.86*DJ)
1100 R=XJF-X
1110 ZI=Z
1120 RI=R-(2*XJF)
1130 'Note:  The following equations calculate the vectors for any given R and
```

```
          Z points of the jet flow.
1140 K=AJ*(VJ)^2
1150 EO=.0161*SQR(K)
1160 ETA=(R*SQR(3*K))/(4*(EO)*Z*SQR(PI))
1170 ETA1=ETA-((ETA^3)/4)
1180 ETA2=(1+((ETA^2)/4))^2
1190 IF -.00001<ETA AND ETA<.00001 OR -2.00001<ETA AND ETA<-1.99999 OR
     1.99999<ETA AND ETA<2.00001 THEN GOTO 1200 ELSE 1220
1200 VRJ=0
1210 GOTO 1230
1220 VRJ=(SQR(3*K)*ETA1)/(4*(ETA2)*Z*SQR(PI))
1230 VZJ=3*K/(8*PI*(EO)*Z*ETA2)
1240 IF VZJ<0 THEN VZJ=0 AND VRJ=0
1250 'Note:  The following calculations are for the effect of the image jet
             field on the flow of the actual jet into the hood. Note that
             K and epsilon-sub-zero have already been calculated for the jet.
1260 ETAI=(RI*SQR(3*K))/(4*EO*ZI*SQR(PI))
1270 ETAI1=ETAI-((ETAI^3)/4)
1280 ETAI2=(1+((ETAI^2)/4))^2
1290 IF -.00001<ETAI AND ETAI<.00001 OR -2.00001<ETAI AND ETAI<-1.99999 OR
     1.99999<ETAI AND ETAI<2.00001 THEN GOTO 1300 ELSE 1320
1300 VRIM=0
1310 GOTO 1330
1320 VRIM=(SQR(3*K)*ETAI1)/(4*ETAI2*ZI*SQR(PI))
1330 VZIM=3*K/(8*PI*EO*ZI*ETAI2)
1340 IF VZIM<0 THEN VZIM=0 AND VRIM=0
1350 'Note:  The following equations add the vectors and then determine
             the next point for vector calculation based on the combined
             values and the desired increment of calculation.
1360 VRTOT=VRC+(COS(RADIANS)*VRJ)+(COS(RADIM)*VRIM)+(SIN(RADIANS)*VZJ)+
          (SIN(RADIM)*VZIM)+(SIN(RDXDF)*VC)+(SIN(XDFIM)*VC)
1370 VZTOT=VZC+(COS(RADIANS)*VZJ)+(COS(RADIM)*VZIM)+(SIN(RADIANS)*VRJ)+
          (SIN(RADIM)*VRIM)+(COS(RDXDF)*VC)+(COS(XDFIM)*VC)
1380 IF VZTOT<=-.00001 THEN GOTO 1390 ELSE GOTO 1410
1390 ANGLE=ATN(VRTOT/VZTOT)+PI
1400 GOTO 1490
1410 IF VZTOT>=.00001 THEN GOTO 1420 ELSE GOTO 1440
1420 ANGLE=ATN(VRTOT/VZTOT)
1430 GOTO 1490
1440 IF -.00001<VZTOT AND VZTOT<.00001 AND VRTOT<0 THEN GOTO 1450 ELSE 1470
1450 ANGLE=3*PI/2
1460 GOTO 1490
1470 IF -.00001<VZTOT AND VZTOT<.00001 AND VRTOT>=0 THEN GOTO 1480
1480 ANGLE=PI/2
1490 X=X+(COS(ANGLE)*INC)
1500 Y=Y+(SIN(ANGLE)*INC)
1510 P(I,1)=X
1520 P(I,2)=Y
1530 IF X<=0 OR X>1 OR Y<=-1 OR Y>=1 THEN I=1600 ELSE COUNT=I+1
1540 'Note: A repetitive cycle is programmed to calculate the new
            magnitude and direction of flow at each subsequent increment.
1550 NEXT I
1560 'Note: The following section is the instructions to the computer
            to draw the hood, and to display the flow into it.
1570 CLS
1580 SCREEN 1
1590 COLOR 16,0
1600 WINDOW (-1.6,-1.1)-(1.6,1.1)
1610 LINE (0,A)-(0,1),2
1620 LINE (0,A)-(-.05,A),2
1630 LINE (-.05,0)-(1,0),3
1640 LINE (0,-A)-(0,-1),2
1650 LINE (0,-A)-(-.05,-A),2
1660 FOR J=1 TO COUNT
1670 G=P(J,1)
1680 H=P(J,2)
```

```
1690 PSET(G,H),1
1700 NEXT J
1710 KEY  OFF
1720 LOCATE 4,4:PRINT "QH/QJ=";Q/QJ
1730 LOCATE 5,4:PRINT "VH/VJ=";VH/VJ
1740 LOCATE 6,4:PRINT "DH/DJ=";2*A/DJ
1750 LOCATE 7,4:PRINT "(Z/D)=";XJF/(2*A)
1760 LOCATE 9,4:PRINT "QH=";Q"CFM"
1770 LOCATE 10,4:PRINT "VH=";VH"FPM"
1780 LOCATE 11,4:PRINT "RH=";A"FT"
1790 LOCATE 13,4:PRINT "QJ=";QJ"CFM"
1800 LOCATE 14,4:PRINT "VJ=";VJ"FPM"
1810 LOCATE 15,4:PRINT "JETX=";XJFIN"IN"
1820 LOCATE 16,4:PRINT "JETY=";YJFIN"IN"
1830 LOCATE 17,4:PRINT "ANG=";DIR"DEG"
1840 LOCATE 18,4:PRINT "JET ORIG=";-1.86*JD"IN"
1850 LOCATE 19,4:PRINT "JETD=";JD"IN"
1860 LOCATE 21,4:PRINT "XDRFT=";VC"FPM"
1870 LOCATE 22,4:PRINT "XDFANG=";XDFA"DEG"
1880 LOCATE 24,1:PRINT "PRINT"
1890 INPUT "ANOTHER(Y/N)";ANN$
1900 IF ANN$="Y" OR ANN$="y" THEN GOTO 1910 ELSE GOTO 1930
1910 CLS
1920 GOTO 150
1930 CLS
1940 PRINT "END OF JET-HOOD FLOW ANALYSIS RUNS"
1950 SYSTEM
Ok
```

APPENDIX B

COMPUTER PREDICTIONS OF $[Z/D]_{50}$'s AT CROSSDRAFT=25 fpm (3 EXAMPLES)

```
QH/QJ= 77.33334
VH/VJ= .321887
DH/DJ= 15.5
(Z/D)= .483871

QH= 145 CFM
VH= 1770.505 FPM
RH= .1614583 FT

QJ= 1.875 CFM
VJ= 5500.394 FPM
JETX= 1.875 IN
JETY= 0 IN
ANG= 90 DEG
JET ORIG=-.465 IN
JETD= .25 IN

XDRFT= 25 FPM
XDFANG= 90 DEG

PRINT
ANOTHER(Y/N)?
```

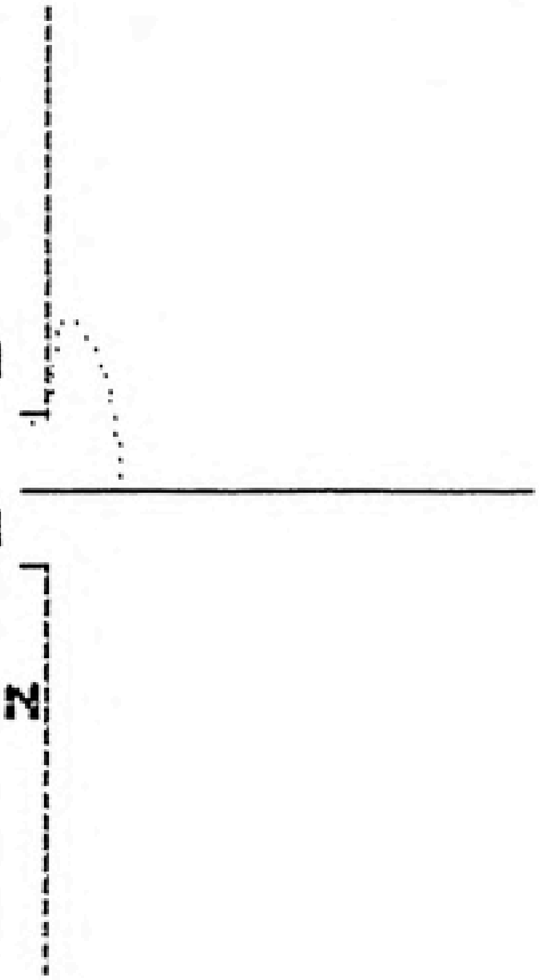

```
QH/QJ= 193.3333
VH/VJ= .8047175
DH/DJ= 15.5
(Z/D)= 1.109678

QH= 145 CFM
VH= 1770.505 FPM
RH= .1614583 FT

QJ= .75 CFM
VJ= 2200.158 FPM
JETX= 4.3 IN
JETY= 0 IN
ANG= 90 DEG
JET ORIG=-.465 IN
JETD= .25 IN

XDRFT= 25 FPM
XDFANG= 90 DEG

PRINT
ANOTHER(Y/N)?
```

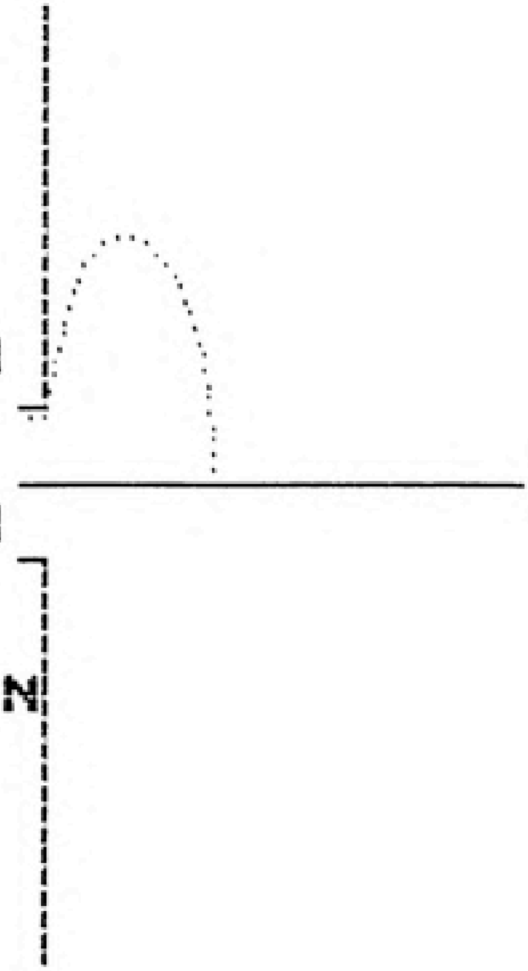

```
QH/QJ= 322.2222
VH/VJ= 1.341196
DH/DJ= 15.5
(Z/D)= 1.516129

QH= 145 CFM
VH= 1770.505 FPM
RH= .1614583 FT

QJ= .45 CFM
VJ= 1320.095 FPM
JETX= 5.875 IN
JETY= 0 IN
ANG= 90 DEG
JET ORIG=-.465 IN
JETD= .25 IN

XDRFT= 25 FPM
XDFANG= 90 DEG

PRINT
ANOTHER(Y/N)?
```

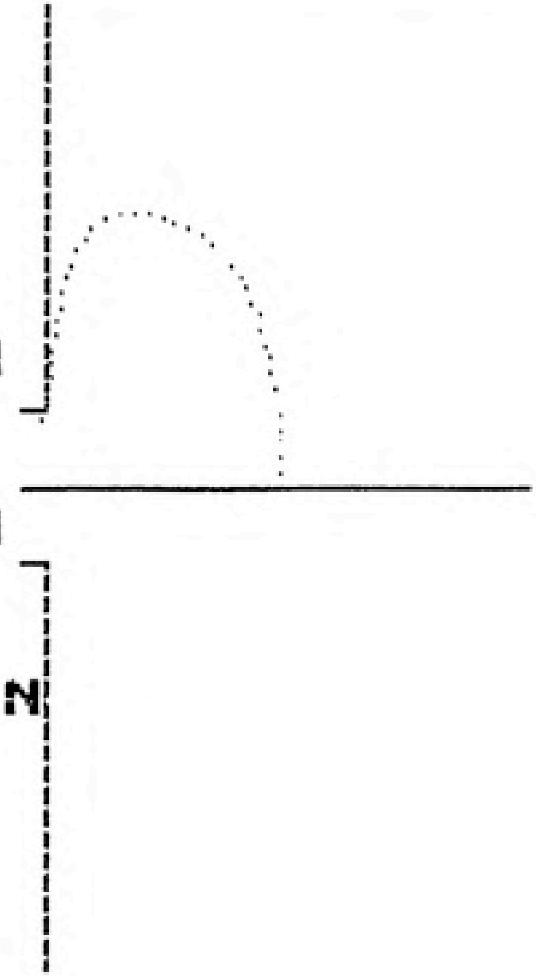

APPENDIX C

EXPERIMENTAL DATA, CALIBRATION THEREOF, AND EFFICIENCY CALCULATIONS

Calibration of Experimental Data & Efficiency Calculation

z	d	regress y	m	exp.peak x	b	theoret. max	ef=y/max	avg.eff.	stdeveff	run
2.5	3.875	241.3756	2.47635	98	-1.3067	246.33	97.98871	95.97811	1.421705	78a
		233.9465		95			94.97282			
		231.4702		94			93.96752			
		238.8992		97			96.98341			
		236.4229		96			95.97811			
3		211.6594		86			85.92514	79.29017	4.477808	78b
		204.2303		83			82.90924			
		191.8486		78			77.88275			
		181.9432		74			73.86156			
		186.8959		76			75.87216			
3.5		157.1797		64			63.80859	60.99375	11.39849	78c
		110.1290		45			44.70793			
		139.8452		57			56.77150			
		147.2743		60			59.78739			
		196.8013		80			79.89335			
4		139.8452		57			56.77150	49.93548	4.689474	78d
		117.5581		48			47.72382			
		117.5581		48			47.72382			
		107.6527		44			43.70263			
		132.4162		54			53.75561			
4.5		120.0344		49			48.72912	41.69203	11.67184	78e
		97.7473		40			39.68144			
		97.7473		40			39.68144			
		142.3216		58			57.77680			
		55.64935		23			22.59138			
5		97.7473		40			39.68144	29.22634	5.600871	78f
		72.9838		30			29.62846			
		68.0311		28			27.61787			
		63.0784		26			25.60727			
		58.1257		24			23.59667			
2		336.4977	3.58133	93	3.43405	361.567	93.06649	98.01900	2.582914	77a
		361.5670		100			100.0000			
		361.5670		100			100.0000			
		357.9857		99			99.00951			
		354.4043		98			98.01900			
2.5		336.4977		93			93.06649	92.07599	3.373529	77b
		311.4284		86			86.13297			
		340.0790		94			94.05699			
		329.3350		91			91.08549			
		347.2417		96			96.03800			
3		282.7777		78			78.20895	78.01085	3.094428	77c
		282.7777		78			78.20895			
		261.2898		72			72.26594			
		293.5217		81			81.18046			
		289.9404		80			80.18996			
3.5		279.1964		77			77.21845	67.51153	5.651942	77d

Calibration of Experimental Data & Efficiency Calculation

z	d	regress y	m	exp.peak x	b	theoret. max	ef=y/max	avg.eff.	stdeveff	run
		221.8951		61			61.37041			
		254.1271		70			70.28494			
		232.6391		64			64.34192			
		232.6391		64			64.34192			
4		232.6391		64			64.34192	59.98371	5.962791	77e
		203.9885		56			56.41790			
		243.3831		67			67.31343			
		221.8951		61			61.37041			
		182.5005		50			50.47489			
4.5		146.6872		40			40.56986	45.52237	5.241246	77f
		153.8499		42			42.55087			
		150.2685		41			41.56036			
		196.8258		54			54.43690			
		175.3378		48			48.49388			
5		175.3378		48			48.49388	36.21165	8.230115	77g
		157.4312		43			43.54137			
		114.4552		31			31.65534			
		103.7112		28			28.68383			
		103.7112		28			28.68383			
2		163.1203	1.73623	93	1.651	175.274	93.06593	92.86782	0.741282	76a
		164.8566		94			94.05651			
		163.1203		93			93.06593			
		161.3841		92			92.07535			
		161.3841		92			92.07535			
2.5		157.9117		90			90.09419	89.89607	4.491602	76b
		163.1203		93			93.06593			
		168.3290		96			96.03767			
		145.7580		83			83.16013			
		152.7030		87			87.12245			
3		119.7146		68			68.30142	66.32026	5.352802	76c
		119.7146		68			68.30142			
		104.0885		59			59.38620			
		130.1320		74			74.24490			
		107.5610		61			61.36736			
3.25		123.1871		70			70.28258	58.98996	7.159642	76d
		90.19873		51			51.46155			
		112.7697		64			64.33910			
		97.14365		55			55.42387			
		93.67119		53			53.44271			
3.5		69.36397		39			39.57459	41.75386	5.582516	76e
		79.78135		45			45.51807			
		67.62774		38			38.58401			
		88.4625		50			50.47097			
		60.68282		34			34.62168			
4		46.79298		26			26.69704	39.57459	18.37253	76f
		114.5059		65			65.32968			
		43.32052		24			24.71588			
		39.84806		22			22.73472			
		102.3523		58			58.39562			
4.5		38.11183		21			21.74414	26.69704	9.186265	76g
		24.22199		13			13.81949			

Calibration of Experimental Data & Efficiency Calculation

z	d	regress y	m	exp.peak x	b	theoret. max	ef=y/max	avg.eff.	stdeveff	run
		71.1002		40			40.56517			
		57.21036		32			32.64052			
		43.32052		24			24.71588			
3		144.3033	1.432617	100	1.04164	144.304	99.99954	99.99954	0	98a
		144.3033		100			99.99954			
		144.3033		100			99.99954			
		144.3033		100			99.99954			
		144.3033		100			99.99954			
3.25		107.0552		74			74.18733	72.99600	4.322857	98b
		115.651		80			80.14400			
		101.3248		70			70.21623			
		105.6226		73			73.19456			
		97.02697		67			67.23789			
3.5		78.40295		54			54.33179	51.35346	9.206635	98c
		49.75061		34			34.47625			
		85.56604		59			59.29568			
		85.56604		59			59.29568			
		71.23987		49			49.36791			
4		65.50940		45			45.39680	32.88781	9.939676	98d
		62.64417		43			43.41125			
		29.69398		20			20.57737			
		44.02015		30			30.50514			
		35.42444		24			24.54848			
4.5		75.53772		52			52.34624	32.09359	11.10136	98e
		48.31800		33			33.48348			
		32.55921		22			22.56293			
		44.02015		30			30.50514			
		31.12659		21			21.57015			
5		32.55921		22			22.56293	21.37159	9.042449	98f
		48.31800		33			33.48348			
		41.15491		28			28.51959			
		15.36781		10			10.64960			
		16.80042		11			11.64238			
2.5		143.4793	1.79844	78	3.201	183.064	78.37658	83.87808	4.241465	97a
		159.6652		87			87.21828			
		148.8746		81			81.32382			
		165.0606		90			90.16551			
		150.6730		82			82.30623			
3		111.1074		60			60.69320	59.51430	8.391419	97b
		125.4949		68			68.55248			
		93.123		50			50.86909			
		89.52612		48			48.90427			
		125.4949		68			68.55248			
3.5		138.084		75			75.42935	51.19656	16.14929	97c
		91.32456		49			49.88668			(6)
		53.55732		28			29.25606			
		64.34796		34			35.15052			
		93.123		50			50.86909			
		121.8980		66			66.58766			
4		30.1776		15			16.48472	33.06290	10.99946	97d
		39.1698		20			21.39677			(8)

Calibration of Experimental Data & Efficiency Calculation

z	d	regress y	m	exp.peak x	b	theoret. max	ef=y/max	avg.eff.	stdeveff	run
		69.74328		37			38.09775			
		67.94484		36			37.11534			
		78.73548		42			43.00981			
		46.36356		24			25.32642			
		57.1542		30			31.22088			
		94.92144		51			51.85150			
4.5		75.1386		40			41.04498	34.65932	10.95068	97e
		37.37136		19			20.41436			(6)
		60.75108		32			33.18570			
		98.51832		53			53.81632			
		44.56512		23			24.34401			
		64.34796		34			35.15052			
5		31.97604		16			17.46713	19.62844	8.086855	97f
		46.36356		24			25.32642			
		58.95264		31			32.20329			
		22.98384		11			12.55508			
		19.38696		9			10.59026			
2		176.7998	1.7298	100	3.81985	176.8	99.99991	99.60855	0.782714	95a
		176.7998		100			99.99991			
		176.7998		100			99.99991			
		176.7998		100			99.99991			
		173.3402		98			98.04312			
2.5		138.7442		78			78.47525	83.56290	3.239059	95b
		143.9336		81			81.41043			
		152.5826		86			86.30240			
		154.3124		87			87.28079			
		149.1230		84			84.34561			
3		71.28205		39			40.31790	46.77529	5.272443	95c
		76.47145		42			43.25308			
		83.39065		46			47.16665			
		83.39065		46			47.16665			
		98.95885		55			55.97220			
3.5		57.44365		31			32.49075	30.53396	2.143553	95d
		52.25425		28			29.55557			
		52.25425		28			29.55557			
		59.17345		32			33.46914			
		48.79465		26			27.59878			
4		26.30725		13			14.87966	18.01052	4.436343	95e
		28.03705		14			15.85805			
		38.41585		20			21.72842			
		22.84765		11			12.92287			
		43.60525		23			24.66360			
2.5		179.1342	1.794434	100	-0.30916	179.134	100.0001	97.79633	2.717617	130a
		179.1342		100			100.0001			
		168.3676		94			93.98976			
		179.1342		100			100.0001			
		170.1620		95			94.99149			
3		114.5346		64			63.93795	76.76005	6.805849	130b
		146.8344		82			81.96904			
		137.8622		77			76.96040			
		148.6288		83			82.97076			

Calibration of Experimental Data & Efficiency Calculation

z	d	regress y	m	exp.peak x	b	theoret. max	ef=y/max	avg.eff.	stdeveff	run
		139.6566		78			77.96213			
3.25		96.59026		54			53.92067	50.51480	7.748992	130c
		64.29045		36			35.88958			
		103.7680		58			57.92758			
		98.38470		55			54.92240			
		89.41253		50			49.91377			
3.5		78.64592		44			43.90340	42.50098	8.584515	130d
		100.1791		56			55.92413			
		80.44036		45			44.90513			
		67.87932		38			37.89304			
		53.52385		30			29.87922			
4		39.16838		22			21.86540	24.46989	4.972443	130e
		44.55168		25			24.87059			
		35.57951		20			19.86195			
		39.16838		22			21.86540			
		60.70158		34			33.88613			
2.5		161.8823	1.59208	100	2.67434	161.884	99.99897	99.99897	0	129a
		161.8823		100			99.99897			
		161.8823		100			99.99897			
		161.8823		100			99.99897			
		161.8823		100			99.99897			
3		99.79122		61			61.64365	66.95439	9.668061	129b
		99.79122		61			61.64365			
		102.9753		63			63.61059			
		99.79122		61			61.64365			
		139.5932		86			86.23039			
3.25		123.6724		76			76.39570	49.25194	13.99985	129c
		58.39714		35			36.07344			
		74.31794		45			45.90814			
		69.5417		42			42.95773			
		72.72586		44			44.92467			
3.5		52.02882		31			32.13956	48.07177	16.42600	129d
		39.29218		23			24.27181			
		98.19914		60			60.66018			
		98.19914		60			60.66018			
		101.3833		62			62.62712			
4		44.06842		26			27.22222	20.33793	5.241072	129e
		26.55554		15			16.40405			
		24.96346		14			15.42058			
		42.47634		25			26.23875			
		26.55554		15			16.40405			
2.5		130.2020	1.293731	100	0.828975	130.2	100.0015	100.0015	0	126a
		130.2020		100			100.0015			
		130.2020		100			100.0015			
		130.2020		100			100.0015			
		130.2020		100			100.0015			
3		70.69044		54			54.29373	72.17942	19.07184	126b
		130.2020		100			100.0015			
		117.2647		90			90.06510			
		79.74656		61			61.24928			
		71.98418		55			55.28738			

Calibration of Experimental Data & Efficiency Calculation

z	d	regress y	m	exp.peak x	b	theoret. max	ef=y/max	avg.eff.	stdeveff	run
3.25		47.40329		36			36.40805	54.88992	13.61842	126c
		82.33402		63			63.23658			
		86.21522		66			66.21752			
		52.57821		40			40.38265			
		88.80268		68			68.20482			
3.5		91.39014		70			70.19212	37.79916	18.12258	126d
		44.81582		34			34.42075			
		18.94120		14			14.54777			
		40.93463		31			31.43981			
		49.99075		38			38.39535			
4		13.76628		10			10.57318	12.56048	2.810463	126e
		21.52867		16			16.53507			
		16.35374		12			12.56048			
		11.17882		8			8.585885			
		18.94120		14			14.54777			
3		203.1016	2.009064	100	2.195281	203.1	100.0008	93.86779	4.781016	195a
		199.0835		98			98.02242			
		176.9838		87			87.14123			
		191.0472		94			94.06563			
		183.0110		90			90.10883			
3.5		160.9113		79			79.22764	82.98659	6.603230	195b
		158.9022		78			78.23844			
		195.0654		96			96.04403			
		162.9204		80			80.21683			
		164.9294		81			81.20603			
4		90.59409		44			44.60566	44.20998	9.582478	195c
		96.62128		47			47.57325			
		102.6484		50			50.54085			
		52.42188		25			25.81087			
		106.6666		52			52.51925			
4.5		96.62128		47			47.57325	33.52662	9.959032	195d
		58.44907		28			28.77847			
		42.37656		20			20.86487			
		86.57596		42			42.62726			
		56.44000		27			27.78927			
5		78.53971		38			38.67046	26.40439	11.74775	195e
		52.42188		25			25.81087			
		28.31311		13			13.94047			
		82.55784		40			40.64886			
		26.30404		12			12.95128			
3.5		155.4185	1.52847	100	2.571589	155.42	99.99909	99.99909	0	193a
		155.4185		100			99.99909			
		155.4185		100			99.99909			
		155.4185		100			99.99909			
		155.4185		100			99.99909			
4		130.9630		84			84.26397	77.37986	12.74690	193b
		94.27978		60			60.66129			
		112.6214		72			72.46263			
		111.0929		71			71.47919			
		152.3616		98			98.03220			
4.5		82.05202		52			52.79373	47.28644	14.40805	193c

Calibration of Experimental Data & Efficiency Calculation

z	d	regress y	a	exp.peak x	b	theoret. max	ef=y/max	avg.eff.	stdeveff	run
		65.23885		41			41.97584			
		39.25486		24			25.25728			
		108.0360		69			69.51230			
		72.88120		46			46.89306			
5		48.42568		30			31.15795	41.38577	9.153964	193d
		54.53956		34			35.09173			(10)
		71.35273		45			45.90962			
		63.71038		40			40.99240			
		65.23885		41			41.97584			
		69.82426		44			44.92618			
		59.12497		37			38.04206			
		83.58049		53			53.77718			
		88.16590		56			56.72751			
		39.25486		24			25.25728			
5.5		23.97016		14			15.42283	24.07714	12.35231	193e
		63.71038		40			40.99240			
		11.74240		6			7.555275			
		33.14098		20			21.32350			
		54.53956		34			35.09173			
3.5		101.8050	1.026046	100	-0.79960	101.8050	99.99999	96.77486	6.450267	189a
		101.8050		100			99.99999			
		101.8050		100			99.99999			
		85.38830		84			83.87432			
		101.8050		100			99.99999			
4		89.49248		88			87.90574	84.07589	8.702633	189b
		73.07574		72			71.78007			
		95.64876		94			93.95287			
		92.57062		91			90.92930			
		77.17993		76			75.81149			
4.25		60.76318		60			59.68582	55.65441	19.04817	189c
		34.08597		34			33.48161			
		34.08597		34			33.48161			
		78.20597		77			76.81934			
		76.15388		75			74.80364			
4.5		56.65900		56			55.65441	32.07062	15.86658	189d
		17.66923		18			17.35594			
		19.72132		20			19.37165			
		47.42458		47			46.58372			
		21.77341		22			21.38736			
5		14.59109		15			14.33238	19.57322	7.278912	189e
		19.72132		20			19.37165			
		13.56504		14			13.32453			
		17.66923		18			17.35594			
		34.08597		34			33.48161			
5		116.2535	1.215357	96	-0.42082	121.115	95.98604	96.18674	2.234842	326a
		112.6074		93			92.97562			
		116.2535		96			95.98604			
		121.1149		100			99.99994			
		116.2535		96			95.98604			
5.5		107.7459		89			88.96172	81.53602	10.93003	326b
		106.5306		88			87.95825			

Calibration of Experimental Data & Efficiency Calculation

z	d	regress y	m	exp.peak x	b	theoret. max	ef=y/max	avg.eff.	stdeveff	run
		77.36206		64			63.87487			
		89.51563		74			73.90961			
		112.6074		93			92.97562			
6		59.13169		49			48.82276	66.68460	12.68352	326c
		72.50063		60			59.86098			
		94.37706		78			77.92351			
		101.6692		84			83.94435			
		76.14670		63			62.87140			
6.5		84.65420		70			69.89572	53.03736	13.15125	326d
		48.19348		40			39.79150			
		81.00813		67			66.88530			
		46.97812		39			38.78802			
		60.34705		50			49.82624			
7		31.17847		26			25.74286	31.42922	5.330914	326e
		31.17847		26			25.74286			(6)
		33.60919		28			27.74981			
		48.19348		40			39.79150			
		42.11669		35			34.77413			
		42.11669		35			34.77413			
7.5		23.88633		20			19.72202	20.47463	2.172584	326f
		28.74776		24			23.73592			(4)
		25.10168		21			20.72549			
		21.45561		18			17.71507			
4		276.0373	2.684206	100	7.6167	275.59	100.1623	99.99999	0.000000	322a
		276.0373		100			100.1623			
		276.0373		100			100.1623			
		276.0373		100			100.1623			
		276.0373		100			100.1623			
4.5		276.0373		100			100.1623	98.60392	3.116752	322b
		254.5636		92			92.37042			
		276.0373		100			100.1623			
		276.0373		100			100.1623			
		276.0373		100			100.1623			
5		265.3004		96			96.26636	98.21433	1.742317	322c
		270.6688		98			98.21433			
		276.0373		100			100.1623			
		265.3004		96			96.26636			
		276.0373		100			100.1623			
5.5		144.5112		51			52.43702	45.37563	11.11314	322d
		157.9322		56			57.30695			(4)
		120.3533		42			43.67116			
		77.40605		26			28.08739			
6		74.72185		25			27.11341	38.47657	11.17138	322e
		80.09026		27			29.06138			(6)
		168.6690		60			61.20289			
		106.9323		37			38.80123			
		109.6165		38			39.77521			
		96.19549		33			34.90529			
6.5		88.14288		30			31.98333	37.24285	8.811202	322f
		106.9323		37			38.80123			
		139.1427		49			50.48905			

Calibration of Experimental Data & Efficiency Calculation

z	d	regress y	m	exp.peak x	b	theoret. max	ef=y/max	avg.eff.	stdeveff	run
		66.66923		22			24.19145			
		112.3007		39			40.74920			
7		74.72185		25			27.11341	30.27886	12.37536	322g
		50.56399		16			18.34754			
		61.30082		20			22.24348			
		147.1954		52			53.41101			
		72.03764		24			26.13942			
4		101.1575	0.9722	98	5.881978	103.102	98.11407	99.62279	0.754359	316a
		103.1019		100			99.99997			
		103.1019		100			99.99997			
		103.1019		100			99.99997			
		103.1019		100			99.99997			
4.5		103.1019		100			99.99997	96.22817	7.543597	316b
		103.1019		100			99.99997			
		103.1019		100			99.99997			
		103.1019		100			99.99997			
		83.65797		80			81.14098			
5		49.63097		45			48.13774	63.97930	9.227426	316c
		72.96377		69			70.76853			
		61.29737		57			59.45314			
		70.04717		66			67.93968			
		75.88037		72			73.59738			
5.5		54.49197		50			52.85249	48.84495	6.613264	316d
		51.57537		47			50.02364			(4)
		56.43637		52			54.73839			
		38.93677		34			37.76529			
6		62.26957		58			60.39609	42.66863	17.19584	316e
		38.93677		34			37.76529			
		65.18617		61			63.22494			
		17.54837		12			17.02040			
		36.02017		31			34.93644			
6.5		59.35297		55			57.56724	30.22170	15.60859	316f
		15.60397		10			15.13450			
		15.60397		10			15.13450			
		30.18697		25			29.27875			
		35.04797		30			33.99349			
7		22.40937		17			21.73515	22.86669	7.599963	316g
		17.54837		12			17.02040			
		38.93677		34			37.76529			
		19.49277		14			18.90630			
		19.49277		14			18.90630			
5		112.5296	1.099967	100	2.53289	115.8375	97.14437	93.72589	2.855057	391a
		112.5296		100			97.14437			
		104.8298		93			90.49733			
		105.9298		94			91.44691			
		107.0297		95			92.39648			
5.5		112.5296		100			97.14437	95.81496	1.761204	391b
		112.5296		100			97.14437			
		107.0297		95			92.39648			
		111.4296		99			96.19480			
		111.4296		99			96.19480			

Calibration of Experimental Data & Efficiency Calculation

z	d	regress y	m	exp.peak x	b	theoret. max	ef=y/max	avg.eff.	stdeveff	run
		116.6323		100			99.99769			
		116.6323		100			99.99769			
		116.6323		100			99.99769			
5.5		116.6323		100			99.99769	97.93095	2.614247	489b
		109.4006		94			93.79746			
		116.6323		100			99.99769			
		111.8112		96			95.86420			
		116.6323		100			99.99769			
6		116.6323		100			99.99769	97.72427	4.546837	489c
		116.6323		100			99.99769			
		116.6323		100			99.99769			
		103.3743		89			88.63060			
		116.6323		100			99.99769			
6.5		81.67937		71			70.02990	79.33025	11.14893	489d
		81.67937		71			70.02990			
		116.6323		100			99.99769			
		87.70574		76			75.19676			
		94.93738		82			81.39699			
7		63.60027		56			54.52932	69.20320	21.61107	489e
		88.91102		77			76.23013			
		116.6323		100			99.99769			
		91.32156		79			78.29688			
		43.11062		39			36.96199			
7.5		66.01082		58			56.59606	60.10953	14.60824	489f
		70.83191		62			60.72955			
		67.21609		59			57.62943			
		99.75848		86			85.53048			
		46.72644		42			40.06211			
8		46.72644		42			40.06211	33.65520	8.068248	489g
		25.03151		24			21.46141			
		51.54753		46			44.19559			
		33.46843		31			28.69501			
		39.49480		36			33.86187			
8.5		26.23679		25			22.49478	23.94150	6.423553	489h
		29.85261		28			25.59490			
		40.70007		37			34.89525			
		17.79987		18			15.26117			
		25.03151		24			21.46141			
5.5		94.94	1.05	92	-1.66	103.34	91.87149	91.46506	7.833579	483a
		83.39		81			80.69479			
		103.34		100			100			
		87.59		85			84.75904			
		103.34		100			100			
6		63.44		62			61.38958	73.78556	12.85872	483b
		63.44		62			61.38958			
		99.14		96			95.93574			
		81.29		79			78.66266			
		73.94		72			71.55022			
6.5		52.94		52			51.22895	59.35746	8.051942	483c
		76.04		74			73.58234			
		55.04		54			53.26107			

Calibration of Experimental Data & Efficiency Calculation

z	d	regress y	m	exp.peak x	b	theoret. max	ef=y/max	avg.eff.	stdeveff	run
		135.4095		70			70.01420			
		150.8745		78			78.01043			
		152.8076		79			79.00996			
		154.7407		80			80.00949			
6		147.0082		76			76.01137	59.41920	9.042280	387e
		94.81410		49			49.02411			
		106.4128		55			55.02128			
		116.0784		60			60.01892			
		110.2790		57			57.02033			
6.5		50.35238		26			26.03495	36.23014	9.616274	387f
		98.68033		51			51.02316			
		60.01797		31			31.03259			
		85.14851		44			44.02646			
		56.15174		29			29.03354			
7		15.55626		8			8.043445	20.63750	6.796793	387g
		46.48615		24			24.03590			
		54.21862		28			28.03401			
		44.55303		23			23.03637			
		38.75368		20			20.03778			
4		100.7442	1.069988	91	3.3753	110.373	91.27613	91.66390	2.572186	379a
		101.8141		92			92.24556			
		106.0941		96			96.12328			
		99.67422		90			90.30670			
		97.53424		88			88.36784			
4.5		95.39426		86			86.42898	86.23510	6.019834	379b
		107.1641		97			97.09270			
		95.39426		86			86.42898			
		88.97434		80			80.61241			
		88.97434		80			80.61241			
5		94.32428		85			85.45955	75.57138	12.28385	379c
		63.29462		56			57.34611			
		88.97434		80			80.61241			
		98.60423		89			89.33727			
		71.85453		64			65.10154			
5.5		29.05501		24			26.32438	39.70250	16.27255	379d
		71.85453		64			65.10154			
		46.17482		40			41.83524			
		51.52476		45			46.68239			
		20.49510		16			18.56895			
6		24.77506		20			22.44666	33.88593	10.51998	379e
		46.17482		40			41.83524			
		41.89486		36			37.95753			
		51.52476		45			46.68239			
		22.63508		18			20.50780			
6.5		10.86521		7			9.844088	17.40563	6.643242	379f
		10.86521		7			9.844088			
		29.05501		24			26.32438			
		20.49510		16			18.56895			
		24.77506		20			22.44666			
3		116.6323	1.205273	100	-3.89505	116.635	99.99769	99.99769	0	489a
		116.6323		100			99.99769			

Calibration of Experimental Data & Efficiency Calculation

z	d	regress y	m	exp.peak x	b	theoret. max	ef=y/max	avg.eff.	stdeveff	run
6		112.5296		100			97.14437	89.35784	6.423527	391c
		99.33001		88			85.74944			
		112.5296		100			97.14437			
		96.03011		85			82.90071			
		97.13007		86			83.85028			
6.5		96.03011		85			82.90071	64.09906	9.746944	391d
		70.73086		62			61.06041			
		70.73086		62			61.06041			
		70.73086		62			61.06041			
		63.03109		55			54.41337			
7		66.33099		58			57.26210	68.27721	9.430986	391e
		75.13073		66			64.85873			
		76.23069		67			65.80830			
		99.33001		88			85.74944			
		78.43063		69			67.70746			
7.5		66.33099		58			57.26210	52.51421	3.343808	391f
		61.93112		54			53.46379			
		60.83115		53			52.51421			
		60.83115		53			52.51421			
		54.23135		47			46.81675			
8		68.53092		60			59.16126	51.37472	9.503372	391g
		55.33132		48			47.76632			
		64.13105		56			55.36295			
		39.93177		34			34.47223			
		69.63089		61			60.11084			
8.5		48.73151		42			42.06886	46.24700	9.080268	391h
		35.53190		30			30.67392			
		57.53125		50			49.66548			
		65.23102		57			56.31252			
		60.83115		53			52.51421			
9		41.03174		35			35.42181	34.28232	3.769716	391i
		36.63187		31			31.62350			
		35.53190		30			30.67392			
		47.63154		41			41.11928			
		37.73184		32			32.57308			
4		172.1388	1.933118	89	0.09132	193.403	89.00524	92.60355	2.331280	387a
		177.9381		92			92.00383			
		185.6706		96			96.00194			
		177.9381		92			92.00383			
		181.8044		94			94.00289			
4.5		189.5368		98			98.00100	95.00241	4.193257	387b
		185.6706		96			96.00194			
		193.4031		100			100.0000			
		170.2057		88			88.00572			
		179.8712		93			93.00336			
5		135.4095		70			70.01420	84.20751	7.436921	387c
		176.0050		91			91.00430			
		170.2057		88			88.00572			
		170.2057		88			88.00572			
		162.4732		84			84.00760			
5.5		170.2057		88			88.00572	79.00996	5.724427	387d

Calibration of Experimental Data & Efficiency Calculation

z	d	regress y	m	exp.peak x	b	theoret. max	ef=y/max	avg.eff.	stdeveff	run
		64.49		63			62.40565			
		58.19		57			56.30927			
7		36.14		36			34.97193	42.49080	14.67640	483d
		43.49		43			42.08438			
		69.74		68			67.48596			
		23.54		24			22.77917			
		46.64		46			45.13257			
7.5		13.04		14			12.61854	20.74704	5.299138	483e
		23.54		24			22.77917			
		25.64		26			24.81130			
		27.74		28			26.84342			
		17.24		18			16.68279			
8		22.49		23			21.76311	16.88600	4.329908	483f
		22.49		23			21.76311			
		16.19		17			15.66673			
		10.94		12			10.58641			
		15.14		16			14.65066			
5		92.8178	0.9986	98	-5.045	94.815	97.89358	99.29786	0.992974	475aII
		94.815		100			100			(3)
		94.815		100			100			
5.5		52.8738		58			55.76522	67.35052	12.95632	475bII
		49.878		55			52.60560			(6)
		84.829		90			89.46791			
		61.8612		67			65.24410			
		58.8654		64			62.08448			
		74.843		80			78.93582			
6		28.9074		34			30.48821	47.10550	14.87622	475cII
		44.885		50			47.33955			(9)
		74.843		80			78.93582			
		26.9102		32			28.38179			
		54.871		60			57.87164			
		30.9046		36			32.59463			
		48.8794		54			51.55239			
		44.885		50			47.33955			
		46.8822		52			49.44597			
6.5		21.9172		27			23.11575	23.95831	12.76774	475dII
		28.9074		34			30.48821			
		6.9382		12			7.317618			
		13.9284		19			14.69008			
		41.8892		47			44.17992			
7		7.9368		13			8.370827	19.42952	9.034502	475eII
		17.9228		23			18.90291			(6)
		10.9326		16			11.53045			
		34.899		40			36.80746			
		18.9214		24			19.95612			
		19.92		25			21.00933			
7.5		17.9228		23			18.90291	13.90017	4.732120	475fII
		6.9382		12			7.317618			(4)
		16.9242		22			17.84970			
		10.9326		16			11.53045			

APPENDIX D

DATA FOR REGRESSION OF LOGIT-TRANSFORMED EFFICIENCY ON [Z/D]; CALCULATION OF ω AND μ

Data for Regression of Logit Efficiency on [Z/D]

	y		x	m	b	y	mu=-b/m=	w=-1/m
efficien	logit eff	Qh/Qj	Z/D	logiteff	regression	predicted	(Z/D)50	spread
0.929	2.567	76	0.516	-5.919	5.539	2.484	0.935799	0.168947
0.899	2.186	76	0.645	-5.919	5.539	1.720		
0.663	0.678	76	0.774	-5.919	5.539	0.957		
0.590	0.364	76	0.839	-5.919	5.539	0.575		
0.418	-0.333	76	0.903	-5.919	5.539	0.193		
0.396	-0.423	76	1.032	-5.919	5.539	-0.571		
0.267	-1.010	76	1.161	-5.919	5.539	-1.335		
						0.000		
0.980	3.902	77	0.516	-5.407	6.027	3.236	1.114666	0.184945
0.921	2.453	77	0.645	-5.407	6.027	2.539		
0.780	1.266	77	0.774	-5.407	6.027	1.841		
0.675	0.731	77	0.903	-5.407	6.027	1.143		
0.600	0.405	77	1.032	-5.407	6.027	0.446		
0.455	-0.180	77	1.161	-5.407	6.027	-0.252		
0.362	-0.566	77	1.290	-5.407	6.027	-0.950		
						0.000		
0.960	3.172	78	0.645	-5.706	6.144	2.463	1.076761	0.175254
0.793	1.343	78	0.774	-5.706	6.144	1.726		
0.610	0.447	78	0.903	-5.706	6.144	0.990		
0.499	-0.003	78	1.032	-5.706	6.144	0.254		
0.417	-0.335	78	1.161	-5.706	6.144	-0.482		
0.292	-0.884	78	1.290	-5.706	6.144	-1.219		
						0.000		
0.996	5.539	95	0.516	-12.836	10.874	4.249	0.847148	0.077905
0.836	1.626	95	0.645	-12.836	10.874	2.593		
0.468	-0.129	95	0.774	-12.836	10.874	0.936		
0.305	-0.822	95	0.903	-12.836	10.874	-0.720		
0.180	-1.516	95	1.032	-12.836	10.874	-2.376		
						0.000		
0.839	1.649	97	0.645	-4.231	3.983	1.253	0.941385	0.236350
0.595	0.385	97	0.774	-4.231	3.983	0.707		
0.512	0.048	97	0.903	-4.231	3.983	0.161		
0.331	-0.705	97	1.032	-4.231	3.983	-0.384		
0.347	-0.634	97	1.161	-4.231	3.983	-0.930		
0.196	-1.410	97	1.290	-4.231	3.983	-1.476		
						0.000		
1.000	12.295	98	0.774			0.000		
0.730	0.994	98	0.839	-4.472	4.33	0.579	0.968246	0.223613
0.514	0.054	98	0.903	-4.472	4.33	0.291		
0.329	-0.713	98	1.032	-4.472	4.33	-0.286		
0.321	-0.749	98	1.161	-4.472	4.33	-0.863		
0.214	-1.303	98	1.290	-4.472	4.33	-1.440		
						0.000		
1.000	16.237	126	0.645			0.000		
0.722	0.953	126	0.774	-11.178	9.593	0.939	0.858203	0.089461
0.549	0.196	126	0.839	-11.178	9.593	0.215		
0.378	-0.498	126	0.903	-11.178	9.593	-0.503		
0.126	-1.940	126	1.032	-11.178	9.593	-1.946		
						0.000		
1.000	11.488	129	0.645			0.000		
0.670	0.706	129	0.774	-7.633	6.579	0.670	0.861915	0.131010
0.493	-0.030	129	0.839	-7.633	6.579	0.177		
0.481	-0.077	129	0.903	-7.633	6.579	-0.315		

Data for Regression of Logit Efficiency on [Z/D]

0.203	-1.365	129	1.032	-7.633	6.579	-1.300		
						0.000		
0.978	3.793	130	0.645	-12.606	11.288	3.155	0.895446	0.079327
0.768	1.195	130	0.774	-12.606	11.288	1.529		
0.505	0.021	130	0.839	-12.606	11.288	0.715		
0.425	-0.302	130	0.903	-12.606	11.288	-0.098		
0.245	-1.127	130	1.032	-12.606	11.288	-1.725		
						0.000		
0.968	3.401	189	0.903	-13.07	14.958	3.153	1.144452	0.076511
0.841	1.664	189	1.032	-13.07	14.958	1.466		
0.557	0.227	189	1.097	-13.07	14.958	0.623		
0.321	-0.751	189	1.161	-13.07	14.958	-0.220		
0.196	-1.413	189	1.290	-13.07	14.958	-1.907		
						0.000		
1.000	11.610	193	0.903			0.000		
0.774	1.230	193	1.032	-5.716	6.911	1.011	1.209062	0.174947
0.473	-0.109	193	1.161	-5.716	6.911	0.273		
0.414	-0.348	193	1.290	-5.716	6.911	-0.464		
0.241	-1.148	193	1.419	-5.716	6.911	-1.202		
						0.000		
0.939	2.728	195	0.774	-7.578	8.294	2.427	1.094484	0.131960
0.830	1.585	195	0.903	-7.578	8.294	1.449		
0.442	-0.233	195	1.032	-7.578	8.294	0.472		
0.335	-0.684	195	1.161	-7.578	8.294	-0.506		
0.264	-1.025	195	1.290	-7.578	8.294	-1.484		
						0.000		
0.996	5.576	316	1.032	-8.139	12.548	4.146	1.541712	0.122865
0.962	3.239	316	1.161	-8.139	12.548	3.096		
0.640	0.574	316	1.290	-8.139	12.548	2.046		
0.488	-0.046	316	1.419	-8.139	12.548	0.996		
0.427	-0.295	316	1.548	-8.139	12.548	-0.054		
0.302	-0.837	316	1.677	-8.139	12.548	-1.105		
0.229	-1.216	316	1.806	-8.139	12.548	-2.155		
						0.000		
1.000	16.118	322	1.032			0.000		
0.986	4.257	322	1.161	-8.71	13.963	3.848	1.603099	0.114810
0.982	4.007	322	1.290	-8.71	13.963	2.724		
0.454	-0.186	322	1.419	-8.71	13.963	1.600		
0.385	-0.469	322	1.548	-8.71	13.963	0.477		
0.372	-0.522	322	1.677	-8.71	13.963	-0.647		
0.303	-0.834	322	1.806	-8.71	13.963	-1.771		
						0.000		
0.962	3.228	326	1.290	-6.709	11.384	2.727	1.696825	0.149053
0.815	1.485	326	1.419	-6.709	11.384	1.862		
0.667	0.694	326	1.548	-6.709	11.384	0.996		
0.530	0.122	326	1.677	-6.709	11.384	0.130		
0.314	-0.780	326	1.806	-6.709	11.384	-0.735		
0.205	-1.357	326	1.935	-6.709	11.384	-1.601		
						0.000		
0.917	2.398	379	1.032	-6.386	9.102	2.510	1.425305	0.156592
0.862	1.835	379	1.161	-6.386	9.102	1.686		
0.756	1.129	379	1.290	-6.386	9.102	0.862		
0.397	-0.418	379	1.419	-6.386	9.102	0.038		
0.339	-0.668	379	1.548	-6.386	9.102	-0.786		
0.174	-1.557	379	1.677	-6.386	9.102	-1.610		
						0.000		

Data for Regression of Logit Efficiency on [Z/D]

0.926	2.527	387	1.032	-5.519	8.823	3.126	1.598659	0.181192
0.950	2.945	387	1.161	-5.519	8.823	2.414		
0.842	1.674	387	1.290	-5.519	8.823	1.702		
0.790	1.326	387	1.419	-5.519	8.823	0.990		
0.594	0.381	387	1.548	-5.519	8.823	0.277		
0.362	-0.565	387	1.677	-5.519	8.823	-0.435		
0.206	-1.347	387	1.806	-5.519	8.823	-1.147		
						0.000		
0.937	2.704	391	1.290	-3.598	7.463	2.820	2.074207	0.277932
0.958	3.131	391	1.419	-3.598	7.463	2.356		
0.894	2.128	391	1.548	-3.598	7.463	1.892		
0.641	0.580	391	1.677	-3.598	7.463	1.428		
0.683	0.767	391	1.806	-3.598	7.463	0.963		
0.525	0.101	391	1.935	-3.598	7.463	0.499		
0.514	0.055	391	2.065	-3.598	7.463	0.035		
0.462	-0.150	391	2.194	-3.598	7.463	-0.429		
0.343	-0.651	391	2.323	-3.598	7.463	-0.894		
						0.000		
0.993	4.952	475	1.290	-9.16	14.964	3.145	1.633624	0.109170
0.674	0.724	475	1.419	-9.16	14.964	1.963		
0.471	-0.116	475	1.548	-9.16	14.964	0.781		
0.240	-1.155	475	1.677	-9.16	14.964	-0.401		
0.194	-1.422	475	1.806	-9.16	14.964	-1.583		
0.139	-1.824	475	1.935	-9.16	14.964	-2.765		
						0.000		
0.915	2.372	483	1.419	-6.113	10.739	2.062	1.756747	0.163585
0.738	1.035	483	1.548	-6.113	10.739	1.274		
0.594	0.379	483	1.677	-6.113	10.739	0.485		
0.425	-0.303	483	1.806	-6.113	10.739	-0.304		
0.207	-1.340	483	1.935	-6.113	10.739	-1.093		
0.169	-1.594	483	2.065	-6.113	10.739	-1.881		
						0.000		
1.000	10.679	489	1.290			0.000		
0.979	3.857	489	1.419	-6.87	13.602	3.851	1.979912	0.145560
0.977	3.760	489	1.548	-6.87	13.602	2.965		
0.793	1.345	489	1.677	-6.87	13.602	2.078		
0.692	0.810	489	1.806	-6.87	13.602	1.192		
0.601	0.410	489	1.935	-6.87	13.602	0.305		
0.337	-0.679	489	2.065	-6.87	13.602	-0.581		
0.239	-1.156	489	2.194	-6.87	13.602	-1.468		

APPENDIX E

LOGIT CAPTURE EFFICIENCY REGRESSION ON [S/D]

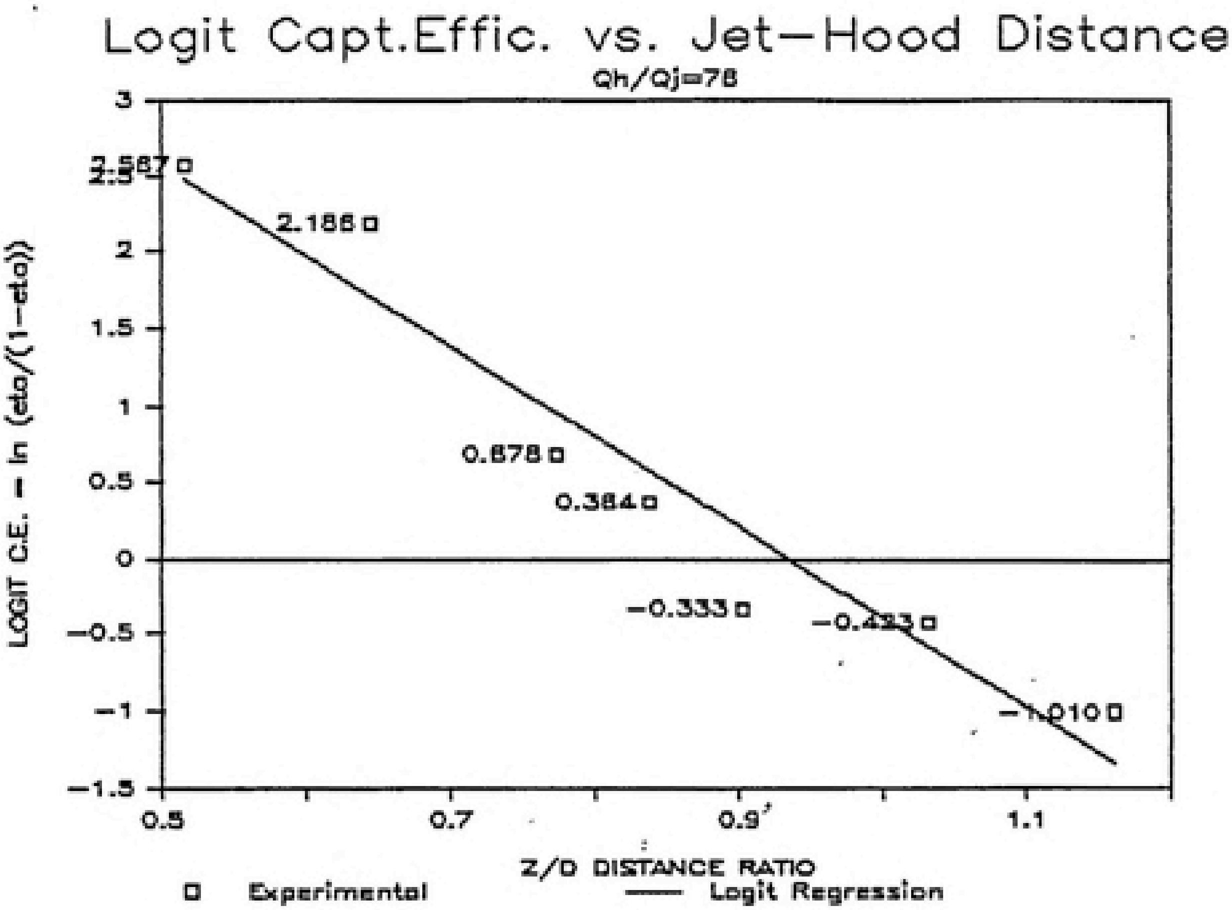

Logit Capt.Effic. vs. Jet-Hood Distance
Qh/Qj=78
LOGIT C.E. = ln (eta/(1-eta))
Z/D DISTANCE RATIO
2.587
2.186
0.678
0.384
-0.333
-0.423
-1.010
3
2.5
2
1.5
1
0.5
0
-0.5
-1
-1.5
0.5
0.7
0.9
1.1
Experimental
Logit Regression

Logit Capt.Effic. vs. Jet–Hood Distance

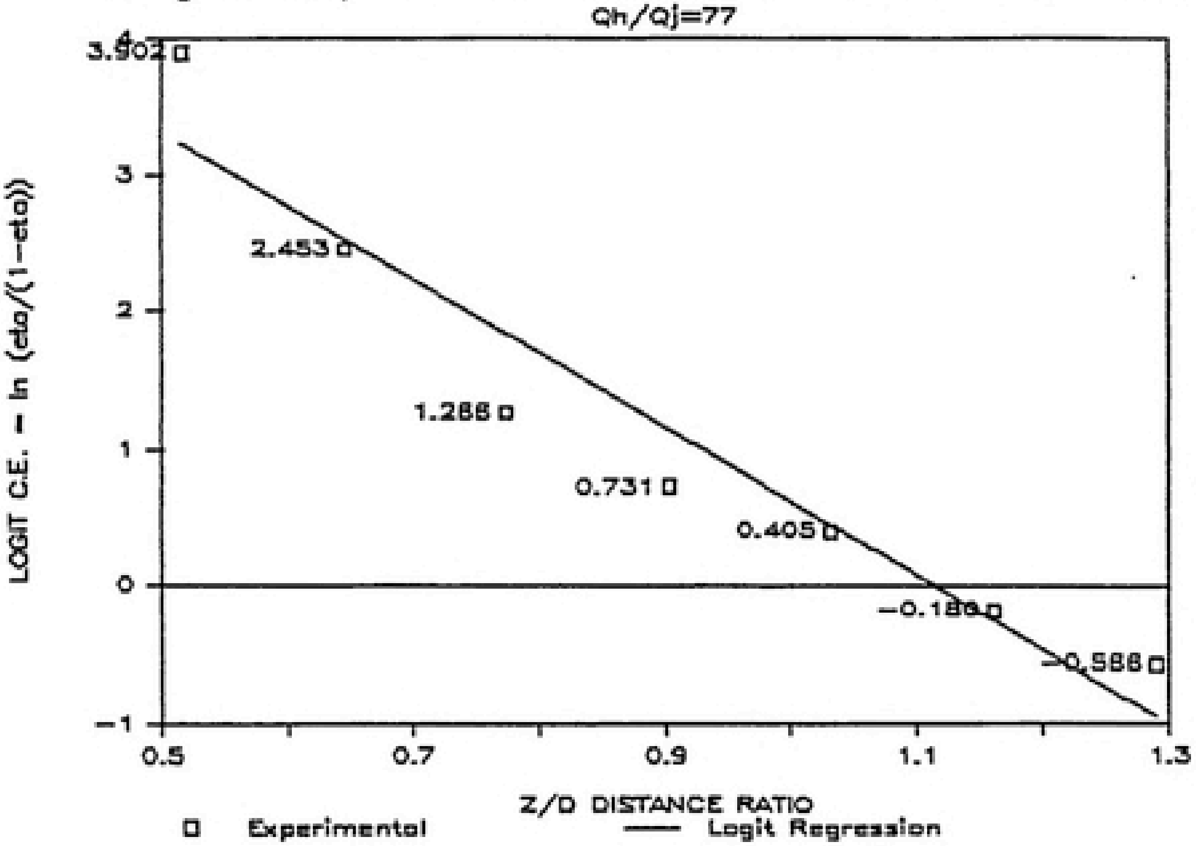

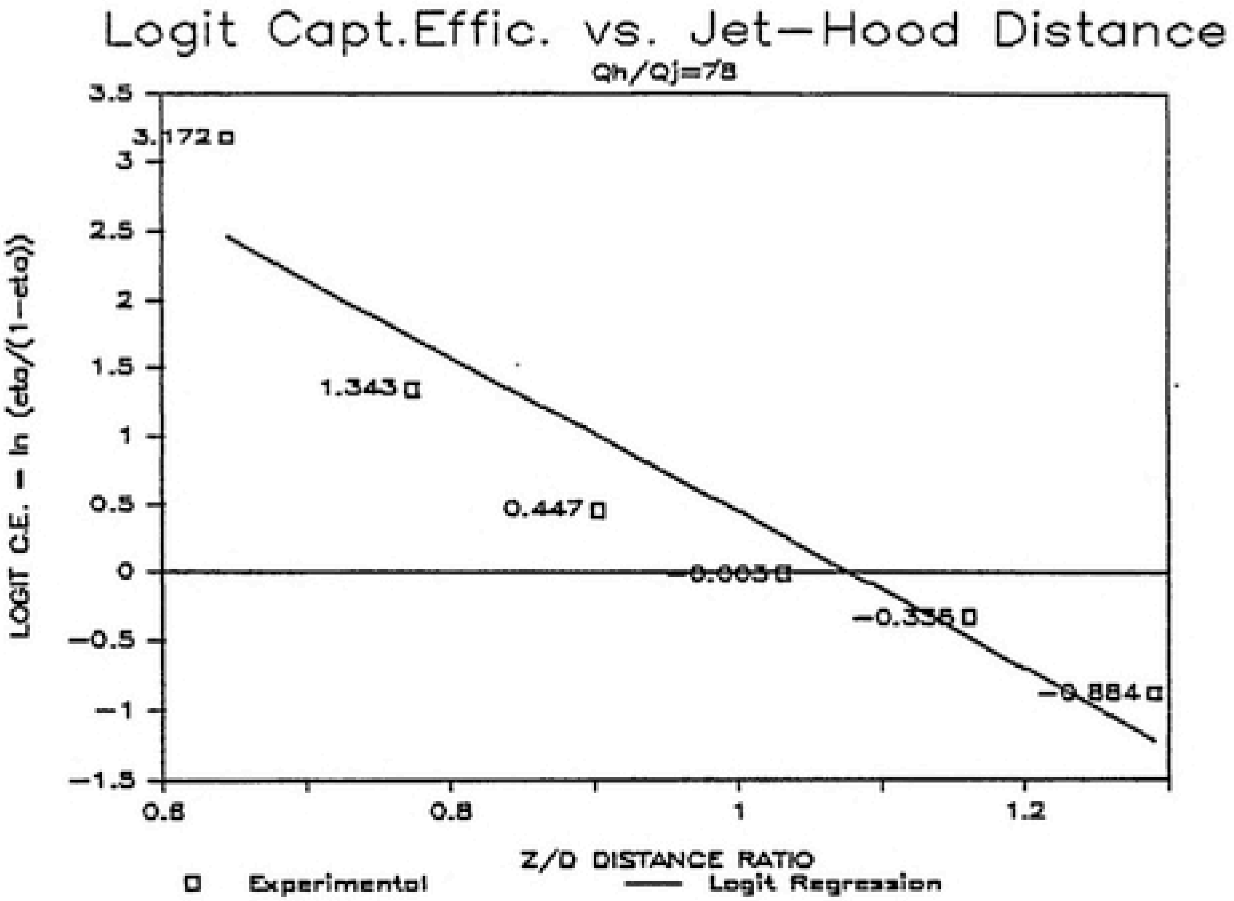
Logit Capt.Effic. vs. Jet-Hood Distance
Qh/Qj=78
LOGIT C.E. = ln (eta/(1-eta))
3.5
3
2.5
2
1.5
1
0.5
0
-0.5
-1
-1.5
3.172
1.343
0.447
-0.003
-0.336
-0.884
0.6
0.8
1
1.2
Z/D DISTANCE RATIO
Experimental
Logit Regression

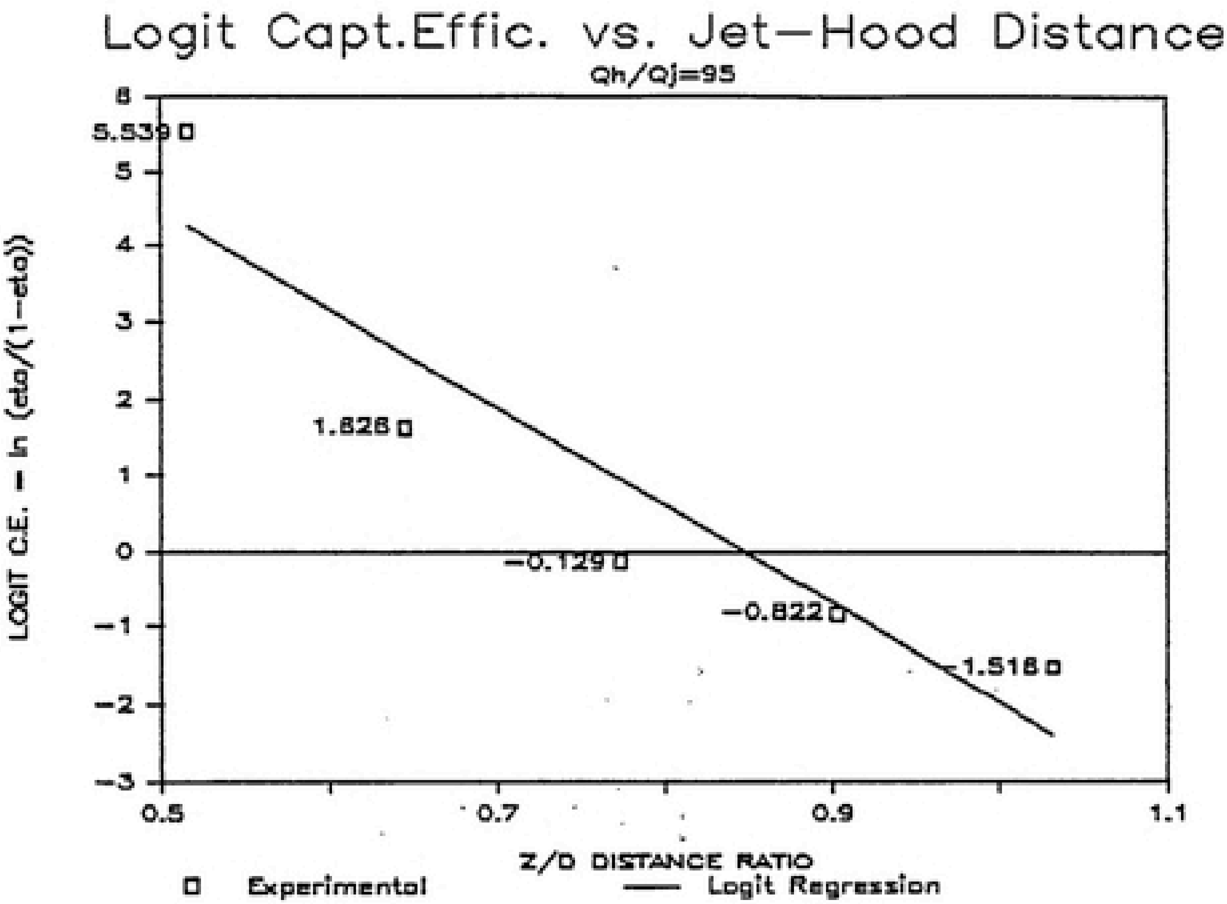

Logit Capt.Effic. vs. Jet–Hood Distance
Qh/Qj=95
LOGIT C.E. = ln (eta/(1–eta))
5.539
1.826
–0.129
–0.822
–1.518
Z/D DISTANCE RATIO
Experimental
Logit Regression

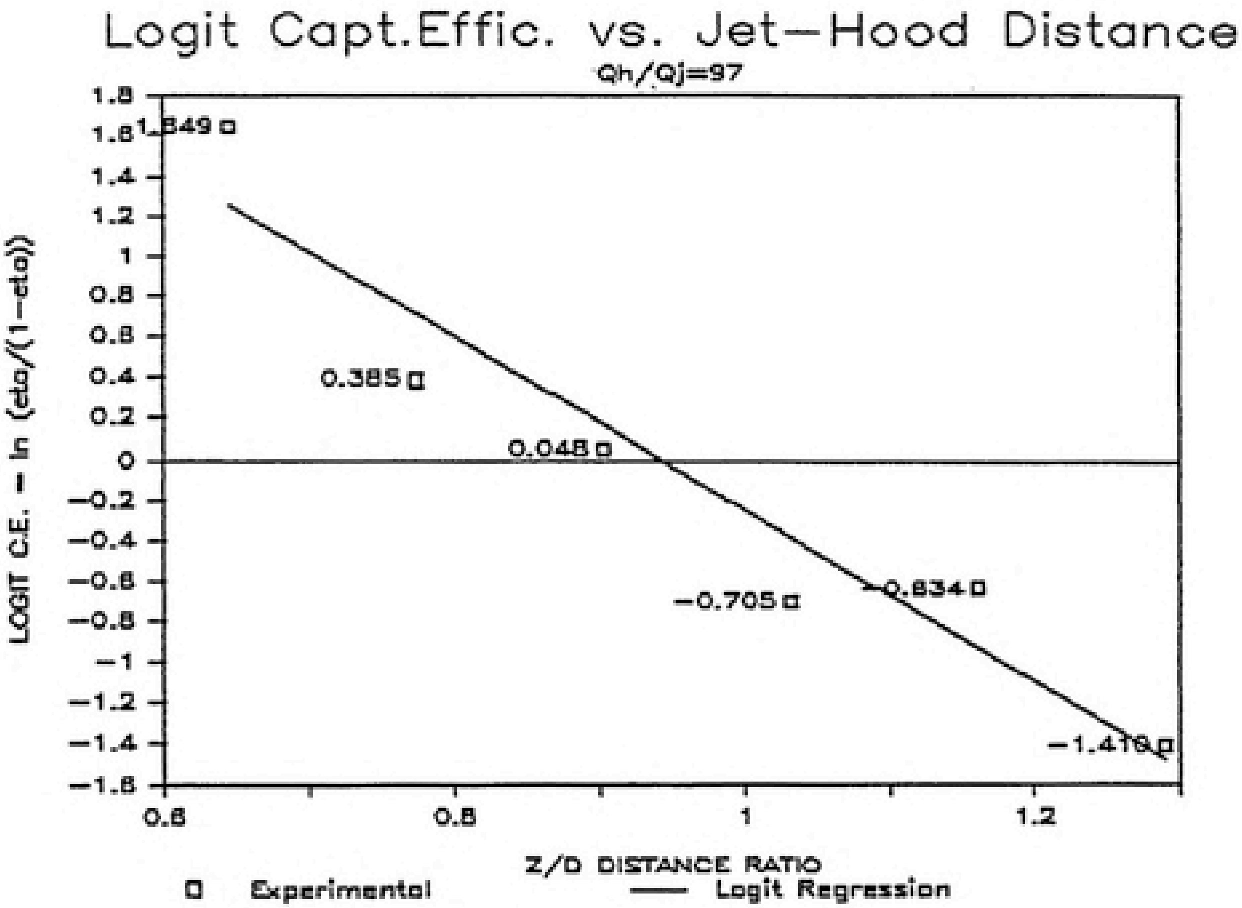

Logit Capt.Effic. vs. Jet-Hood Distance
Qh/Qj=97
LOGIT C.E. = ln (eta/(1-eta))
Z/D DISTANCE RATIO
1.849
0.385
0.048
-0.705
-0.834
-1.416
Experimental
Logit Regression

Logit Capt.Effic. vs. Jet-Hood Distance

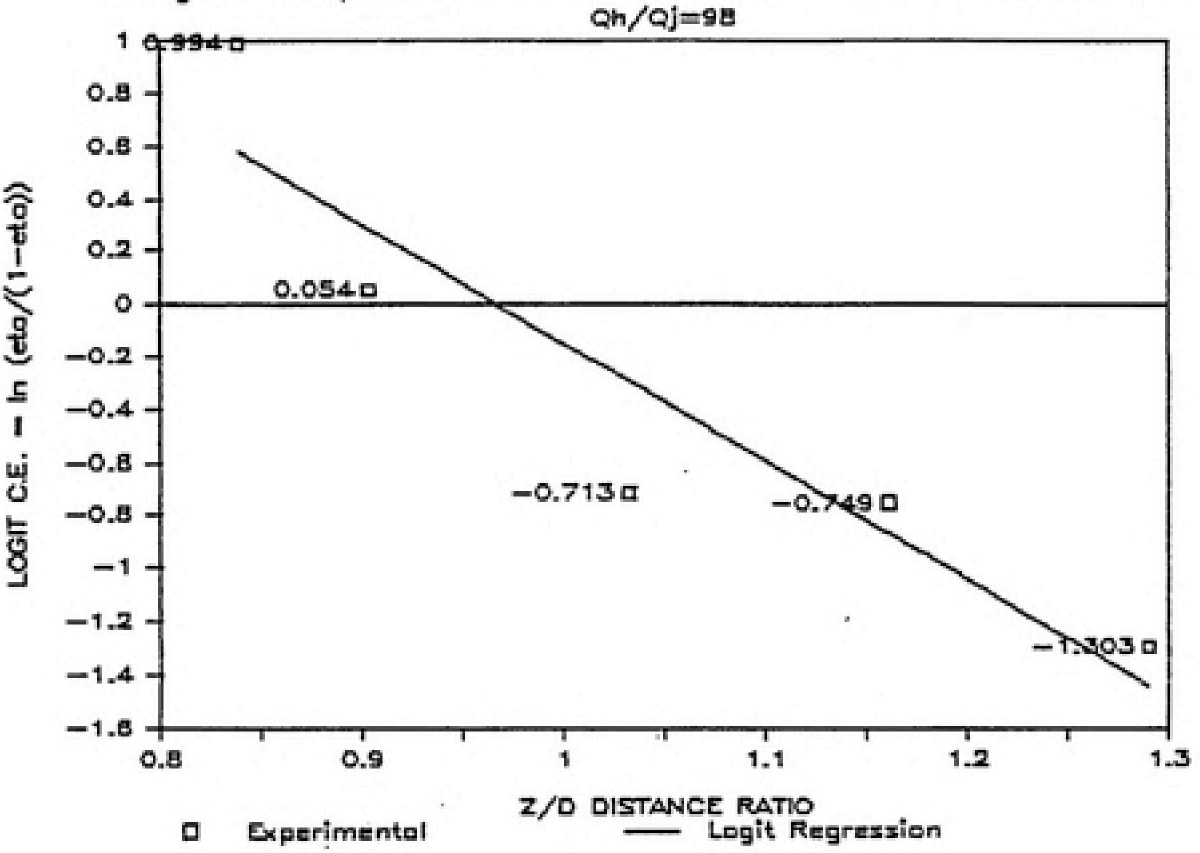

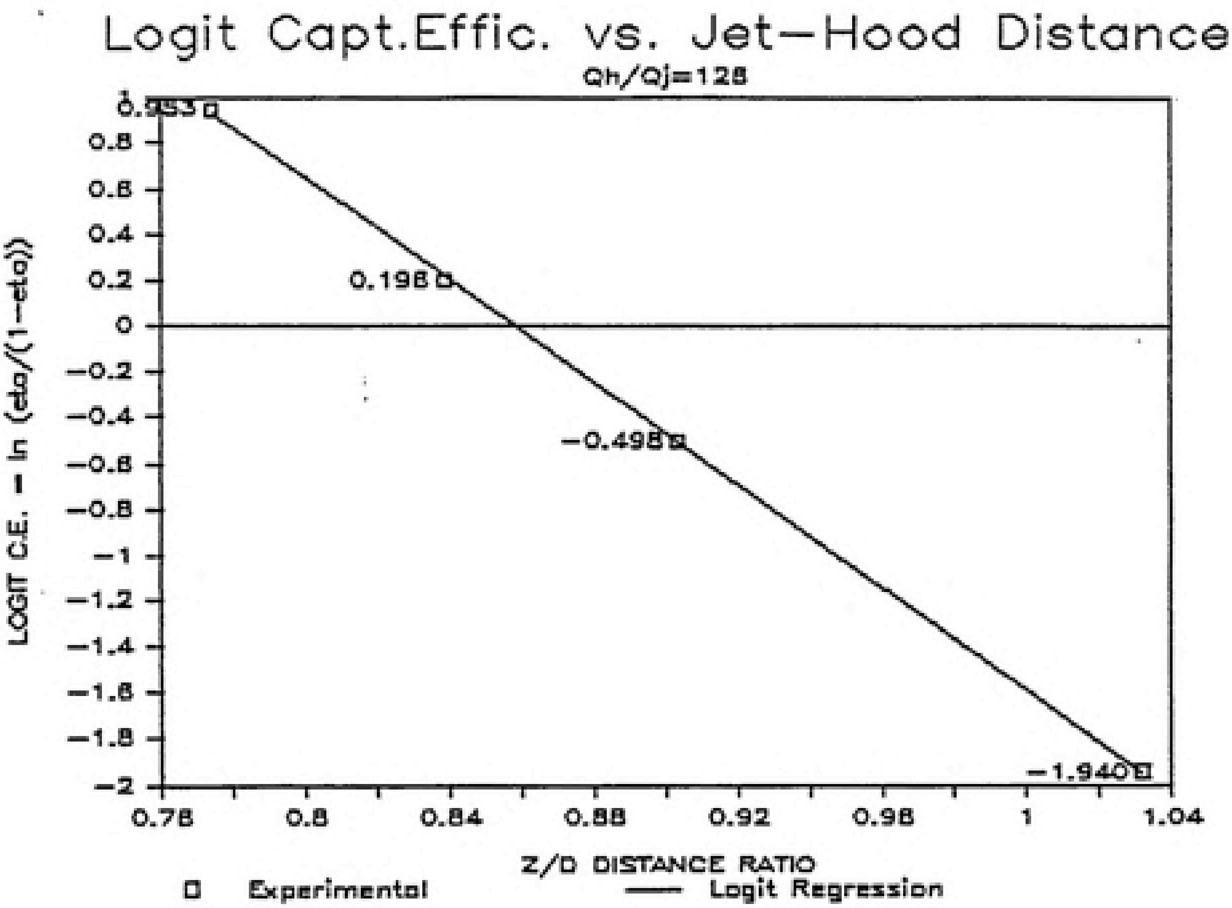

Logit Capt.Effic. vs. Jet-Hood Distance
Qh/Qj=128
LOGIT C.E. = ln (eta/(1-eta))
0.953
0.198
-0.498
-1.940
Z/D DISTANCE RATIO
Experimental
Logit Regression

Logit Capt.Effic. vs. Jet-Hood Distance

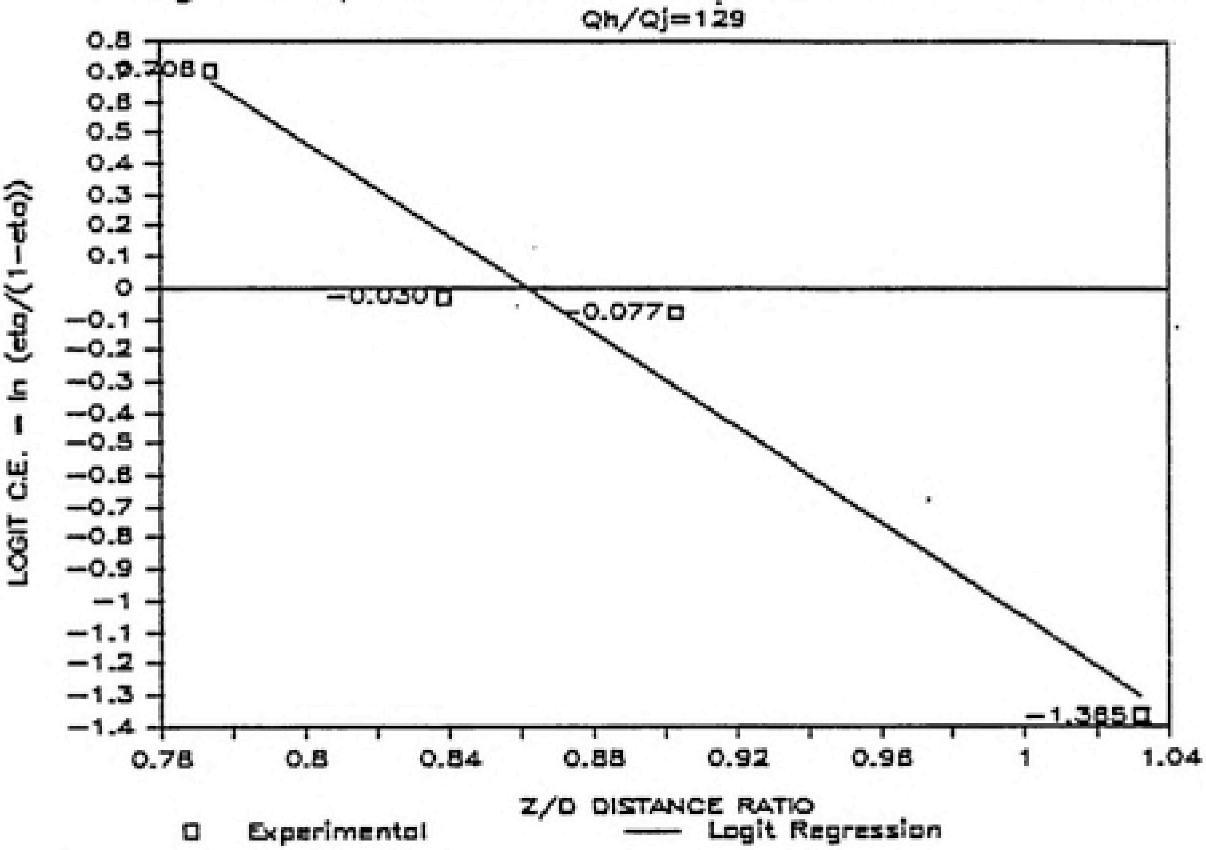

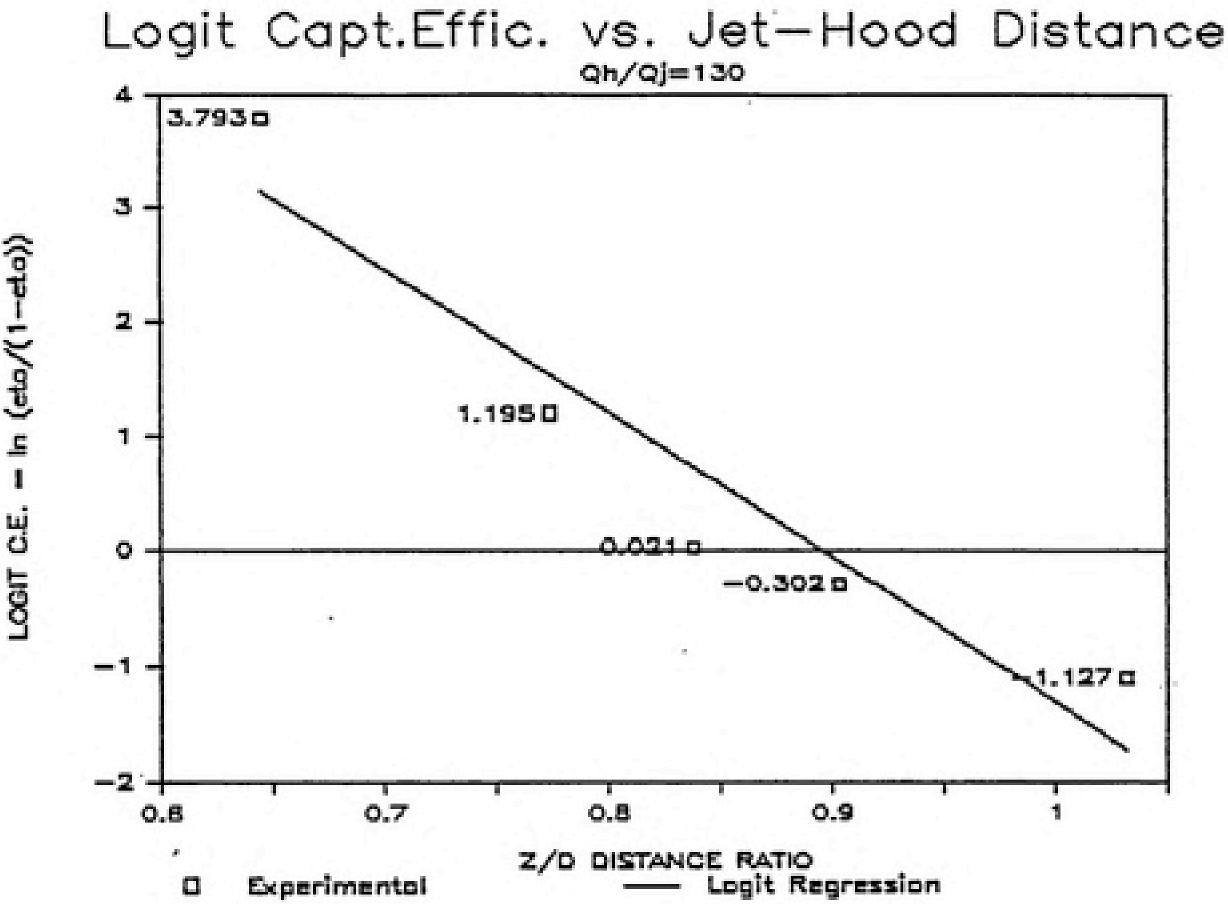

Logit Capt.Effic. vs. Jet-Hood Distance
Qh/Qj=130
LOGIT C.E. = ln (eta/(1-eta))
Z/D DISTANCE RATIO
3.793
1.195
0.021
-0.302
-1.127
4
3
2
1
0
-1
-2
0.6
0.7
0.8
0.9
1
Experimental
Logit Regression

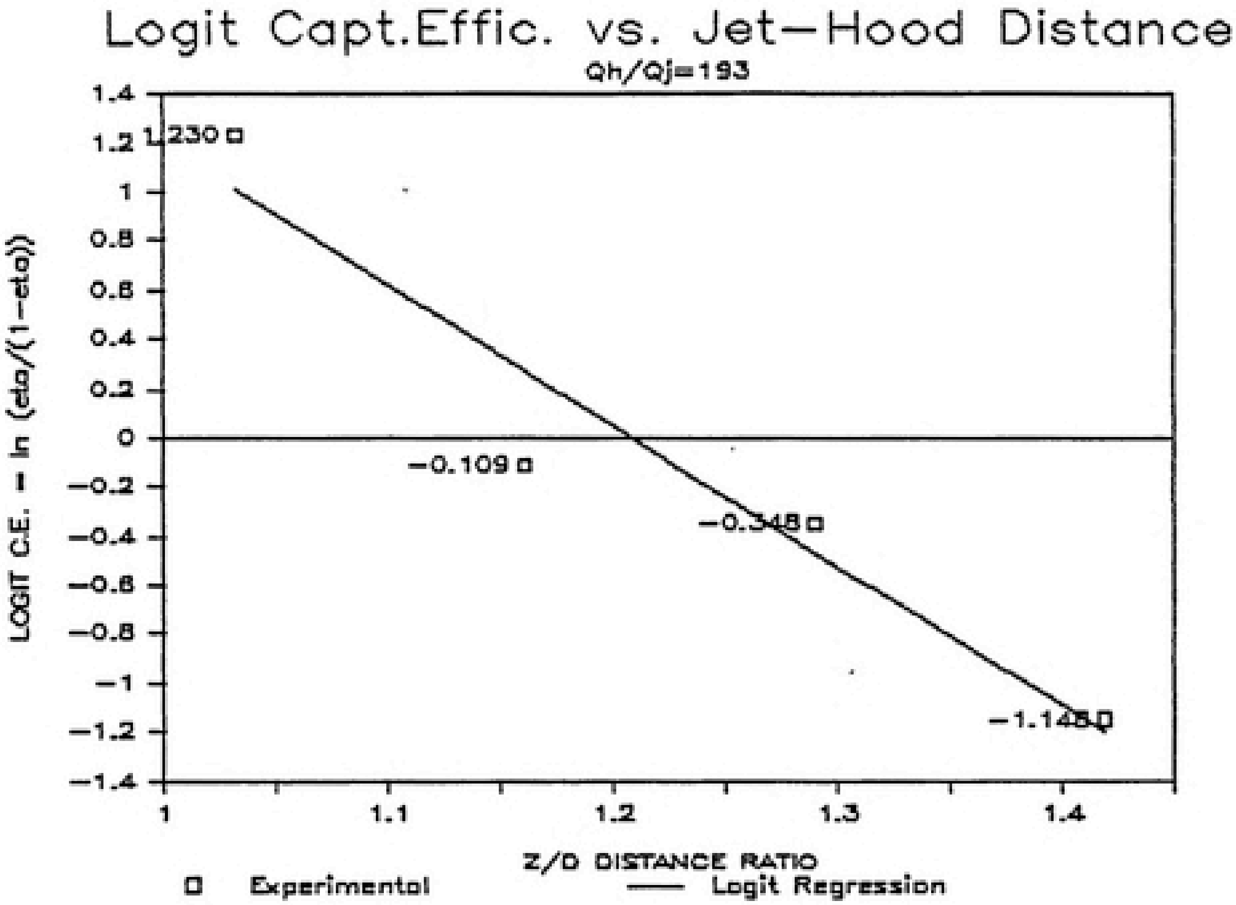
Logit Capt.Effic. vs. Jet−Hood Distance
Qh/Qj=193
LOGIT C.E. = ln (eta/(1−eta))
1.230
−0.109
−0.348
−1.148
Z/D DISTANCE RATIO
Experimental
Logit Regression

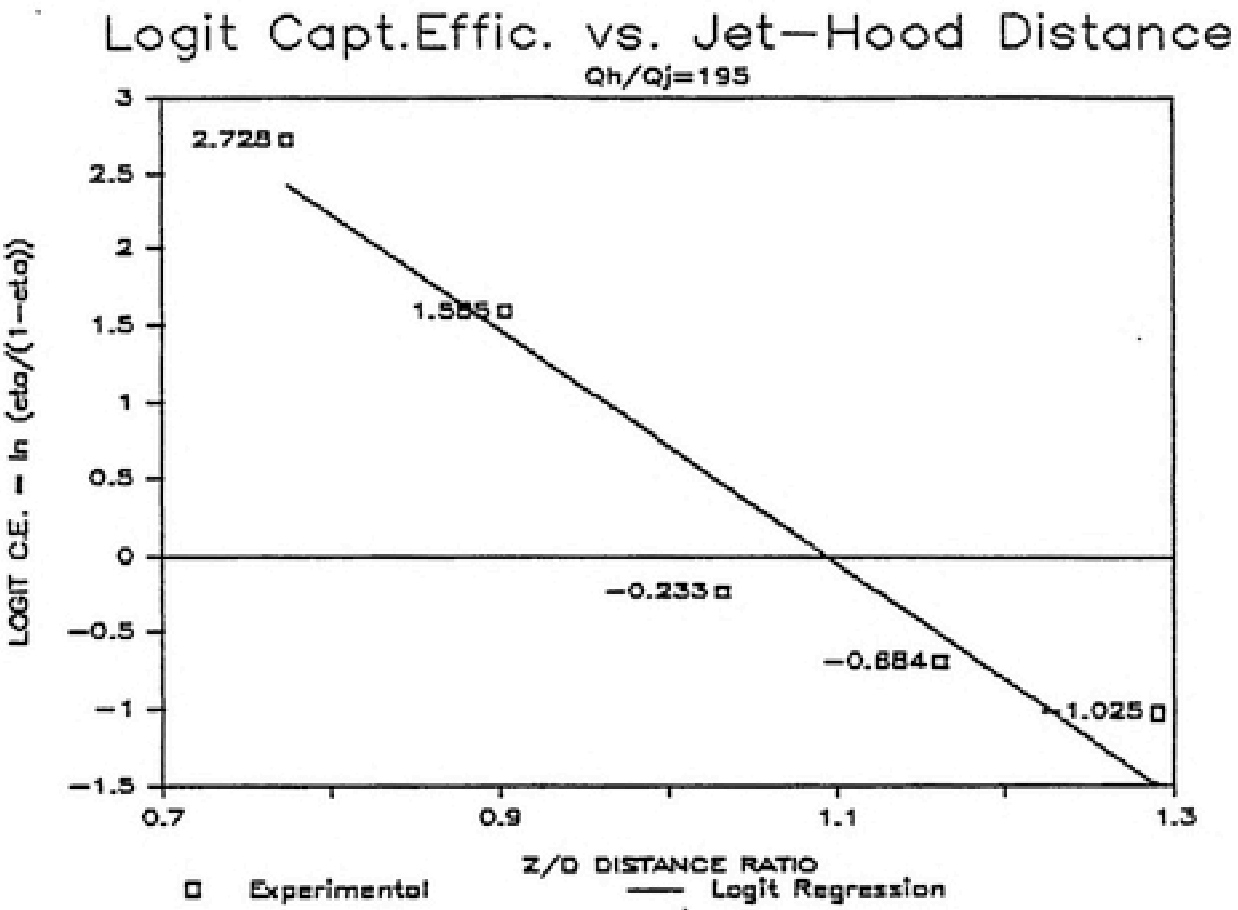

Logit Capt.Effic. vs. Jet-Hood Distance
Qh/Qj=195
LOGIT C.E. = ln (eta/(1-eta))
3
2.5
2
1.5
1
0.5
0
-0.5
-1
-1.5
0.7
0.9
1.1
1.3
2.728
1.585
-0.233
-0.684
-1.025
Z/D DISTANCE RATIO
Experimental
Logit Regression

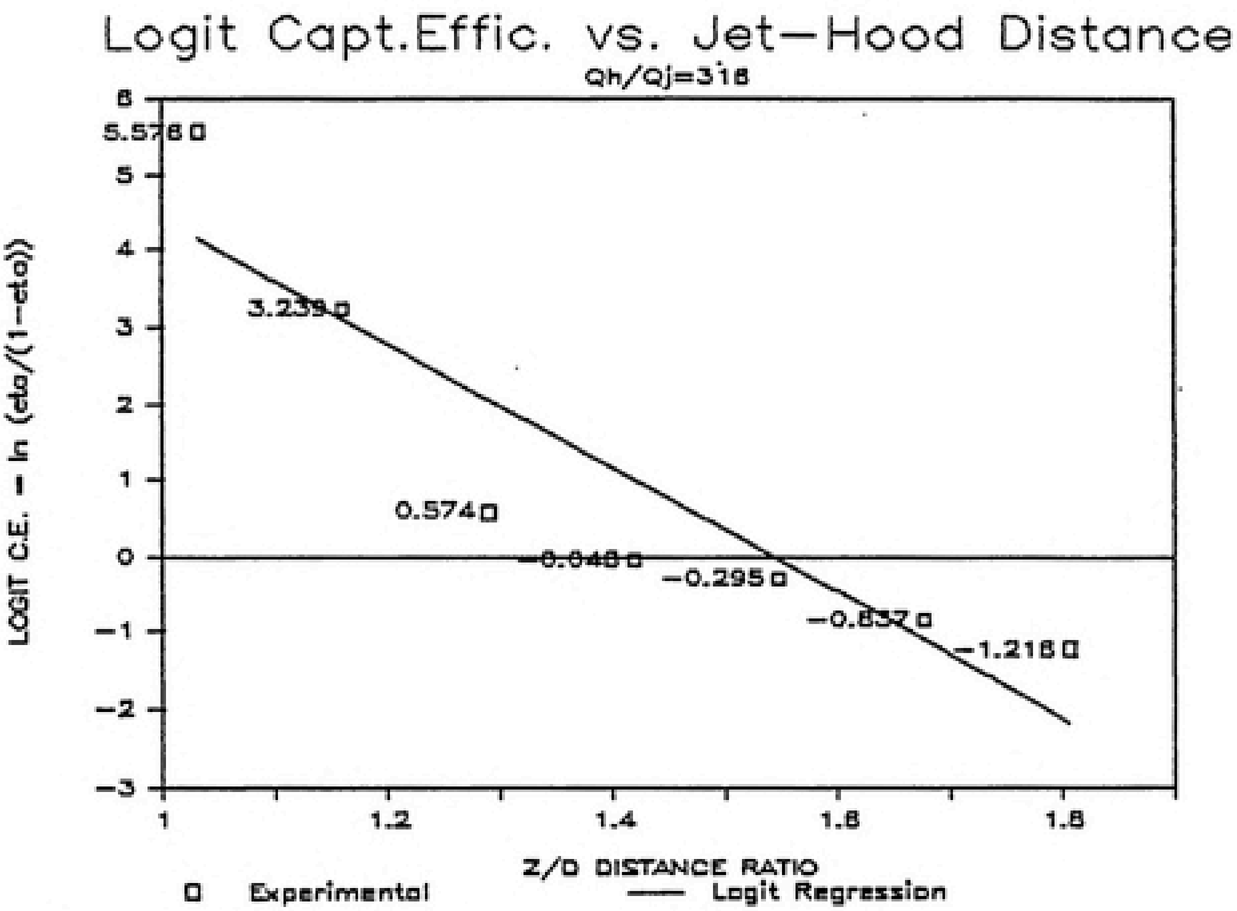
Logit Capt.Effic. vs. Jet-Hood Distance
Qh/Qj=318
LOGIT C.E. = ln (eta/(1-eta))
Z/D DISTANCE RATIO
5.576
3.239
0.574
-0.048
-0.295
-0.837
-1.218
Experimental
Logit Regression

Logit Capt.Effic. vs. Jet-Hood Distance

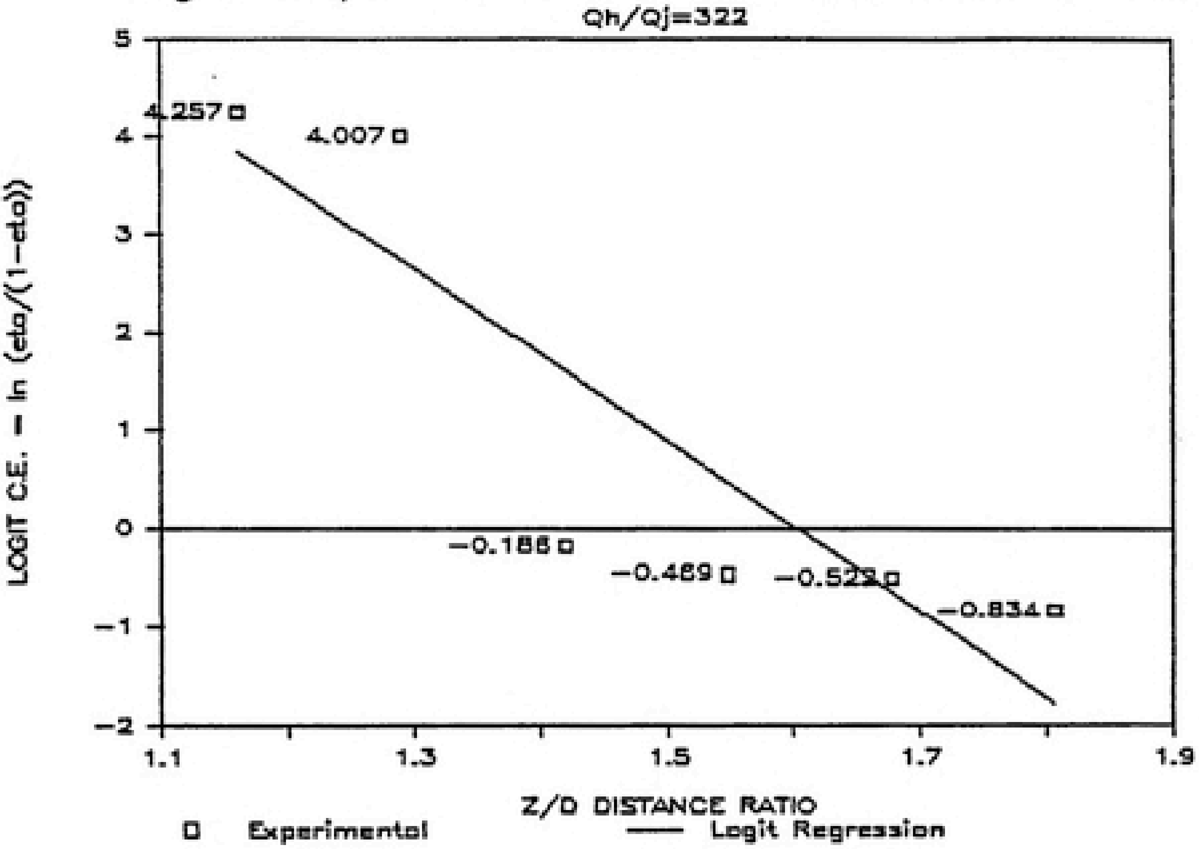

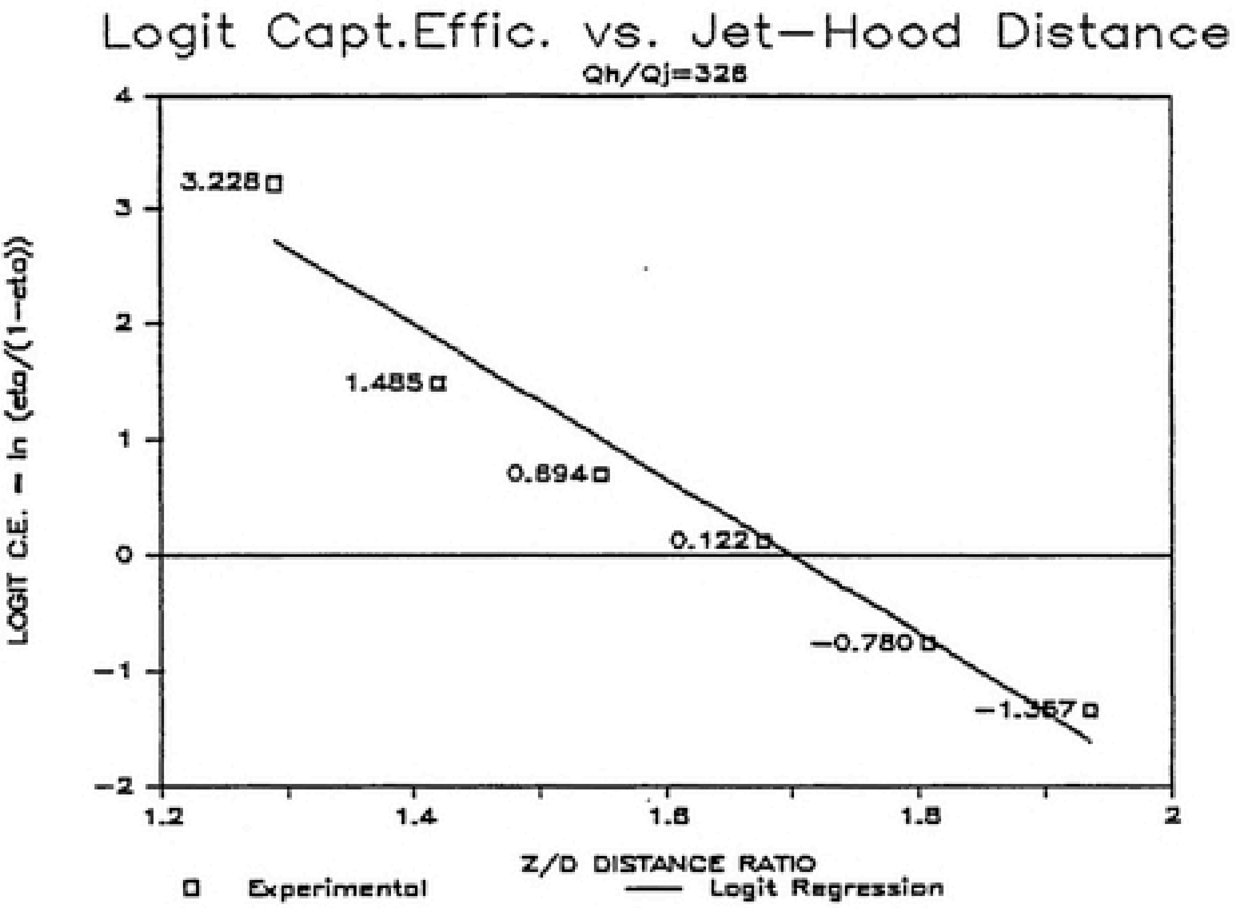
Logit Capt.Effic. vs. Jet-Hood Distance
Qh/Qj=328
LOGIT C.E. = ln (eta/(1-eta))
Z/D DISTANCE RATIO
3.228
1.485
0.894
0.122
-0.780
-1.367
Experimental
Logit Regression

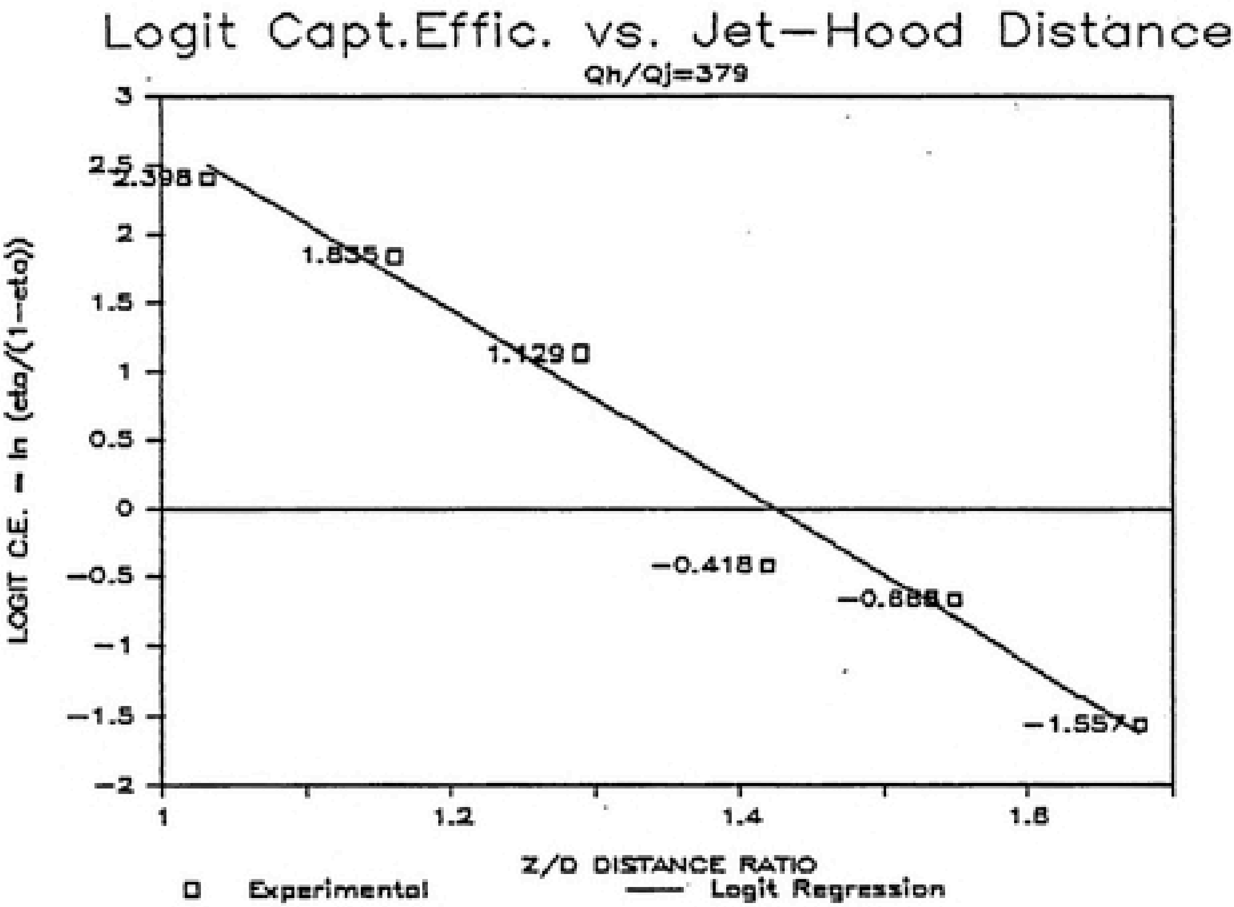

Logit Capt.Effic. vs. Jet-Hood Distance
Qh/Qj=379
LOGIT C.E. = ln (eta/(1-eta))
3
2.5
2
1.5
1
0.5
0
-0.5
-1
-1.5
-2
2.398
1.835
1.129
-0.418
-0.888
-1.557
1
1.2
1.4
1.6
Z/D DISTANCE RATIO
Experimental
Logit Regression

Logit Capt.Effic. vs. Jet–Hood Distance

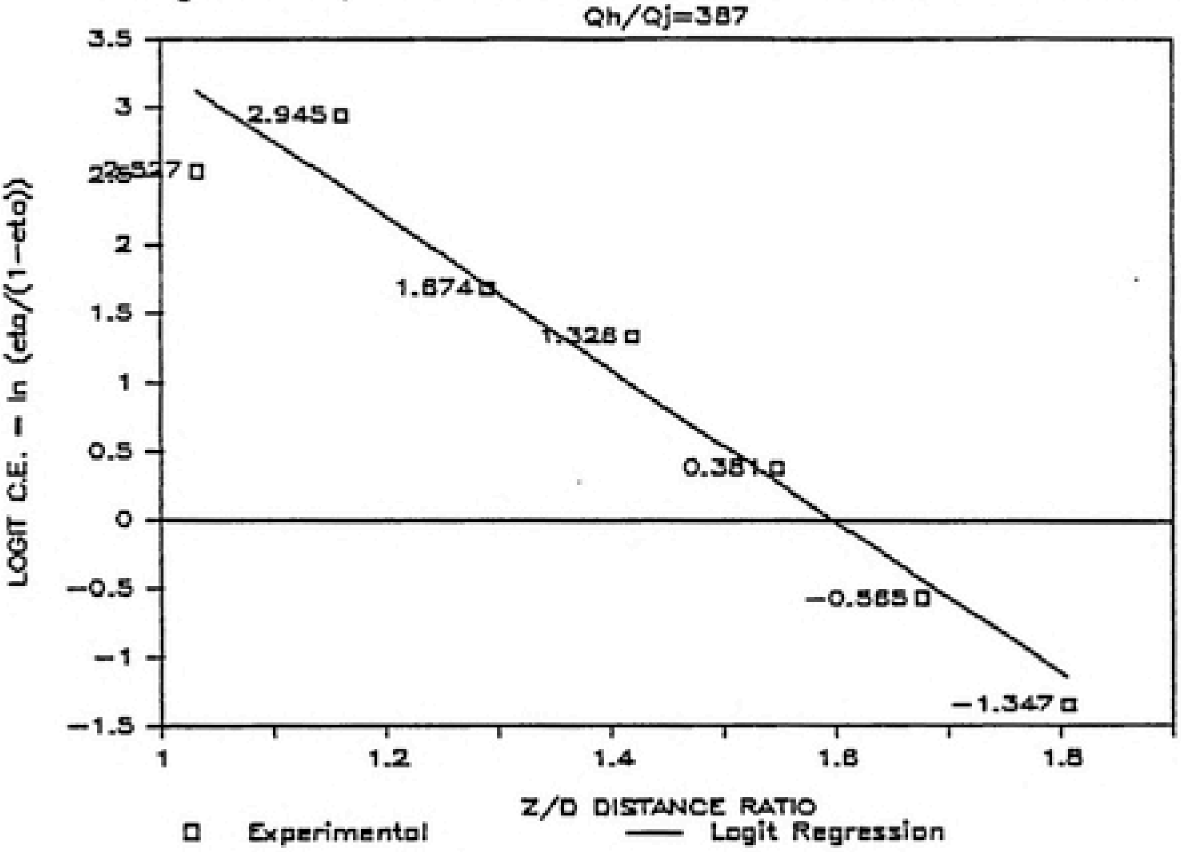

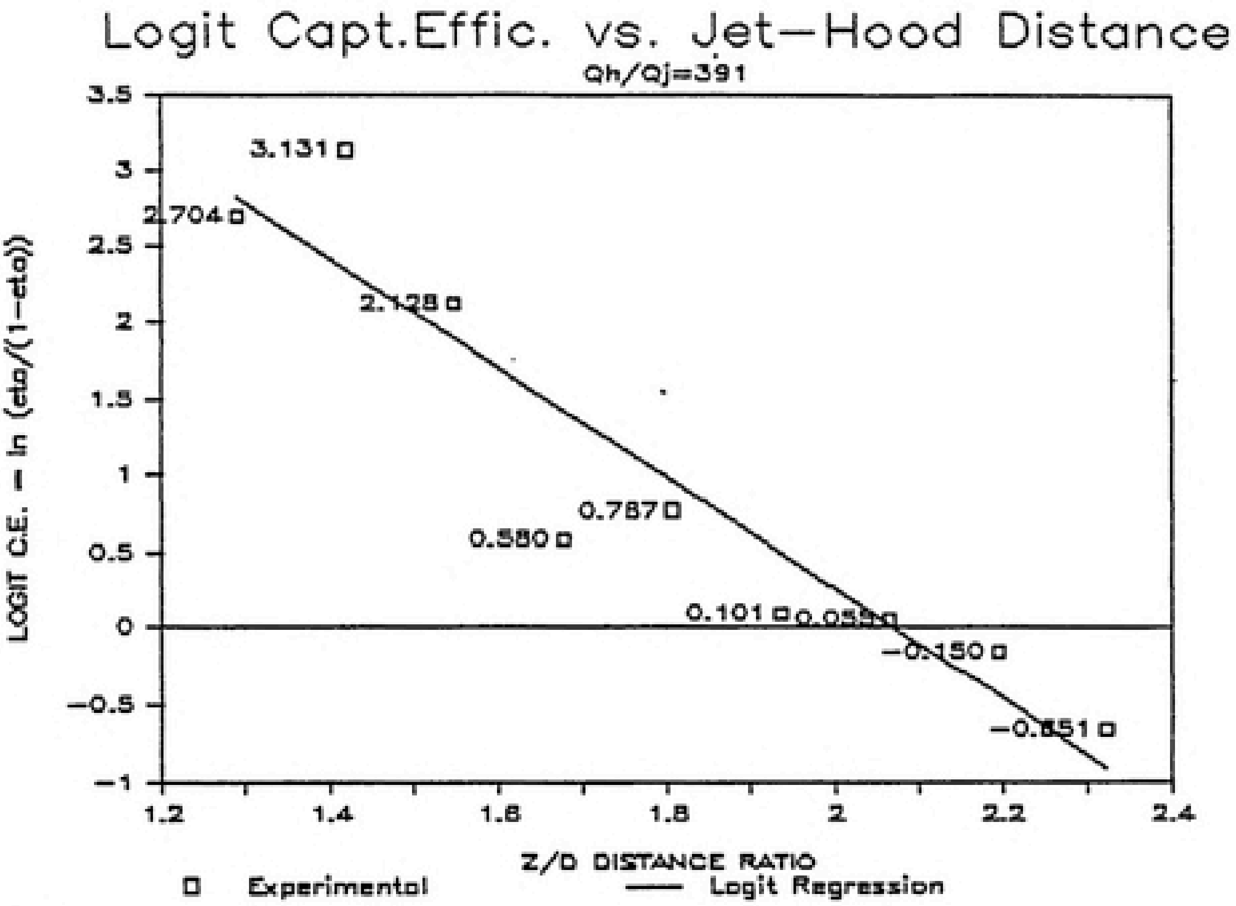

Logit Capt.Effic. vs. Jet-Hood Distance
Qh/Qj=391
LOGIT C.E. = ln (cta/(1-cta))
Z/D DISTANCE RATIO
3.131
2.704
2.128
0.787
0.580
0.101
0.055
-0.150
-0.851
Experimental
Logit Regression

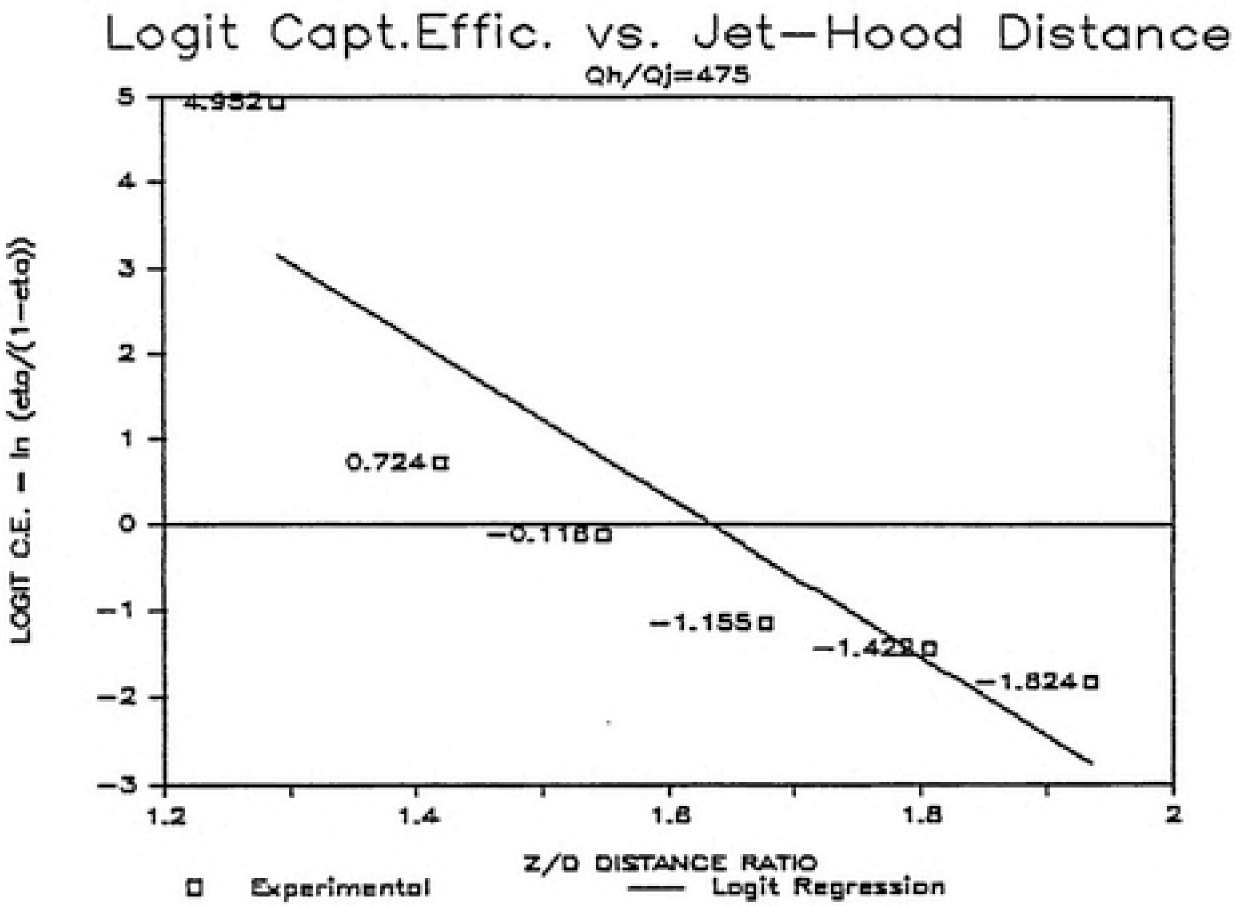

Logit Capt.Effic. vs. Jet-Hood Distance
Qh/Qj=475
LOGIT C.E. = ln (eta/(1-eta))
4.952
0.724
-0.118
-1.155
-1.429
-1.824
5
4
3
2
1
0
-1
-2
-3
1.2
1.4
1.6
1.8
2
Z/D DISTANCE RATIO
Experimental
Logit Regression

Logit Capt.Effic. vs. Jet–Hood Distance

Qh/Qj=483

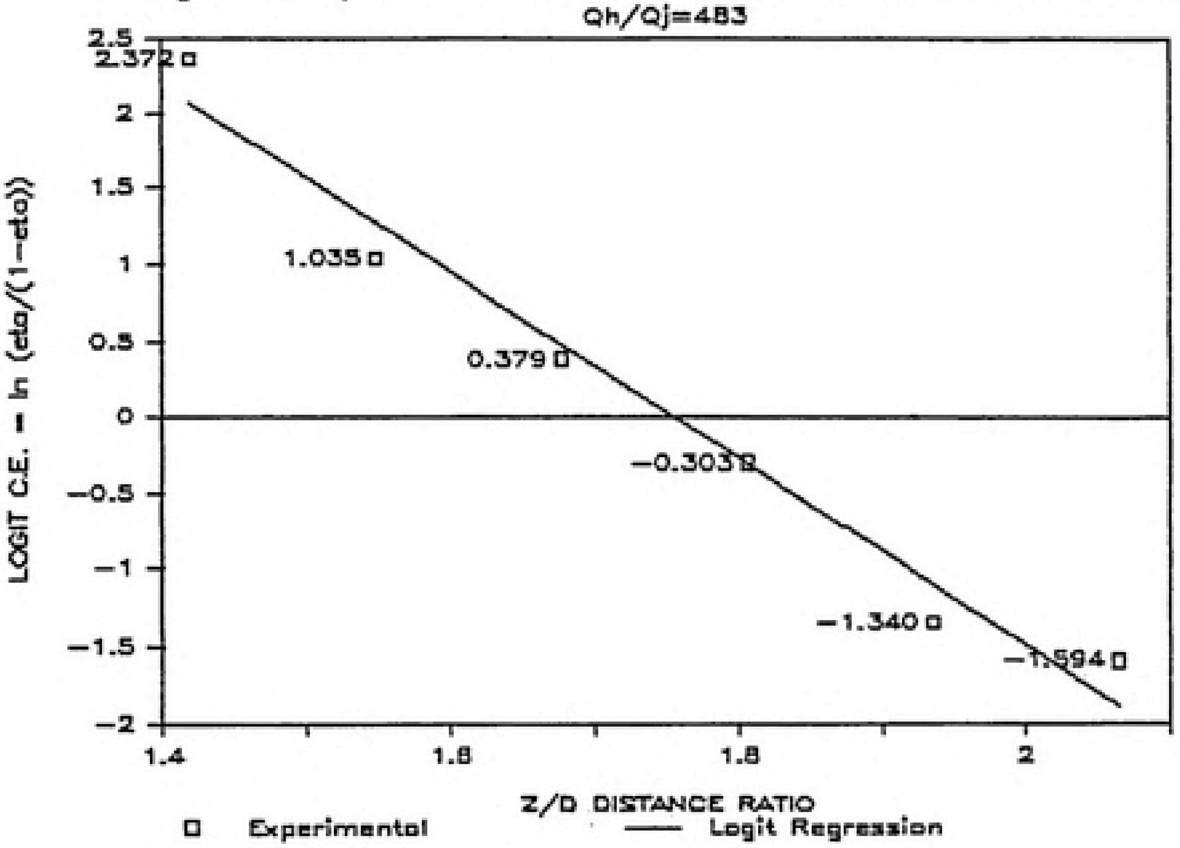

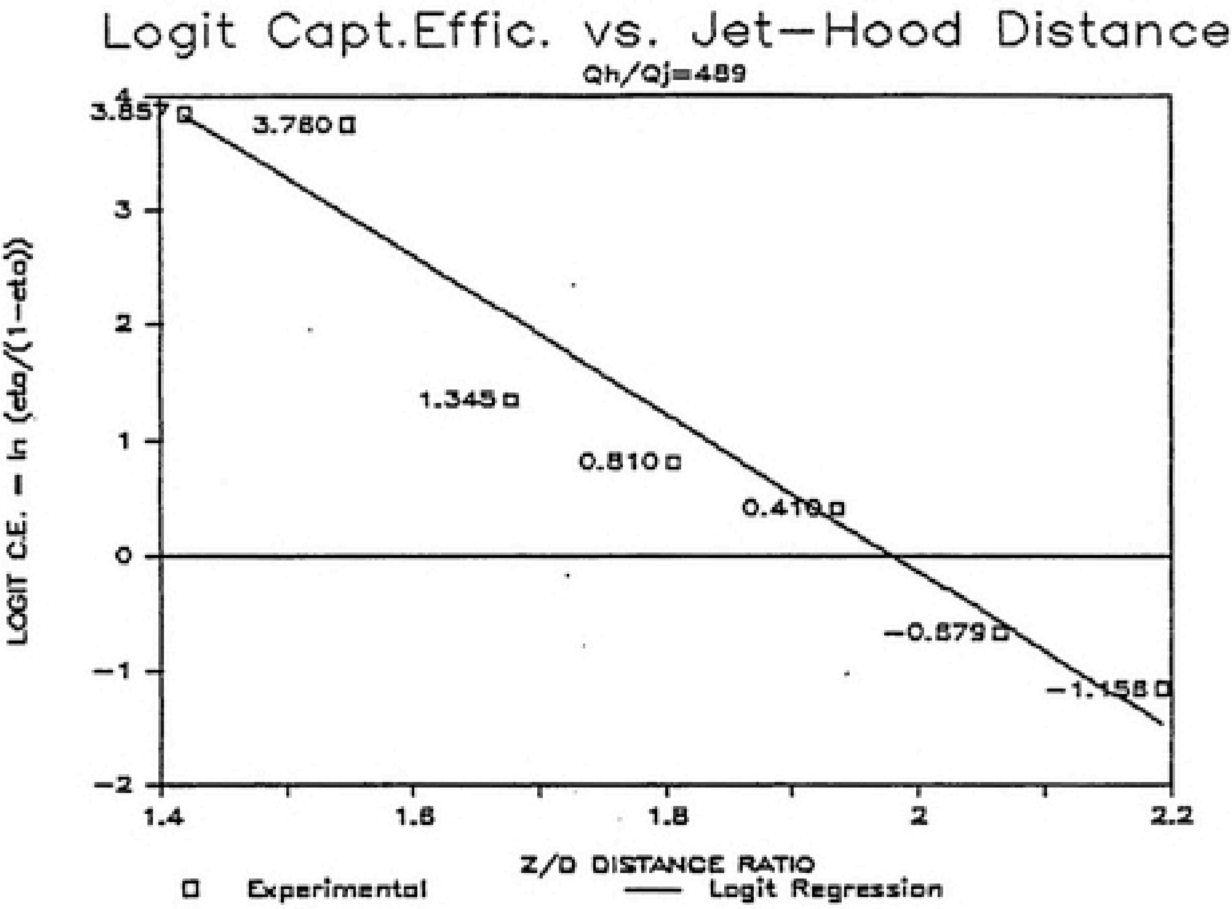

Logit Capt.Effic. vs. Jet-Hood Distance
Qh/Qj=489
LOGIT C.E. = ln (eta/(1-eta))
3.857
3.760
1.345
0.810
0.419
-0.879
-1.158
4
3
2
1
0
-1
-2
1.4
1.6
1.8
2
2.2
Z/D DISTANCE RATIO
Experimental
Logit Regression

APPENDIX F

EXPERIMENTAL DATA: RESULTS SUMMARY

Experimental Results Data Summary

Qh/Qj ratio	Qh cfm	Vh fpm	Vh/25	Projected Crossdraf	Vh/ideal or/25	(Z/D)50 logit mu	(Z)50, inches
76	75	916	36.64	25	36.64	0.9358	3.626
77	145	1770.5	70.82	25	70.82	1.1147	4.319
78	220	2686	107.44	25	107.44	1.0768	4.173
95	75	916	36.64	25	36.64	0.8742	3.388
97	145	1770.5	70.82	25	70.82	0.9414	3.648
98	220	2686	107.44	25	107.44	0.9683	3.752
126	75	916	36.64	5	183.2	0.8582	3.326
129	145	1770.5	70.82	24	73.77083	0.8619	3.340
130	220	2686	107.44	32	83.9375	0.8955	3.470
189	75	916	36.64	10	91.6	1.1445	4.435
193	145	1770.5	70.82	21	84.30952	1.2091	4.685
195	220	2686	107.44	59	45.52542	1.0945	4.241
316	75	916	36.64	16	57.25	1.5417	5.974
322	145	1770.5	70.82	33	53.65151	1.6031	6.212
326	220	2686	107.44	25	107.44	1.6968	6.575
379	75	916	36.64	19	48.21052	1.4253	5.523
387	145	1770.5	70.82	28	63.23214	1.5987	6.195
391	220	2686	107.44	17	158	2.0742	8.038
475	75	916	36.64	20	45.8	1.6336	6.330
483	145	1770.5	70.82	27	65.57407	1.7568	6.808
489	220	2686	107.44	29	92.62068	1.9799	7.672

Experimental Results Data Summary

w=-1/m spread	(Z/D)50 modlogit	(Z)50, modlogt"	25fpmPred inches	25fpmPred (Z/D)50	5fpmPred Z,inches	5fpmPred (Z/D)50	Qh/Qj ratio
0.168947	0.865	3.352	1.875	0.484	2.125	0.548	76
0.184945	1.1147	4.319	1.875	0.484	2.125	0.548	77
0.175254	1.03	3.991	1.875	0.484	2.125	0.548	78
0.077905	0.75	2.906	2.125	0.548	2.625	0.677	95
0.23635	0.9414	3.648	2.375	0.613	2.625	0.677	97
0.223613	0.92	3.565	2.625	0.677	2.625	0.677	98
0.089461	0.8582	3.326	2.875	0.742	3.625	0.935	126
0.13101	0.82	3.178	3.125	0.806	3.625	0.935	129
0.079327	0.84	3.255	3.375	0.871	3.625	0.935	130
0.076511	1.1445	4.435	3.625	0.935	5.125	1.323	189
0.174947	1.15	4.456	4.375	1.129	5.375	1.387	193
0.13196	1.03	3.991	4.625	1.194	5.375	1.387	195
0.122865	1.4	5.425	4.875	1.258	7.625	1.968	316
0.11481	1.4	5.425	5.875	1.516	8.125	2.097	322
0.149053	1.6968	6.575	6.625	1.710	8.375	2.161	326
0.156592	1.4253	5.523	5.125	1.323	8.375	2.161	379
0.181192	1.5987	6.195	6.375	1.645	9.125	2.355	387
0.277932	2.0742	8.038	7.375	1.903	9.625	2.484	391
0.10917	1.52	5.890	5.375	1.387	9.625	2.484	475
0.163585	1.7568	6.808	7.125	1.839	10.875	2.806	483
0.14556	1.9799	7.672	8.125	2.097	11.125	2.871	489

Experimental Results Data Summary

OfpmPred Z,inches	OfpmPred (Z/D)50	Projected Crossdraf	Vh/Vc Projected	Z"for PredXdrft	(Z/D)50 fromXdrft	Qh/Qj ratio
2.125	0.548	25	36.640	1.875	0.484	76
2.125	0.548	25	70.820	1.875	0.484	77
2.125	0.548	25	107.440	1.875	0.484	78
2.625	0.677	25	36.640	2.125	0.548	95
2.625	0.677	25	70.820	2.375	0.613	97
2.625	0.677	25	107.440	2.625	0.677	98
3.63	0.937	5	183.200	3.325	0.858	126
3.64	0.939	24	73.771	3.18	0.821	129
3.675	0.948	32	83.938	3.255	0.840	130
5.38	1.388	10	91.600	4.43	1.143	189
5.475	1.413	21	84.310	4.46	1.151	193
5.625	1.452	59	45.525	3.991	1.030	195
8.52	2.199	16	57.250	5.425	1.400	316
8.69	2.243	33	53.652	5.425	1.400	322
8.725	2.252	25	107.440	6.575	1.697	326
9.8	2.529	19	48.211	5.52	1.425	379
9.95	2.568	28	63.232	6.195	1.599	387
10.125	2.613	17	158.000	8.04	2.075	391
11.575	2.987	20	45.800	5.89	1.520	475
11.625	3.000	27	65.574	6.81	1.757	483
11.875	3.065	29	92.621	7.67	1.979	489

APPENDIX G

"EPSILON" MODIFICATION OF COMPUTER PROGRAM

```
10 'Title:   EPSILON
20 'Author: This program was prepared by Kirby N. Smith.
30 'Date:    This program was finalized in March, 1988.
40 'Purpose:To evaluate the effect of sequential changes in epsilon sub-zero
            on the calculation of jet flow.
50 'Note:    The equations of the Prandtl mixing length hypothesis,
            which takes viscosity into account, describe the jet flow.
60 'Note:    The line of 50% Capture Efficiency can be determined as a function
            of the dimensionless variables (Qh/Qj) and (Z/D)50, and of e-o.
70 CLS
80 SCREEN 0
90 COLOR 5
100 PRINT "EPSILON RUNNING--PLEASE STAND BY."
110 DIM P(600,2)
120 PI=3.1415927#
130 DH=3.875                    ''''Hood diameter in inches.
140 RH=DH/2
150 A=RH/12                     ''''A is the hood radius in feet.
160 AH=PI*(A^2)
170 JD=.25                      ''''Jet diameter in inches.
180 DJ=JD/12
190 RJ=DJ/2
200 AJ=PI*(RJ)^2
211 FOR MM=1 TO 21
220 IF MM=1 THEN Q=220
230 IF MM=2 THEN Q=145
240 IF MM=3 THEN Q=75
250 IF MM=4 THEN Q=220
260 IF MM=5 THEN Q=145
270 IF MM=6 THEN Q=75
280 IF MM=7 THEN Q=220
290 IF MM=8 THEN Q=145
300 IF MM=9 THEN Q=75
310 IF MM=10 THEN Q=220
320 IF MM=11 THEN Q=145
330 IF MM=12 THEN Q=75
340 IF MM=13 THEN Q=220
350 IF MM=14 THEN Q=145
360 IF MM=15 THEN Q=75
370 IF MM=16 THEN Q=220
380 IF MM=17 THEN Q=145
390 IF MM=18 THEN Q=75
400 IF MM=19 THEN Q=220
410 IF MM=20 THEN Q=145
420 IF MM=21 THEN Q=75
430 IF MM=1 THEN QJ=Q/489
440 IF MM=2 THEN QJ=Q/483
450 IF MM=3 THEN QJ=Q/475
460 IF MM=4 THEN QJ=Q/391
470 IF MM=5 THEN QJ=Q/387
480 IF MM=6 THEN QJ=Q/379
490 IF MM=7 THEN QJ=Q/326
500 IF MM=8 THEN QJ=Q/322
510 IF MM=9 THEN QJ=Q/316
520 IF MM=10 THEN QJ=Q/195
530 IF MM=11 THEN QJ=Q/193
540 IF MM=12 THEN QJ=Q/189
550 IF MM=13 THEN QJ=Q/130
560 IF MM=14 THEN QJ=Q/129
570 IF MM=15 THEN QJ=Q/126
580 IF MM=16 THEN QJ=Q/98
590 IF MM=17 THEN QJ=Q/97
600 IF MM=18 THEN QJ=Q/95
610 IF MM=19 THEN QJ=Q/78
620 IF MM=20 THEN QJ=Q/77
```

```
630 IF MM=21 THEN QJ=Q/76
640 IF MM=1 THEN XJFIN=7.67
650 IF MM=2 THEN XJFIN=6.81
660 IF MM=3 THEN XJFIN=5.89
670 IF MM=4 THEN XJFIN=8.04
680 IF MM=5 THEN XJFIN=6.195
690 IF MM=6 THEN XJFIN=5.52
700 IF MM=7 THEN XJFIN=6.575
710 IF MM=8 THEN XJFIN=5.425
720 IF MM=9 THEN XJFIN=5.425
730 IF MM=10 THEN XJFIN=3.99
740 IF MM=11 THEN XJFIN=4.46
750 IF MM=12 THEN XJFIN=4.43
760 IF MM=13 THEN XJFIN=3.255
770 IF MM=14 THEN XJFIN=3.18
780 IF MM=15 THEN XJFIN=3.325
790 IF MM=16 THEN XJFIN=3.57
800 IF MM=17 THEN XJFIN=3.65
810 IF MM=18 THEN XJFIN=2.91
820 IF MM=19 THEN XJFIN=4
830 IF MM=20 THEN XJFIN=4.32
840 IF MM=21 THEN XJFIN=3.35
850 IF MM=1 THEN GG=-2
860 IF MM=2 THEN GG=-1
871 IF MM=3 THEN GG=0
880 IF MM=4 THEN GG=0
890 IF MM=5 THEN GG=-1
900 IF MM=6 THEN GG=0
910 IF MM=7 THEN GG=-1
919 IF MM=8 THEN GG=-2
930 IF MM=9 THEN GG=0
939 IF MM=10 THEN GG=-2
950 IF MM=11 THEN GG=0
960 IF MM=12 THEN GG=0
970 IF MM=13 THEN GG=-1
979 IF MM=14 THEN GG=0
989 IF MM=15 THEN GG=0
999 IF MM=16 THEN GG=0
1009 IF MM=17 THEN GG=0
1019 IF MM=18 THEN GG=0
1029 IF MM=19 THEN GG=0
1040 IF MM=20 THEN GG=1
1041 IF MM=21 THEN GG=0
1042 IF MM=1 THEN FF=4
1043 IF MM=2 THEN FF=4
1044 IF MM=3 THEN FF=4
1045 IF MM=4 THEN FF=3
1046 IF MM=5 THEN FF=4
1047 IF MM=6 THEN FF=4
1048 IF MM=7 THEN FF=9
1049 IF MM=8 THEN FF=1
1050 IF MM=9 THEN FF=5
1051 IF MM=10 THEN FF=1
1052 IF MM=11 THEN FF=2
1053 IF MM=12 THEN FF=4
1054 IF MM=13 THEN FF=9
1055 IF MM=14 THEN FF=2
1056 IF MM=15 THEN FF=3
1057 IF MM=16 THEN FF=4
1058 IF MM=17 THEN FF=5
1059 IF MM=18 THEN FF=4
1060 IF MM=19 THEN FF=8
1061 IF MM=20 THEN FF=2
1062 IF MM=21 THEN FF=8
1064 FOR DD=.1 TO .9 STEP .2
1070 VH=Q/AH
```

```
1080 VJ=QJ/AJ
1090 RATIO=Q/QJ
1100 YJFIN=0                    ''''radial coord of the jet face(+to-12in)
1110 YJF=YJFIN/12
1120 XJF=XJFIN/12               ''''jet tip location on Z axis, in .ft
1130 DIR=90                     ''''jet direction (0,90,180,270)from Z axis
1140 RADIANS=PI*DIR/180
1150 XDFA=90                    ''''crossdraft angle
1160 RDXDF=PI*XDFA/180
1171 VC=25                      ''''crossdraft velocity
1180 INC=.03                    ''''increment to recalculation, in feet
1190 'Note:  The following three equations set the angle of the image jet.
1200 IF RADIANS=0 THEN RADIM=PI
1210 IF 0(RADIANS(=PI THEN RADIM=PI-RADIANS.
1220 IF PI(RADIANS(2*PI THEN RADIM=(3*PI)-RADIANS
1230 '   Note:The following equations set the angle of the image crossdraft.
1240 IF RDXDF=0 THEN XDFIM=PI
1250 IF 0(RDXDF(=PI THEN XDFIM=PI-RDXDF
1260 IF PI(RDXDF(2*PI THEN XDFIM=(3*PI)-RDXDF
1270 'Note:  The following equations calculate the vectors for each increment
             of hood flow.
1280 'Note:  Hood coordinates Z and R are named in hood flow calculations
             as X and Y, respectively.
1290 X=XJF
1300 Y=YJF
1310 FOR I1=1 TO 600            ''''points of the jet flow in the hood's field
1320 GAMMA1=SQR(X^2+(A+Y)^2)
1330 GAMMA2=SQR(X^2+(A-Y)^2)
1340 ECC=(2*A)/(GAMMA1+GAMMA2)
1350 ECC2=ECC^2
1360 T1=A+Y
1370 T2=Y-A
1380 T3=GAMMA1+GAMMA2
1390 T4=GAMMA1*GAMMA2
1400 T5=4*A^2
1410 T6=SQR(T3^2-T5)
1420 T7=-Q/PI
1430 T8=(T1*GAMMA2)+(T2*GAMMA1)
1440 T9=T3*T4*T6
1450 VR1=(T8/T9)*T7
1460 VZ1=(T7*X)/(T4*T6)
1470 V=SQR(VR1^2+VZ1^2)
1480 VTF=(Q*ECC2*SQR(3))/(2*PI*A^2*SQR(3-2*ECC2))
1490 VR2=(VR1/V)*VTF
1500 VZ2=(VZ1/V)*VTF
1510 VRC=(2.6*ECC^18+.853)*VR2
1520 VZC=.9*VZ2
1530 'Note:  The following equations transform the coordinates of the jet and
             its image to the coordinates of the hood.
1540 'Note:  The virtual point in the Prandtl mixing length hypothesis of jet
             flow is taken as the actual origin of the jet.
1550 IF DIR=0 OR DIR=360 THEN GOTO 1560 ELSE 1610
1560 Z=X-XJF+(1.86*DJ)
1570 R=YJF-Y
1580 ZI=2*(1.86*DJ)-(2*XJF)-Z
1590 RI=-R
1600 GOTO 1790
1610 IF DIR=90 THEN GOTO 1620 ELSE GOTO 1670
1620 Z=Y-YJF+(1.86*DJ)
1630 R=X-XJF
1640 ZI=Z
1650 RI=(2*XJF)+R
1660 GOTO 1790
1670 IF DIR=180 THEN GOTO 1680 ELSE GOTO 1730
1680 Z=XJF-X+(1.86*DJ)
1690 R=Y-YJF
```

```
1700 ZI=2*((1.86*DJ)+XJF)-Z
1710 RI=-R
1720 GOTO 1790
1730 IF DIR=270 THEN GOTO 1740 ELSE PRINT "DIRECTION"
1740 Z=YJF-Y+(1.86*DJ)
1750 R=XJF-X
1760 ZI=Z
1770 RI=R-(2*XJF)
1780 'Note:  The following equations calculate the vectors for any given R and
              Z points of the jet flow.
1790 K=AJ*(VJ)^2
1800 EO=.0161*SQR(K)*(FF-1+DD)*10^GG
1810 F=(FF-1+DD)*10^GG
1820 ETA=(R*SQR(3*K))/(4*(EO)*Z*SQR(PI))
1830 ETA1=ETA-((ETA^3)/4)
1840 ETA2=(1+((ETA^2)/4))^2
1850 IF -.00001<ETA AND ETA<.00001 OR -2.00001<ETA AND ETA<-1.99999 OR
     1.99999<ETA AND ETA<2.00001 THEN GOTO 1860 ELSE 1880
1860 VRJ=0
1870 GOTO 1890
1880 VRJ=(SQR(3*K)*ETA1)/(4*(ETA2)*Z*SQR(PI))
1890 VZJ=3*K/(8*PI*(EO)*Z*ETA2)
1900 IF VZJ<0 THEN VZJ=0 AND VRJ=0
1910 'Note:  The following calculations are for the effect of the image jet
              field on the flow of the actual jet into the hood. Note that
              K and epsilon-sub-zero have already been calculated for the jet.
1920 ETAI=(RI*SQR(3*K))/(4*EO*ZI*SQR(PI))
1930 ETAI1=ETAI-((ETAI^3)/4)
1940 ETAI2=(1+((ETAI^2)/4))^2
1950 IF -.00001<ETAI AND ETAI<.00001 OR -2.00001<ETAI AND ETAI<-1.99999 OR
     1.99999<ETAI AND ETAI<2.00001 THEN GOTO 1960 ELSE 1980
1960 VRIM=0
1970 GOTO 1990
1980 VRIM=(SQR(3*K)*ETAI1)/(4*ETAI2*ZI*SQR(PI))
1990 VZIM=3*K/(8*PI*EO*ZI*ETAI2)
2000 IF VZIM<0 THEN VZIM=0 AND VRIM=0
2010 'Note:  The following equations add the vectors and then determine
              the next point for vector calculation based on the combined
              values and the desired increment of calculation.
2020 VRTOT=VRC+(COS(RADIANS)*VRJ)+(COS(RADIM)*VRIM)+(SIN(RADIANS)*VZJ)+
          (SIN(RADIM)*VZIM)+(SIN(RDXDF)*VC)+(SIN(XDFIM)*VC)
2030 VZTOT=VZC+(COS(RADIANS)*VZJ)+(COS(RADIM)*VZIM)+(SIN(RADIANS)*VRJ)+
          (SIN(RADIM)*VRIM)+(COS(RDXDF)*VC)+(COS(XDFIM)*VC)
2040 IF VZTOT<=-.00001 THEN GOTO 2050 ELSE GOTO 2070
2050 ANGLE=ATN(VRTOT/VZTOT)+PI
2060 GOTO 2150
2070 IF VZTOT>=.00001 THEN GOTO 2080 ELSE GOTO 2100
2080 ANGLE=ATN(VRTOT/VZTOT)
2090 GOTO 2150
2100 IF -.00001<VZTOT AND VZTOT<.00001 AND VRTOT<0 THEN GOTO 2110 ELSE 2130
2110 ANGLE=3*PI/2
2120 GOTO 2150
2130 IF -.00001<VZTOT AND VZTOT<.00001 AND VRTOT>=0 THEN GOTO 2140
2140 ANGLE=PI/2
2150 X=X+(COS(ANGLE)*INC)
2160 Y=Y+(SIN(ANGLE)*INC)
2170 P(II,1)=X
2180 P(II,2)=Y
2190 IF X<=.01 OR X>=1 OR Y<=-1 OR Y>=1 THEN II=600 ELSE COUNT=II+1
2200 'Note:  A repetitive cycle is programmed to calculate the new
              magnitude and direction of flow at each subsequent increment.
2210 NEXT II
2220 'Note:  The following section is the instructions to the computer
              to draw the hood, and to display the flow into it.
2230 CLS
2240 SCREEN 1
```

```
2250 COLOR 16,0
2260 WINDOW (-1.6,-1.1)-(1.6,1.1)
2270 LINE (0,A)-(0,1),2
2280 LINE (0,A)-(-.05,A),2
2290 LINE (-.05,0)-(1,0),3
2300 LINE (0,-A)-(0,-1),2
2310 LINE (0,-A)-(-.05,-A),2
2320 FOR JJ=1 TO COUNT
2330 G=P(JJ,1)
2340 H=P(JJ,2)
2350 PSET(G,H),1
2360 NEXT JJ
2370 KEY  OFF
2380 LOCATE 8,4:PRINT "QH/QJ=";RATIO
2390 LOCATE 9,4:PRINT "QH=";Q"CFM"
2400 LOCATE 10,4:PRINT "JETX=";XJFIN"IN"
2410 LOCATE 17,4:PRINT "VZJ=";VZJ"FPM"
2420 LOCATE 16,4:PRINT "VJ=";VJ"FPM"
2430 LOCATE 15,4:PRINT "(Z/D)=";XJF/(2*A)
2440 LOCATE 18,4:PRINT "epsilon-O=";EO
2450 LOCATE 19,4:PRINT "F=";F
2460 PRINT
2470 PRINT
2480 INPUT "BREAKPT?(Y/N)";AN$
2490 IF AN$="Y" OR AN$="y" THEN GOTO 2510 ELSE GOTO 2630
2500 PRINT "BREAKPT FILE"
2510 OPEN "EPSICALC.DAT" FOR APPEND AS #1
2520 WRITE #1, RATIO, Q, VJ, VZJ, XJFIN, XJF/(2*A), EO, F
2530 CLOSE #1
2540 LPRINT "QH/QJ=";RATIO
2550 LPRINT "QH=";Q"CFM"
2560 LPRINT "VJ=";VJ"FPM"
2570 LPRINT "VZJ=";VZJ"FPM"
2580 LPRINT "JETX=";XJFIN"IN"
2590 LPRINT "(Z/D)50=";XJF/(2*A)
2600 LPRINT "epsilon-O=";EO
2610 LPRINT "eoFACTOR=";F
2620 LPRINT "--------------------------------------------------"
2630 CLS
2640   '''''  SCREEN 0
2650   ''''   COLOR 4
2660   ''''   INPUT "ANOTHER?(Y/N)";ANN$
2670   ''''   IF ANN$="Y" OR ANN$="y" THEN GOTO 1977 ELSE GOTO 1970
2680   ''''   PRINT "END OF PROGRAM"
2690   ''''   SYSTEM
2700   ''''   END
2710 SCREEN 0
2720 COLOR 5
2730 PRINT "EPSILON LOOPS RUNNING--PLEASE STAND BY."
2741 NEXT DD
2750 NEXT MM
2760 CLS
2770 COLOR 3
2780 PRINT "END OF EPSILON LOOPS."
2790 OPEN "EPSICALC.DAT" FOR INPUT AS #2
2800 LPRINT"                    EPSICALC DATA          DATE_________________"
2810 LPRINT"______________________________________________________________________"
2820 LPRINT "---------------------------------------------------------------------"
2830 LPRINT "QH/QJ", "QH", "VJ", "VZJ", "XJFIN", "ZD50", "E-O", "eoFACTOR"
2840 LPRINT"----------------------------------------------------------------------"
2850 IF EOF(2) THEN CLOSE #2:SYSTEM
2860 INPUT #2, RATIO, Q, VJ, VZJ, XJFIN, XJF/(2*A), EO, F
2870 LPRINT RATIO, Q, VJ, VZJ, XJFIN, XJF/(2*A), EO, F
2880 GOTO 2850
Ok
system
```